Modification Of An Ignition Quality Tester™ And Its Use In Characterising Middle Distillate Fuels

February 11, 2015

Written By: Aidan Lloyd Ehrenreich

Supervised By: Dr. Gareth Floweday and Mr. Paul Schaberg

A dissertation submitted in partial fulfillment of the requirements for the degree of Master of Science in Mechanical Engineering

Declaration

1. I know that plagiarism is wrong. Plagiarism is to use another's work and pretend that it is one's own.
2. Each contribution to, and quotation in, this dissertation from the work(s) of other people has been attributed, and has been cited and referenced.
3. This dissertation is my own work.
4. I have not allowed, and will not allow, anyone to copy my work with the intention of passing it off as their own.
5. I acknowledge that copying someone else's work, or part of it, is wrong and declare that this is my own work.

Signed: ——————————

Aidan Lloyd Ehrenreich

Abstract

The Ignition Quality Tester (IQT^{TM}) is a constant volume combustion chamber based device which is used to determine the derived cetane number of diesel fuel oils when used in conjunction with ASTM D6890. During a test, the fuel sample is injected into heated, pressurised gas where it combusts. Suitable measurements are made during the combustion event to determine the ignition delay of the fuel and the latter is used with a correlation to determine the derived cetane number of the sample.

The IQT offers improved repeatability and reproducibility when compared with the conventional method of determining cetane number, namely ASTM D613. Despite these advantages, the device features a fuel injection system not indicative of the state of the art, in terms of direct injection diesel components and associated fuel spray behavior. Therefore this project sought to make suitable mechanical, electrical and control modifications to incorporate a more technologically appropriate injector. It is believed that by improving the spray characteristics of the IQT along with the incorporation of a flexible control system, that it can be leveraged to a greater extent in a fuels research context.

The modifications made to the system included the incorporation of a single hole common rail diesel injector along with a custom control system. The control system allowed flexible control of all variables considered to be significant to the study of auto-ignition delays. Additionally, an optical sensor was added to detect luminous emissions from the reacting fuels. The modified system was used to rate diesel fuels with varied composition including solvents, diesel primary reference fuels, crude derived as well as Low Temperature Fischer Tropsch (LTFT) products. These tests were performed at two temperatures and oxygen concentrations and the resulting data was used to redevelop correlations between the cetane number of the respective samples and their ignition delays in order to surmise the optimal operating conditions of the modified IQT.

The device worked as required, however problems with the fuel injector limited the number of tests that were performed. Nonetheless, the data gathered suggests that the use of a fuel injector and pressures typical of common rail injection systems may be an effective means to extend the range over which the IQT could reliably rate the cetane numbers of diesel fuels.

Contents

List of Figures

List of Tables

List of Acronyms

IQT - Ignition Quality Tester

ID - Ignition delay

ASTM - American Society for Testing and Materials

TDC - Top dead centre

ULSD - Ultra Low Sulphur Diesel

CN - Cetane Number

DCN-Derived cetane number

SAFL - Sasol Advanced Fuels Laboratory

FIT-Fuel Ignition Tester

AFIDA - Advanced Fuels Ignition Delay Analyser

PRF(s) - Primary Reference Fuel(s)

CFR- Co-operative Fuels Research

SRF (s) -Secondary Reference Fuel(s)

Φ- phi, equivalence ratio

HP-High pressure

CR-Common Rail

HeNe - Helium Neon

Op-amp - Operational Amplifier

FPGA - Field Programmable Gate Array

RTC - Real Time Controller

VIs - Virtual Instruments

GUI - Graphic User Interface

GND - Ground

NI - National Instruments

CJ - Cold Junction

UPS - Uninterrupted Power Supply

GTL (Diesel) - Gas to Liquids Diesel

Chapter 1

Introduction

1.1 Background

The Ignition Quality Tester ^{TM} (IQT) is a device used to determine the derived cetane number (DCN) of a fuel sample. The system is based on an electrically heated constant volume combustion chamber which is charged with synthetic air, where synthetic air is a commercially available gas mixture featuring 21% oxygen in nitrogen. Once heated, the fuel sample is pressurised and injected by a custom fuel pump and injector into the vessel. The injector features a needle lift sensor, which is used to define the start of the auto-ignition delay period. The end of the combustion chamber is fitted with a piezoelectric pressure transducer which measures the pressure rise due to combustion and therefore defines the end of the auto-ignition delay.

The ignition delay (ID) is defined as the time between injector needle lift and significant pressure rise within the combustion chamber. The average ignition delay of a predetermined number of combustion cycles is used with a correlation, based on the diesel reference fuels' ignition delays, to interpolate the derived cetane number of the sample. Allard et al. [1] state that the device offers better repeatability and reproducibility than the original ASTM D613 [2] method and in later work the IQT was shown to be able to determine the derived cetane number of cetane-improved fuels indicating the robustness of the device [3]. The IQT was formally recognised as a method of determining DCN when used in conjunction with ASTM D6890 [4]. The standard indicates that it can be used for biodiesel, cetane improved and tar sands based fuels within a range of 33-64 DCN [4].

While useful in its original form, the IQT suffers from certain drawbacks that limit its use in a fuels research context. These limitations include:

- A fixed control system, preventing variation of test conditions required to perform ignition delay (ID) characterisation studies.

- The fuel injection system is not indicative of current production diesel common rail systems.
- No means exist at the facility to alter the charge gas composition in order to study its effect on ignition delay.

This project therefore sought to address these and related issues by suitably modifying an IQT so that it can be used as a more flexible fuels research device to complement those already present at the Sasol Advanced Fuels Laboratory (SAFL).

1.2 Project Objectives

In line with the shortcomings previously mentioned, this project sought to make suitable control, mechanical and electrical modifications to an existing IQT so that it would be more useful in a fuels research context. It then sought to re-establish the correlation between CN and ID by performing suitable Primary Reference Fuel (PRF) parametric tests. The specific objectives include:

- Design, manufacture and commissioning of suitable fittings and fixtures such that single hole common rail diesel injectors available for use with this project could be incorporated with the existing combustion chamber.
- Develop a means to detect the onset of fuel injection to define the beginning of the auto-ignition delay period.
- Development of a new control system based on National Instruments^{TM} components, to allow flexible control of the operating conditions using components widely used within Sasol.
- Design and implement a means to alter the charge gas composition of the IQT.
- Redevelop the correlation between ignition delay and cetane number through adequate testing.
- Use the correlation to analyse fuels from a variety of sources to determine its suitability.

1.3 Thesis Outline

The thesis outline is as follows:

- Review of pertinent literature to inform and better understand the following:

  - Cetane and its estimation by various methods.
  - The effect of operating conditions on the auto-ignition delay of middle distillate fuels in the IQT.
  - Methods used to detect the onset of fuel injection.
  - Systems that can be used to generate fuel pressure indicative of common rail injection systems.

- Discussion of the adopted design solution and its operation.
- Experimental method development including data analysis techniques driven by initial testing results.
- Results and discussion of the testing procedure.
- General discussion based on analysis of the results.
- Conclusions
- Recommendations for future work.

Chapter 2

Literature Review

2.1 Cetane Measurement

The cetane number of a fuel is an indication of its propensity to auto-ignite, with fuels of higher cetane number being more susceptible to auto-ignition. Auto-ignition is defined as the spontanenous, fast and highly energetic release of thermal energy from a fuel when exposed to critical conditions [5]. Commercially available diesel fuels are mandated to satisfy a minimum cetane number for e.g. SANS 342 [6] requires a CN of 45. Therefore the accurate determination of a diesel fuel's CN is key to refiners, while the advent and promulgation of fuels from alternative sources, such as bio-fuels and tar sands, have necessitated the robust estimation of cetane number in a research context as well [1].

Traditionally the cetane number of a fuel sample was determined using the ASTM D613 method [2] in conjunction with the Co-ordinating Fuels Research (CFR) cetane engine. This method made use of a variable compression ratio engine, which allowed for the in-cylinder conditions to be critically adjusted so that the fuel being tested auto-ignited at top dead centre (TDC). Next, two blends of the two PRFs, namely hexadecane and heptamethylnonane, were tested at similar compression ratios to bracket the test fuel's compression ratio. The aforementioned fuels define the cetane scale with cetane numbers of 100 and 15 respectively. The cetane number of the tested fuel was thus determined by the composition of reference fuel blends, based on the respective PRF blends cetane numbers' differing by five or less and appropriate interpolation of the compression ratio required to achieve TDC auto-ignition.

While the ASTM D613 method defines cetane number, it has relatively poor repeatability and reproducibility according to Allard et al. [1] . Furthermore, it is expensive to implement, requires a relatively skilled operator and requires a large volume of fuel (500 ml) in order to perform a test. Therefore several other means of estimating the cetane number of a fuel sample have been devised and these alternative methods typically rely on either:

- The bulk physical characteristics of the fuel, such as density and volatility, to extrapolate a cetane index based on the performance of other fuels with similar characteristics e.g. ASTM D4737 [7] or ASTM D976 [8].
- The use of combustion bomb apparatus which derive the cetane number based on a correlation between ignition delay and cetane number e.g. ASTM D6890 [4].

The cetane index methods are limited to fuels with a composition similar to those that were used to develop the correlations. Therefore they cannot be reliably used on fuels derived from other sources, nor are they sensitive to cetane improver additives. This limitation is stated in the respective standards and neither method may be definitively used as a replacement for combustion based methods. Their limitations were studied by Bezaire et al. [9] who tested an ultra low sulphur diesel (ULSD) separately blended with a soybean based biodiesel and with a cetane improver additive. Neither cetane index method previously mentioned was able to indicate the change in auto-ignition quality of the fuel after blending. However, it did register with the IQT when used as part of ASTM D6890.

Other devices similar to the IQT also exist, including the Fuel Ignition Tester (FIT) [10], Advanced Fuels Ignition Delay Analyser (AFIDA) and the Herzog CID 510[11] . All three devices work on a principle similar to the IQT as previously discussed, however the FIT, which has been formalised in ASTM D7170 [10] operates at a slightly lower temperature and slightly higher pressure than the IQT as depicted in Table 2.1 . Allard et al. [1] found that at lower temperatures and/or pressures a prototype IQT exhibited the characteristic of higher ignition delay sensitivity to cetane number while the ignition delay repeatability worsened. It is therefore interesting to note, as depicted in Figure 2.1, that the IQT has a better 95% DCN confidence interval than the FIT despite the similarity in their respective operating conditions as indicated in Table 2.1. This suggests that tighter control of the charge gas pressure, basing a DCN estimation on more cycles and a faster cycle speed may be beneficial in terms of improving the repeatability of a DCN determination when considering the information presented in Table 2.1.

	Units	IQT	FIT
Charge Temperature	ºC	545 ± 30	510 ± 50
Charge Pressure	Bar	21.37 ± 0.07	24 ± 0.2
Total number of cycles		47	27
No. of cycles for DCN		32	25
Test time	min	≈20	≈20

Table 2.1: Major parameters of IQT and FIT derived cetane number tests [4],[10]

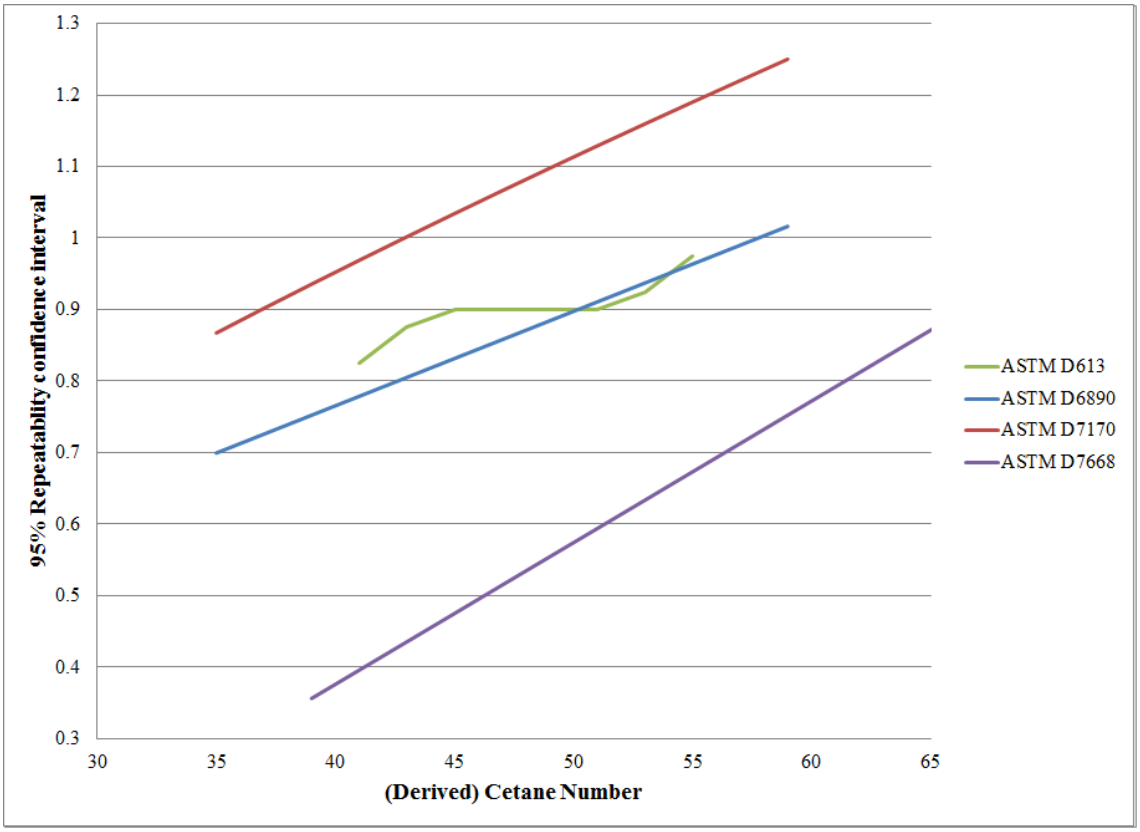

Figure 2.1: Comparison of the DCN determination repeatability of various methods at 95% confidence level [2, 4, 10, 11].

Despite the relatively good repeatability of the IQT relative to the CFR cetane engine, the use of an Ignition Delay (ID) correlation to predict DCN has limitations.

Yates et al. [12] discuss that a fuel's auto-ignition traits typically have a unique response to temperature and pressure. Also, the CFR cetane engine's temperature and pressure changes with compression ratio. Therefore two fuels with the same D613 cetane number may not necessarily return the same ID at the fixed IQT operating conditions. This can be better understood by referring to Figure 2.2 which shows the polytropic curve corresponding to the CFR cetane engine as well as curves indicating constant ignition delay for two hypothetical fuels. The figure shows that the two fuels cross the CFR engine's polytropic curve at 50 CN, however they do not coincide at the IQT's operating point. This implies they would have different ID's and therefore different DCNs when tested in the IQT even though they have the same CN. The IQT's reference fuel, n-heptane, exhibits this discrepancy with a DCN of 53.8 [4] and a D613 CN of 52.2 [13] and similarly the PRFs and Secondary Reference Fuels (SRFs) also exhibit this incongruity [14].

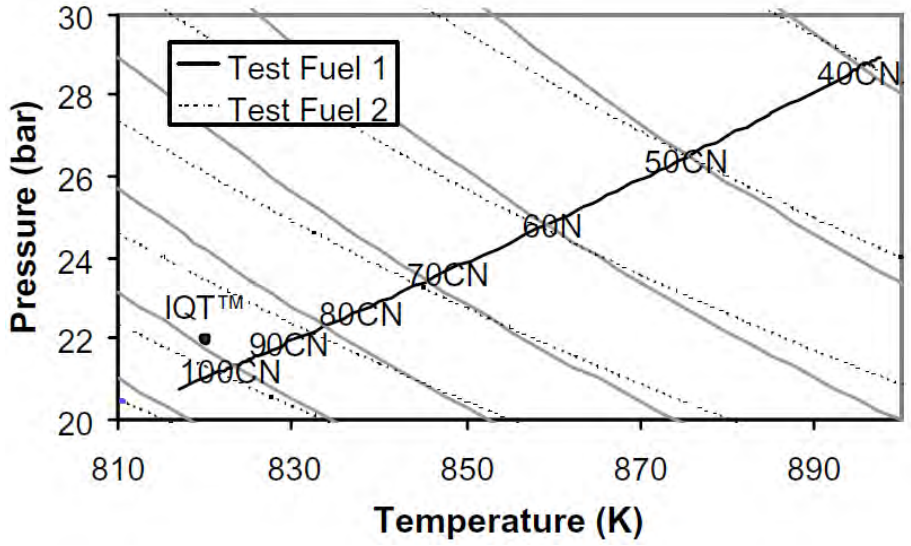

Figure 2.2: Hypothetical response of two fuels with the same D613 cetane number but differing ID at the IQT operating point [12].

In an attempt to remedy this situation, Yates [12] et al. used an IQT with modified controls to generate parametric ID data, at different pressures and temperatures, to use with an ignition delay model based on a combination of three Arrhenius functions to mimic the cool, intermediate and hot flame chemistry typical of middle distillate hydrocarbon fuels. The ignition delay model was then used with a quasi dimensional, numerical, CFR engine model to estimate the compression ratio required to achieve TDC auto-ignition. Finally the compression ratio was linked with the engine's guide curve allowing the cetane number to be estimated and the engine model to be suitably tuned to the PRFs. While Yates et al.[13] were able to show an improved agreement between the D613 CN and the results of their measurement and modeling work for a limited group of fuels, the need to test each fuel at a number of different conditions greatly increases the testing time per fuel as well as the level of analysis required to achieve a result. Furthermore, the method would require more validation before it could be considered as a replacement for methods such as ASTM D6890. Their method also tacitly relies on the temperature measured within the IQT to be homogeneous for the engine model to be "tuned" to having boundary conditions which are representative of the engine and simultaneously achieving accurate DCN estimation.

It has been noted by researchers such as Metcalf [15] and Savage [16], that a temperature gradient exists within the IQT's combustion chamber and therefore the temperature used as the base of the ignition delay model may not be appropriate. It would therefore seem that a significant number of potential problems are remedied by suitable calibration of the model with the PRF data. However, the PRFs do not cover the full distillation range of diesel fuels and therefore a fuel with different volatility may not fit the CFR engine model of Yates et al. [12] well. Also, it is not clear if the CFR

engine's knock sensor will respond to the cool or hot flame and therefore a two stage igniting fuel may require a slightly different hand wheel setting if actually tested in the engine. This may result in the numerical model triggering off the incorrect heat release point and result in a compression ratio estimate via the model which is not representative.

2.2 Factors Influencing the Ignition Delay of Middle Distillate Fuels in the IQT

Various factors have been shown to effect the ignition delay of middle distillate fuels and therefore they will be considered and discussed.

2.2.1 Temperature and Pressure

It was previously alluded to in Section 2.1 that fuel ignition delays are dependent on the temperature and pressure of the gas into which they are introduced. It is also important to note that in the context of diesel auto-ignition and combustion, the ignition delay is a combination of both the physical, spray-mixing and evaporation effects, as well as the chemical reactivity of the fuel [17] . Therefore the ambient temperature and pressure can alter both facets of the ignition delay and are considered separately.

With respect to the chemical reactivity, according to Heywood [5], the ignition mechanism is temperature dependent and can be divided into three categories based on the prevailing fuel air mixture temperature:

1. Cool flame(s): After an induction period, preliminary reactions occur where only a small fraction of the total heat release occurs, typically accompanied by blue luminosity before the reactions are quenched.

2. Two stage ignition: An induction period occurs followed by a cool flame. A second induction period occurs after the cool flame and finally there is a so called hot flame, where the remainder of the fuel energy is rapidly released.

3. Hot flame: Under suitably high temperature conditions, a single stage ignition process occurs. There is an induction period followed by one main, fast, heat release.

While these ignition mechanisms have been separated, it is possible under typical diesel operating conditions for both two stage as well as single stage hot flame ignition to occur. This may occur if fuel initially sprayed into an elevated temperature environment sufficiently reacts to cause a rise in temperature and pressure high enough to force subsequently sprayed fuel straight into a hot flame condition.

Floweday [18] collected ignition delay data from simulation runs of CHEMKIN ™ detailed chemical kinetic models, at a homogenous, stoichiometric air/fuel ratio and constant pressure conditions. The data showed the change in ignition delay of n-heptane with respect to temperature over a wide range as depicted in Figure 2.3. N-heptane has a cetane number of 52.2 [13] which is relatively close to that of full boiling range diesel fuels and it can therefore be considered as a diesel surrogate, given its CN similiarity. The figure shows, in blue, that the ID decreases with increasing temperature up until the negative temperature coefficient (NTC) region where the ignition delay *increases* with increasing temperature until initial temperatures of 950 K and above, where it once again decreases. It is thought that in the NTC region, the reaction pathways dominant at lower temperatures are shut-off and other reaction pathways dominate [5] changing the response of the fuel to the elevated temperature.

An interesting consequence of the cool flame is that the bulk gas temperature after the cool flame is higher, as indicated by *Tcf* in Figure 2.3, and that the 2nd stage ignition delay (ID-t1) is shorter than expected after a cool flame, even if a hot flame auto-ignition test starts at *Tcf [18]*. This suggests that the cool flame expedites the hot flame due to a change in chemistry as well as an increase in temperature. In the IQT, combustion occurs at constant volume, not constant pressure and therefore the rise in temperature caused by a cool flame would also increase the pressure. An increase in pressure always decreases the ignition delay and therefore the cool flame acts to expedite the subsequent hot flame, exacerbating the cool flame influence on the hot flame auto-ignition.

The original IQT has a main injection duration of approximately 2.4 ms [19] and its ignition delays span the range of 2 to 25 ms [20] over the full CN range, indicating that high cetane fuels undergo flame liftoff and a partial mixing controlled burn while low cetane fuels only undergo premixed combustion. In this context, flame lift off implies that a flame ignites and forms on the boundary of the fuel spray and that the reaction rate is limited by the rate at which air (oxygen) can be entrained into the fuel vapour [21]. However, the engine based tests always nominally have the same injection duration (13 ml/min fuel flow rate [2]) and ignition delay, 13 crank angle degrees (CAD). Therefore it may be possible that auto-ignition in the IQT is more susceptible to air fuel ratio effects because auto-ignition occurs at varying points within the injection period when compared to the cetane engine. At typical diesel combustion conditions, the ignition delay is short and therefore fuel which is sprayed into an engine is heterogeneously distributed inside the combustion chamber when it ignites. However, since the IQT operates at a reduced pressure condition, the ignition delays are relatively longer and therefore more time is available for mixing. With low cetane fuels, the ignition delay may be long relative to the physical evaporation time and therefore the fuel/air mixture may be closer to homogeneous conditions. It has been shown [18] that at homogenous conditions, the ignition delay increases

with decreasing equivalence ratio (Φ) and therefore the equivalence ratio may become significant if conditions such as changing the injector enhance mixing.

CFD simulations of the original device at standard test conditions using n-heptane by [15, 22, 23] indicate that auto-ignition occurs at a locally rich condition, with Φ>2 at least. It is interesting to note that none of the previously mentioned CFD models were able to accurately predict the ignition delay of n-heptane and it would appear, based on the assumptions made in those respective studies, that modeling the IQT's injector is a limiting factor.

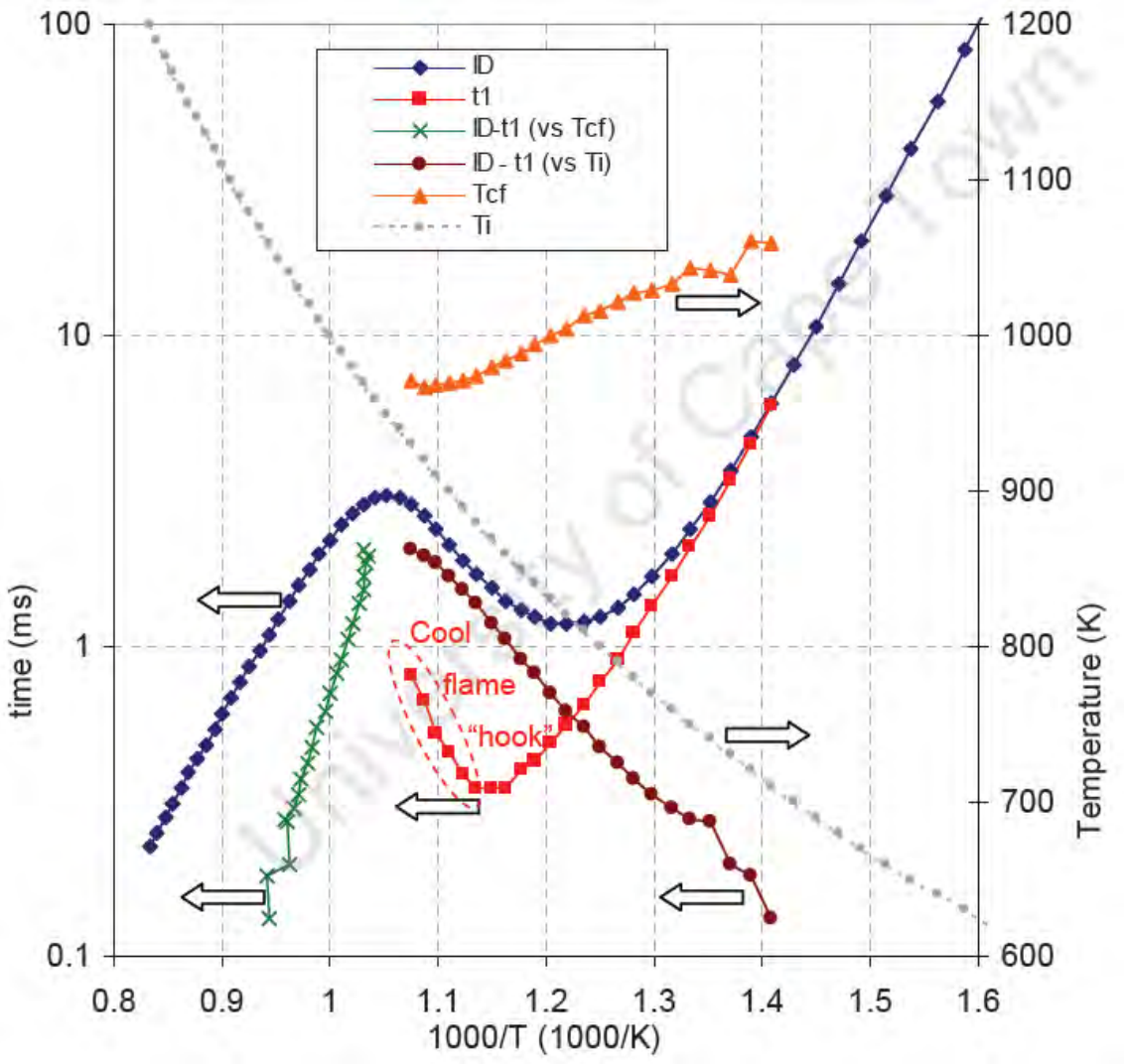

Figure 2.3: Ignition delay of stoichiometric n-heptane at various temperatures and constant pressure of 20 bar [18]. The primary axis is logarithmically scaled.

The IQT makes use of the pressure recovery method [4] to define the end of ID period. This method considers the point when the combustion chamber pressure increases passed the initial pressure, subsequent to fuel evaporation, as indicative of the end of the ID phase. It is not clear if this method of defining the end of the ignition

delay period may respond to the cool flame typically, but in certain circumstances respond to the hot flame. Zheng et al. [24] tested four fuels in a DCN range of 25-61 and showed that the lowest DCN fuel underwent two stage ignition while the others did not. The pressure rise associated with the fuel which underwent the cool flame was minor and therefore the possibility exists for a fuel to have a cool flame heat release insufficient for the pressure recovery to occur and therefore the end of the ignition delay would coincide with the hot flame instead, resulting in a very different DCN being determined. The fuel which underwent the cool flame is outside of the applicable range of the ASTM D6890, but it suggests the possibility of such an event occurring.

In comparison, engine based ignition delay studies determine auto-ignition based on the heat release rate inferred from in-cylinder pressure measurements. However, the IQT combustion pressure measurement is subject to large fluctuations [24, 25] which makes this approach difficult to use as is shown in Figure 2.4.

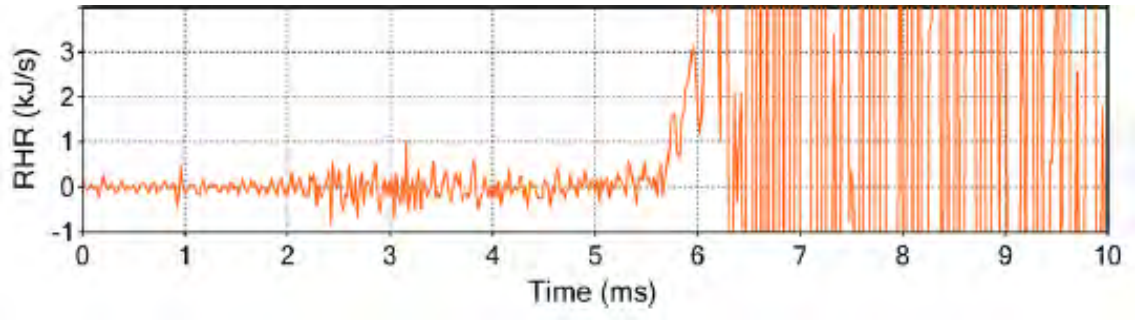

Figure 2.4: Rate of heat release (RHR) after start of measurement for N-heptane under standard IQT operating conditions using the original device [24].

The pressure trace can be filtered, but then the ID is likely to change with the degree of filtering used. Rabl et al. [26] made use of a 5% total heat release to define the end of the ignition delay for their constant volume combustion work. At constant volume, a fraction heat release is equivalent to a fraction pressure rise since there is no work done, if heat losses are assumed to be negligible. Given the IQT's pressure fluctuations, this may be a useful way of defining the end of the auto-ignition delay phase.

2.2.2 Physical Effects

With regards to the physical effects that the ambient temperature and pressure have on the ignition delay, the following is noted:

Siebers [21] noted that at constant density, increasing the ambient temperature decreased the liquid length of diesel sprays as shown in Figure 2.5. The liquid length is defined as the maximum penetration of liquid fuel when it enters a combustion

chamber. The liquid length is an important characteristic because spray contact with the heated walls of the IQT may lead to erroneous ignition delays, thereby placing a limit on conditions which can be tested with confidence. At the standard IQT point of 818 K and 21.37 bar, the density is approximately 9.1 kg/m^3. With the 246 μm orifice sized injector used by Siebers, the liquid lengths of heptamethylnonane and cetane are approximately 50 and 60 mm respectively at the IQT operating conditions, based on Figure 2.5. The injectors available for use in this project had orifice sizes of 135 and 160 μm respectively and therefore the liquid lengths were expected to even shorter than previously mentioned.

Additionally, the spray spreading angle, as depicted in Figure 2.6, was shown to be weakly dependent on gas temperature and density, and spray angles of the order of 14 degrees are expected. There is at least 100 mm from the injector tip to the back wall of the combustion chamber and therefore by ensuring that the liquid length was reasonable in comparison to the combustion chamber length, significant quantities of fuel impingment on the walls was avoided.

Siebers [21] further showed that the liquid length remained approximately constant with increasing fuel pressure, indicating that the evaporation rate increased with increasing fuel pressure monotonically over a range of 50-170 MPa. The evaporation rate must increase because the mass flow rate of fuel increases and therefore if the penetration is same the fuel droplets have less time to evaporate. Pastor et al. [27] found a similar trend with five full boiling range diesel fuels, with the liquid length being longest for the fuel with the lowest volatility. This suggests that the ignition delay would decrease with increasing fuel pressure since the evaporation rate must increase for the liquid length to remain the same and the sooner fuel is volatilized the earlier it can react.

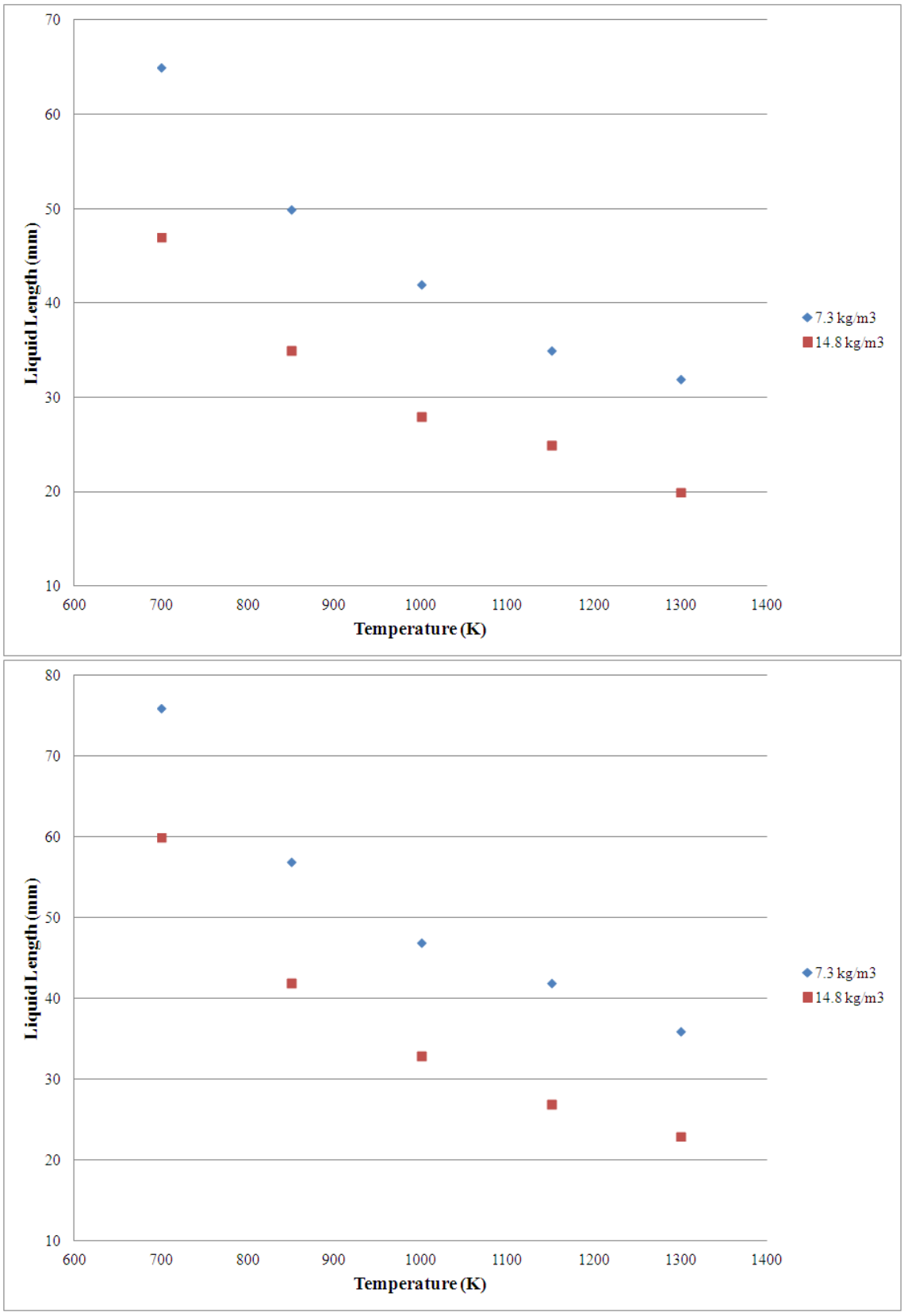

Figure 2.5: Liquid length of heptamethylnonane (Top) and cetane (Bottom) at constant densities. Injector orifice size 246 μm, injection pressure 136 MPa and fuel temperature 438 K. Adapted from [21].

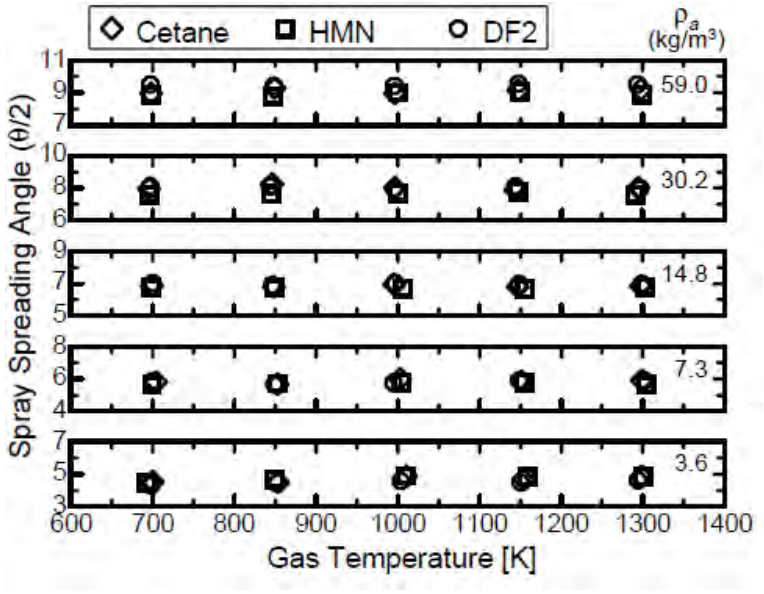

Figure 2.6: Spray spreading angles of hexadecane (cetane), heptamethylnonane (HMN) and no.2 diesel (DF2) as a function of temperature at different densities. [21]

2.2.3 Oxygen Concentration

Allard et al. [20] tested three PRF blends at different oxygen concentrations with an IQT. As expected the ignition delays increased for all of the blends with decreasing oxygen concentration, but of interest to this work is that the DCN correlation flattened out as shown in Figure 2.7, which means that the correlation could distinguish between high cetane fuels more easily. Also, the relative response between check fuels and the PRF blends changed with oxygen concentration i.e. at some oxygen concentrations the nominally identical cetane fuels had either shorter or longer ignition delays. This led the researchers to optimise the oxygen concentration in order to get the best agreement between the results, which was achieved with an oxygen concentration of 6.7%. At this oxygen concentration the equivalence ratio is 2.14 which would be overall rich for the reference fuels given that the standardised injected mass of n-hexadecane is 98 mg [28] and the chamber contains approximately 2 g of gas at the standard conditions.

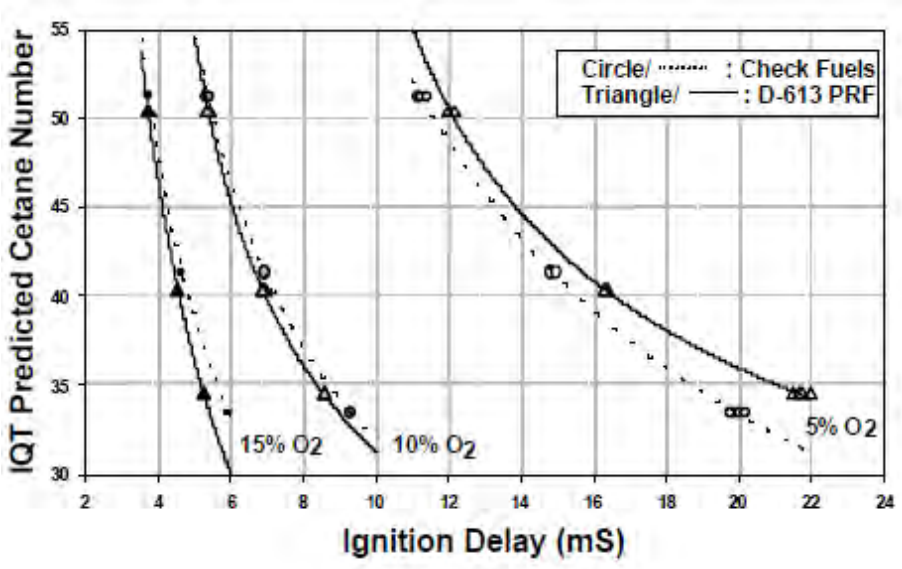

Figure 2.7: DCN and ignition delay of three check fuel blends and their nominally identical PRF blends as a function of oxygen concentration using the original IQT device [20].

2.3 Detection of Fuel Injection

The IQT's ignition delay is based on the time between the detection of fuel sprayed into the combustion chamber and the time taken for a standardised increase in combustion pressure to take place. The original device featured a delay pintle type injector [4], which is not indicative of the mini-sac injectors typical in contemporary diesel research facilities [29]. The original device made use of a Hall effect sensor to measure the injector's needle rise and assumed that fuel flow was immediate. Cross [30] showed that fuel flow does not commence immediately for common rail injectors relative to energising of the injector actuator, as indicated in Figure 2.8. Also, the IQT needle lift sensor was custom made for the application which made it difficult to incorporate with a production injector. Therefore alternatives were sought which would be more appropriate for the purposes of this project.

In this application, injection is expected to occur approximately twice a minute based on the data represented in Table 2.1.

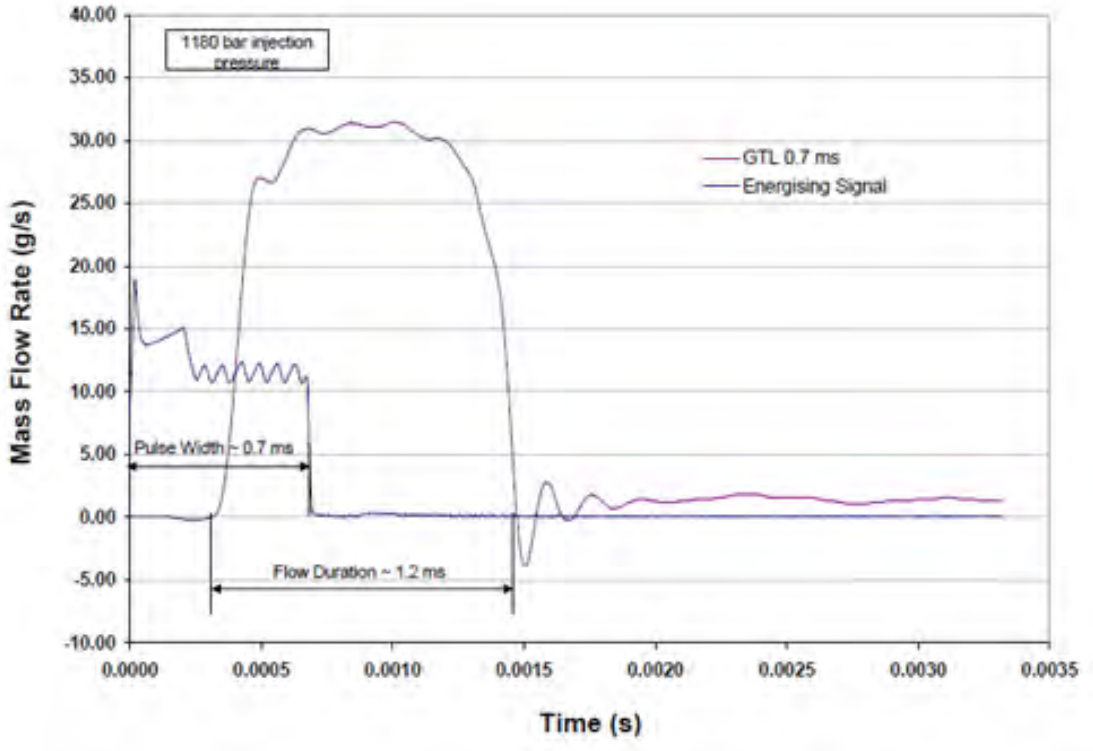

Figure 2.8: Comparison of injector actuator current and GTL diesel mass flow rate indicating the time delay between the injector current and actual fuel flow [30].

Fryskowski and Mazur [31] compared the performance of an accelerometer and piezoelectric strain transducer in determining the injection timing and duration of an engine. Both sensors were fitted onto the high pressure tube connected to the injector being analysed. The piezoelectric material was incorporated within a clamp as shown

in Figure 2.9 while the uni-axial accelerometer, ADXL150, was fitted perpendicular to the axis of the tube. A comparison of the respective output signals for both sensors is shown in Figure 2.10 and shows that both sensors are sensitive to the vibrations present within the engine as manifested by the high noise levels in each case.

The noise is a concern because determination of the onset of injection requires careful processing of the signals to deduce the onset of injection. However, with the relatively low injection frequency and vibration of the IQT, the noise may be significantly lower if the fuel pump does not run continuously. Fryskowski and Mazur [31] used a digital tachometer as a reference value to measure engine speed and compared it with the speed deduced using the aforementioned sensors. They found that the piezoelectric signal had a maximum 2% error while the accelerometer error was approximately 0.75% at 4000 RPM. The trend in their work was that the error would be lower at lower speeds.

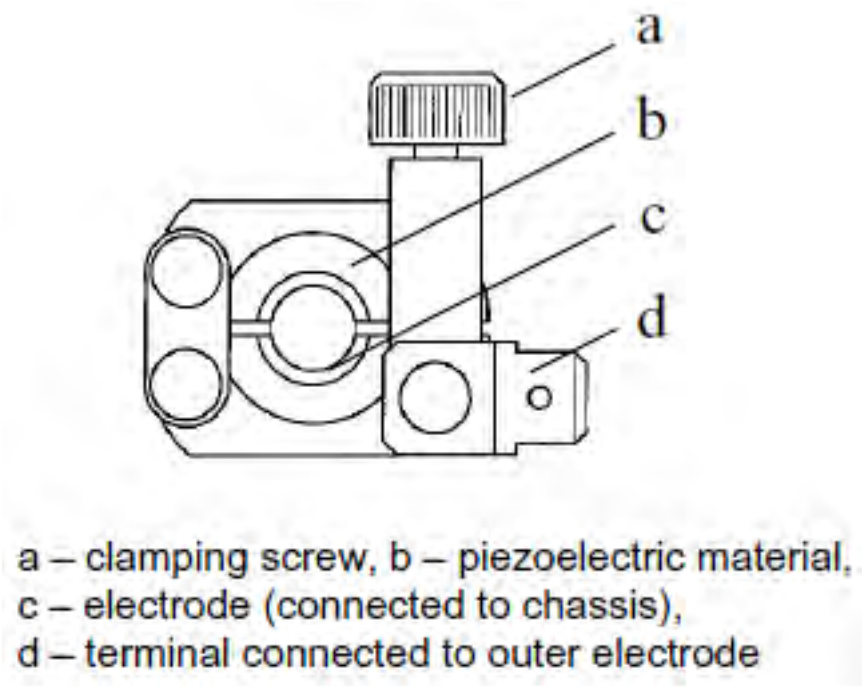

Figure 2.9: Clamp used by Fryskowski and Mazur [31] to detect injection timing and duration of an distribution pump injector.

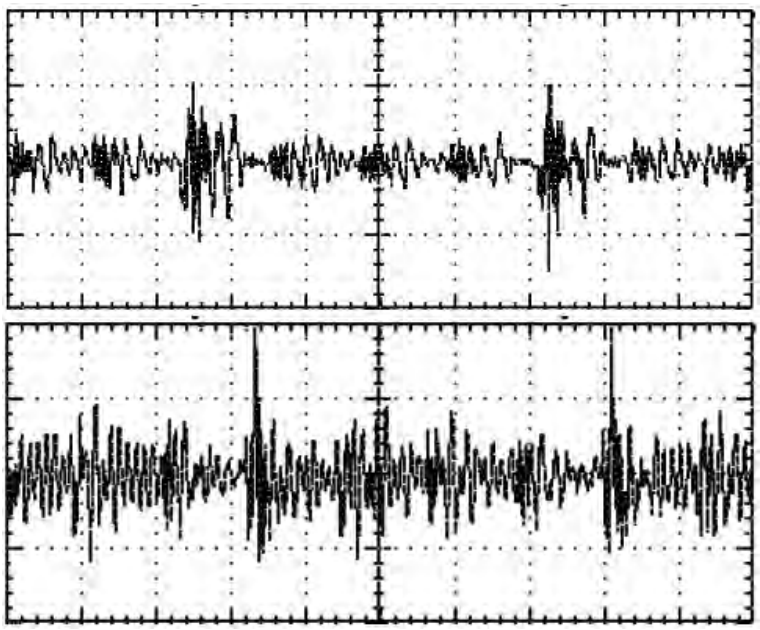

Figure 2.10: Comparison of piezoelectric (top) and accelerometer (bottom) signals at the same engine operating conditions. Time scale 25 ms per division, voltage scale 2 V per division [31].

Kistler [32] and AVL [33] both have a pressure transducers which are able to measure the fuel pressure within the high pressure (HP) injector tube. The transducer fits into a Briden adapter as shown in Figure 2.11. A hole is drilled into the HP tubing before the injector and the Briden adapter seals against the tube, allowing the fuel pressure to be measured at high speed. This system is also susceptible to harmonics, which may be introduced by a fuel pump which is running continually, but it is accurate and less noisy than the strain based measurements because a change in fuel pressure will only occur when fuel actually begins to flow out of the injector and it is directly measuring the physical variable which is changing. Additionally, if a fuel pump is used which can produce static pressures then the only assumption required to determine the start of injection would be the time taken for the fuel pressure pulse to reach the sensor which is negligible. The need to drill into the injector tube is a downside as well as the relatively high cost of such a system which can easily be R40 000.

In a research context however, the ability to measure the dynamic fuel pressure is useful because other properties of the fuel can be deduced using this kind of transducer.

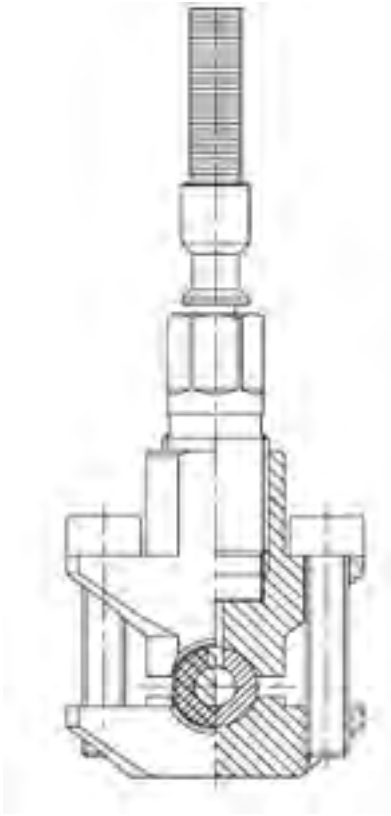

Figure 2.11: Kistler Briden adapter to fit HP tubing [32]

For example, Dernotte et al. [34] made use of such a pressure transducer to determine the time taken for reflected waves to propagate within a length of tube after fuel injection. Given a set length of tube, this allowed the sonic velocity and bulk modulus of the fuels to be determined. The sensor also allowed the fuel mass flow rate out of the injector to be determined and in their work they could deduce injector cavitation by a decrease in the coefficient of discharge of the injector as the fuel pressure was increased.

Szybist and Boehman [35] compared the injection timing performance of three systems namely, high speed photography, injector fuel line pressure and laser beam interference. The high speed photography requires optical access and illumination of the injector tip, which is not practical in this context but the laser beam interference is of interest. This system makes use of a laser beam placed directly in front of the injector tip, perpendicular to the injector's axis and an optical receiver sensitive to the laser's output light frequency. When the fuel is injected, the droplets scatter the laser light, decreasing the intensity of light impinging on the optical receiver and therefore allowing the injection timing to be deduced. Siebers [29] made use of a Helium Neon (HeNe) laser with a photodiode in the same manner as described previously with SANDIA's constant volume combustion chamber. The spray detection was used to trigger high speed photography, and the photography indicated at least that

the spray was detected correctly, based on the position of the spray plume within the vessel at the time when the camera was triggered.

Szybist and Boehman [35] concluded that the laser interference method had comparable accuracy to the pressure based injection detection. Furthermore, their work showed that for an engine with a distributor pump based injection system, the difference in sonic velocity between a biodiesel and petrodiesel blend caused as much as 1 CAD difference in injection timing at 3600 RPM. This indicates the varied effect of fuel composition on engine performance and that at least a minor error is introduced by assuming that the start of injector coil energising is the beginning of fuel flow, even though this example made use of mechanical injection.

Chapter 3

Fuel System and Injection Timing Solution Development

This section describes the fuel system and the associated injection timing sensor solution adopted. These systems are described first, because they constrain the subsequent mechanical and electrical design considerations.

The injector used in this project is a Bosch single hole diesel injector, part number 044 5110 131. It has a 135 μm orifice which was measured by using a microscope. It is not known if the orifice is cylindrical or tapered.

3.1 High Pressure Fuel System

It was desirable to develop a system capable of generating fuel pressures in the range of 400-1800 bar, which is indicative of typical direct injection diesel engine injection pressures and in line with the pressure limits of the fuel rail and injectors which were available for use in this project. The requirements of the fuel system were specified as followed:

- Ability to generate pressures typical of CR Diesel systems (400-1800 bar) accurately, with limited pressure fluctuations or ripples. If there are ripples they must be predictable so that the injection event can be synchronized to correspond to the same pressure value for each combustion cycle.
- Have a sufficiently high fuel flow rate to ensure that the required pressure range can be met despite the combined injector static leakage and injection fuel consumption. Fuel injection is likely to occur only twice per minute and therefore the return flow is the significant flow requirement.
- Ideally require no fuel bypass during periods when no injection events occur.

- Controllable directly with National Instruments components.
- Be able to pump a wide variety of hydrocarbons especially single component fuels which may have low lubricity.
- Require no additional lubricant other than the fuel being pumped unless the required lubricant is isolated from the fuel so as to prevent contamination.
- Be able to generate the required pressure with small fuel volumes i.e. not have a large swept volume due to the high cost of reference fuels.
- Be easy to prime and flush during fuel change over.
- Use connections for which HP piping is readily available.

The following systems were considered as potential solutions:

3.1.1 High Pressure Fuel Pump from an Engine

A previous project at the SAFL adapted a high pressure fuel pump from a 2002 BMW 320D engine. The pump was coupled via a reducing belt drive to a three phase 2.2 kW induction motor as depicted in Figure 3.1.

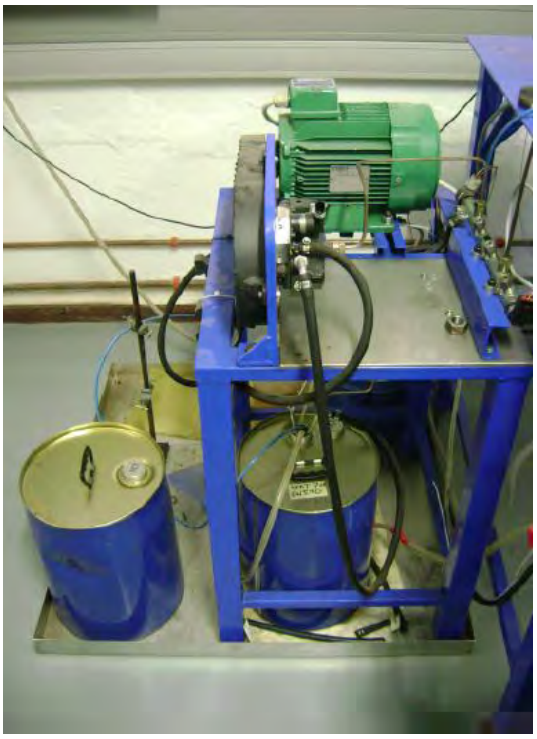

Figure 3.1: Modified high pressure pump stand developed by [36].

Fuel pressure control was provided by making use of a pulse width modulation strategy to control the relief valve of a common rail (CR) attached to the system. While

the pump was able to generate the required fuel pressure, its flow rate far exceeded that required and therefore much of the fuel was bypassed through the CR. The consequence of this is that the fuel needed to be cooled, adding to the volume of the fuel system and additionally requiring more equipment for cooling in the form of a air to liquid heat exchanger and fan.

Fundamentally the pump is intended to convey full boiling range fuels, which conform to strict lubricity requirements e.g. [6]. The reference fuels do not meet these requirements and therefore it is likely that the pump would fail prematurely if operated on these fuels. Also the volume of the HP pump and the low pressure pump required to lift fuel to the high pressure pump's suction would require a relatively large volume of fuel, thereby increasing the cost per test.

3.1.2 Hydraulic Intensifier

The intensifier makes use of a rod with a piston on each end of a different size. The force acting on each respective piston is equal to the product of the pressure and the area and therefore if the area is smaller on one side than the other, the pressure must be higher to achieve a force balance. This pressure ratio allows the pump to generate high discharge liquid pressures by only using laboratory compressed air. A cutaway picture of a "Maximator" air to liquid pump is shown in Figure 3.2.

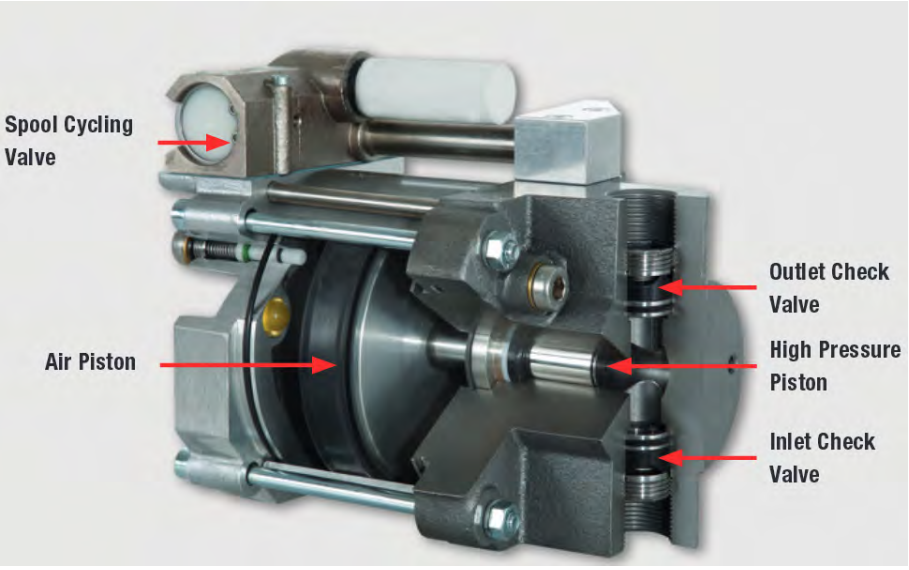

Figure 3.2: Cutaway view of a Maximator hydraulic intensifier [37].

For the required fuel pressure range, Maximator offers a G250 pump [37]. It has a piston area ratio of 265:1 and therefore with the available laboratory compressed air pressure of 8 bar, it can produce a maximum outlet pressure of 2120 bar. The outlet

pressure is controlled by changing the inlet laboratory compressed air pressure via a regulator.

The pump wetted materials are made from stainless steel and it has a liquid swept volume of 3.8cm^3. The pump has Viton® seals which are compatible with the paraffinic reference fuels from a chemical reactivity perspective. Additionally, this version of the pump is intended for water use, and therefore should not be lubricity constrained. Additionally, the pump supplier has a standard range of tubing and fittings rated to 4500 bar. The pump has a flow rate of approximately 0.65 litres/min at an outlet pressure of 2000 bar and additionally has the benefit of being able to stall and hold the outlet pressure, allowing injection to occur with a static CR pressure. This type of pump has been used by other diesel combustion researchers successfully such as Zhu et. al. [38].

3.1.3 Syringe Pump

The syringe pump finds typical use in high pressure liquid chromatography devices where it is used to drive a fluid through a filter bed so that particles can be extracted from the fluid stream. The device is useful in this context because it allows very precise pressure and flow rate control. The pump is a positive displacement type and is usually driven with a cam or a power screw. Certain pump manufacturers, such as Telydyne, allow more than one pump to be controlled via a common interface which allows “constant flow” to be achieved. This is done by making use of a series of check valves on each pump so that one pump has an intake stroke while the other discharges. Figure 3.3 shows the required valve arrangement so that two pumps can be used simultaneously.

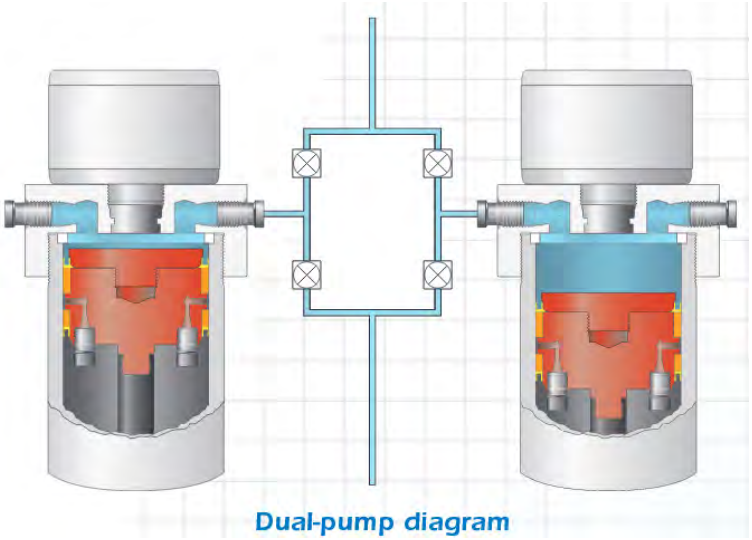

Figure 3.3: Pipe coupling between two Teledyne 65D pumps which allows for continuous flow [39]

The pump(s) can typically be controlled either with its own micro controller or using a computer via a RS 232 port connection. Teledyne pumps come standard with National Instruments software drivers which may make incorporating such a pump into the IQT control system easier. In its normal form the pumps have relatively low liquid storage capacity (70 ml) but it is possible to pipe them so that they can be connected to a larger reservoir. The pumps are designed for use with aggressive chemicals and should therefore be able to pump diesel fuel [39]. The cylinders are made of stainless steel and the piston can be ordered with any of a variety of seal materials so that it can be optimized for this application.

A major issue with this type of pump is that it has relatively low flow rates at elevated pressures. Figure 3.4 below shows the flow rate of an Agilent 1290 pump in comparison to other pumps by the same manufacturer.

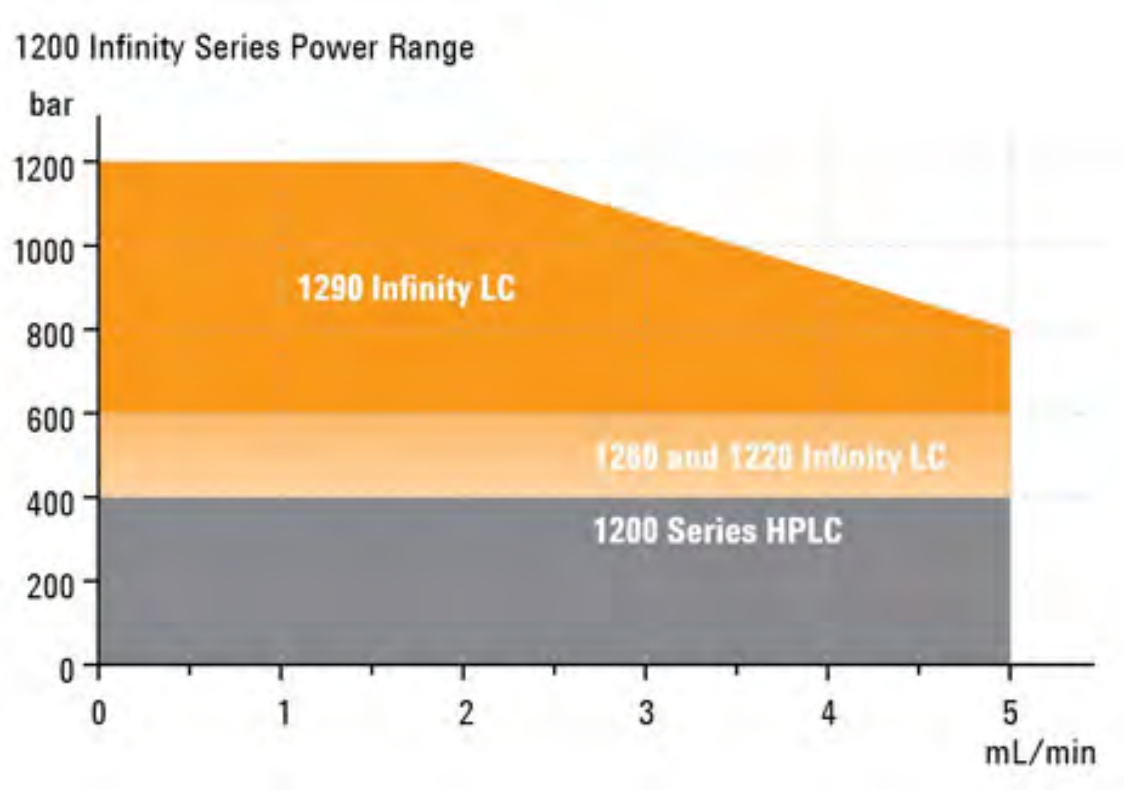

Figure 3.4: Graph indicating different HPLC pumps' discharge pressure dependence on flow rate [40]

It is evident from Figure 3.4 that the typical flow rates achievable with one pump is quite low at elevated pressure. Given the expected cycle time of 25s, one HPLC pump may not be able to meet the combined flow rate required to satisfy injection and static leakage through the injector. Multiple pumps may have worked but they were found to be prohibitively expensive.

Between the three types of pumps previously mentioned, it was decided to procure

the Maximator G250 pump because it offered robust chemical compatibility and has a flow rate high enough to meet the demands of the injection system. The availability of high pressure tubing and fittings from the same supplier simplified procurement and added confidence that the system would work as required. The pump was driven by laboratory compressed air, so it could be controlled by fitting a normally closed solenoid valve before its drive air inlet. As was mentioned previously, the fuel pressure could be controlled via an air pressure regulator on the supply line. The low swept volume of the pump means that fuel flushing can be done with a relatively low volume of fuel.

3.2 Injection Timing Sensor

3.2.1 Diode Laser

While the method of Siebers [29] for fuel spray detection seemed effective, as discussed in Section 2.3, the relatively high cost of the HeNe gas laser (R10 000) discouraged its use. A search of the internet revealed that diode lasers are used to detect sewing thread breakage when it is being spooled. Given that the thread was well below 1 mm in diameter, it was thought that the diode laser could serve the same purpose as the HeNe laser, but at a much lower cost (R90). Another search indicated the availability of a Quarton VLM 635-01 LPA diode laser module locally. The diode module incorporated the diode laser, an aspherical lens and power supply all in a cylindrical brass package as depicted in Figure 3.5. The laser module was constrained to an operating temperature of 40°C and also required a current limiting resistor to ensure that it did not overload.

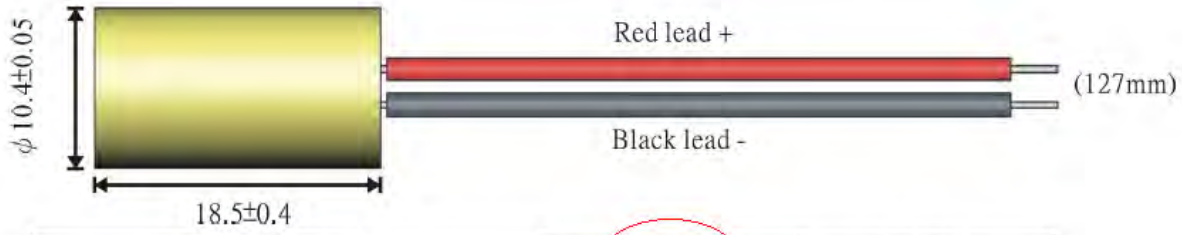

	SPECIFICATIONS	635-01	650-01
1	Operating voltage (Vop)	3~5V	
2	Operating current (Iop)	< 50mA	< 35mA
3	Cw output power (Po)	≦3mW	
4	Wavelength at peak emission (λp)	630~645nm	645~665nm
5	Collimating lens	Aspherical plastic (ø7)	
6	Spot size at 5M	5±1 mm	
7	Divergence	1.0 mrad	
8	Operating temp. range	+10°C ~+40°C	
9	Storage temp. range	-20°C ~+65°C	
10	Housing	Brass	
11	Mean time to failure (MTTF) 25℃	5000hrs	10000hrs

Figure 3.5: Quarton VLM 635-01 LPA diode laser module external form, dimensions and technical specifications

3.2.2 Phototransistor

On the receiver side, it was desirable to have a low cost sensor, which is sized appropriately given the 12mm windows available. The receiver should have a response

time as short as possible and a high signal to noise ratio. Additionally, a small optical acceptance angle was sought because it ensures good coupling with the laser and decreases the quantity of scattered light that will reach and register with the receiver. For these reasons an Optek 803 SL phototransistor was chosen. A phototransistor was chosen, instead of a photodiode like in Siebers [29] case, because the transistor acts to amplify the photodiode's photo-current, thereby increasing the signal to noise ratio and making it easier to measure the response of the transducer.

In terms of the combined performance, the phototransistor had a nonlinear output current with changing incident light wavelength. Therefore the monochromicity of the laser was desirable as it ensured that the phototransistor's output did not vary other than due to injection.

Chapter 4

Mechanical Design

With the fuel system specified, the various components required in order to achieve the project aims needed to be mechanically incorporated.

The combustion chamber of the original IQT was used for this project. It is depicted as a cross section in Figure 4.1. The combustion chamber in its original form had a volume of 0.213 L [4] and was designed according to Canadian pressure vessel requirements [28]. The envisaged changes, depicted and discussed later, were not expected to increase the volume to more than 0.25 L.

The standard charge pressure was 21.37 bar [4], and the rise in pressure due to combustion was not expected to be more than 20 bar based on the estimated mass of fuel than can be injected with the single hole injectors available for use in this project [41]. Additionally, a relief valve was fitted so that the pressure does not exceed the approximately 42 bar total pressure.

Based on a design pressure of 42 bar and with the aforementioned volume, the vessel conformed to "Sound Engineering Practice" according to SANS 347 [42] and therefore did not require professional assessment. In comparison, the original device had a peak total pressure of approximately 80 bar [25] and therefore the combustion chamber will be operated well within its tolerable pressure. Additionally, it was found that under the conditions considered in this project, the maximum pressure during testing was found to be 26 bar, which indicates that the device operated well within its limits.

The original end cap, which holds the injector, and the pressure transducer housing, were not suitable for the components used in this project and hence were redesigned.

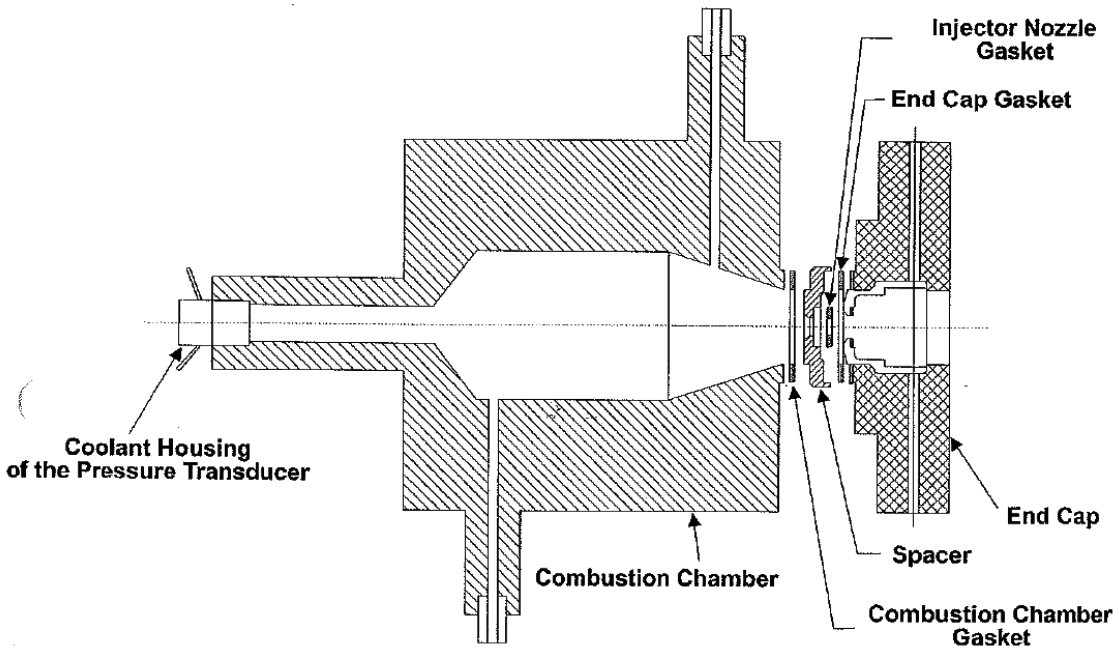

Figure 4.1: Cross section of the IQT's combustion chamber, indicating original configuration [28]

4.1 Injector Mounting and Sealing

Initially the injector was designed to be mounted as depicted in Figure 4.2.

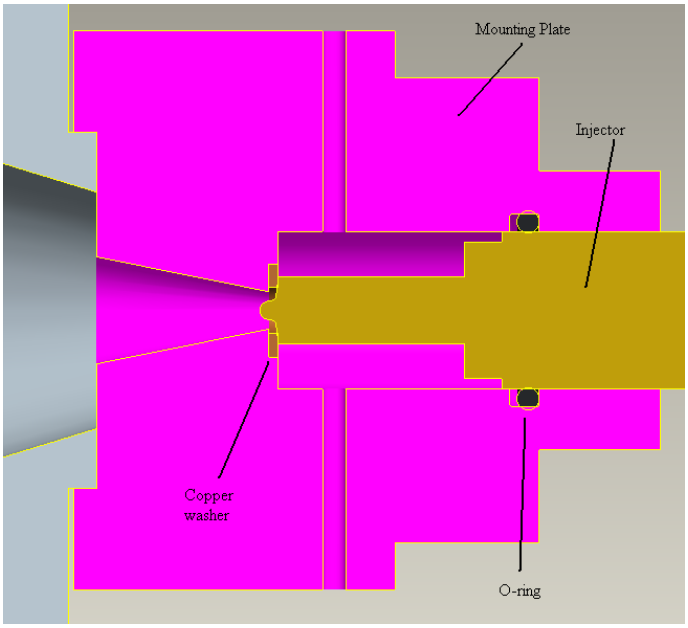

Figure 4.2: 1st injector mounting configuration.

It became apparent during manufacturing that the conical volume in front of the injector tip would likely pool cooler gas, potentially resulting in spray and auto-ignition characteristics which were not representative of the bulk temperature within the combustion chamber. This led to the first modification as depicted in Figure 4.3. This design was thought to be better as the gas was not as restricted as before. Also, the injector tip was now 7 mm from the edge of the combustion chamber, decreasing the effect of the injector's cooling on the gas into which the spray was first introduced.

After performing preliminary tests it became apparent that the copper washer used to seal the injector tip was succumbing to low strain rate plastic deformation (creep). This caused gas to ingress into the coolant system as well as sporadically causing coolant to leak into the combustion chamber in small quantities. The problem was narrowed down to the size of the copper washer. It was deliberately chosen to be narrow (6 mm inside diameter, 7 mm outside diameter) so that it would take a low clamping force to plastically deform it and seal the injector without damaging its tip. The myopia was that the clamping force needed to keep the joint together was difficult to control, due to friction between the injector and the o-ring (indicated in black). This resulted in the copper washer load being higher than necessary to yield the washer and therefore the actual stress on the washer when the injector was installed was far in excess of the yield strength of the material, making it highly susceptible to creep. This design was therefore also unacceptable and it was again modified.

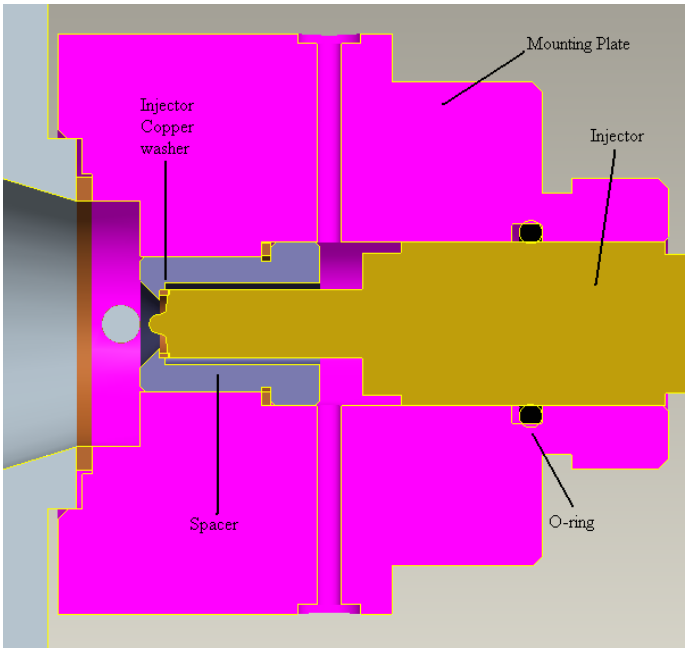

Figure 4.3: 2nd injector mounting design. The housing depicted in Figure 4.2 was re-machined and threaded to incorporate the purple spacer indicated in this figure.

Figure 4.4 indicates the final injector mounting configuration. The injector housing was once again machined, this time to incorporate an indirect cooling jacket for the

injector tip. The injector was sealed on its shoulder, using a much wider OEM copper washer. The cooling jacket was suitably sized to provide a sliding fit with the injector tip, and a high performance heat paste, Deepcool Z9®, was forced into the annular space between the injector tip and the cooling jacket bore to promote cooling. The cooling jacket was welded into the housing on the front side, providing the gas seal. This configuration has proved successful, providing adequate sealing while still providing optical access to the injector tip for spray detection.

However, the injector tip temperature is still of concern. In an earlier mechanical configuration as depicted in Figure 4.3 a thermocouple was placed through a port into the counterbore where the injector tip is positioned. It indicated a gas temperature of 580 K with a set-point combustion chamber surface temperature of 848 K, which is half way between the two conditions used in this work. The temperature gradients were expected to be steep in this region of the combustion chamber, given the proximity of the thermocouple to the walls. However, this temperature was quite high and may have contributed to the generally much shorter ignition delays found in this work, as will be shown later in Chapter 9, due to excessive heating of the fuel prior to injection.

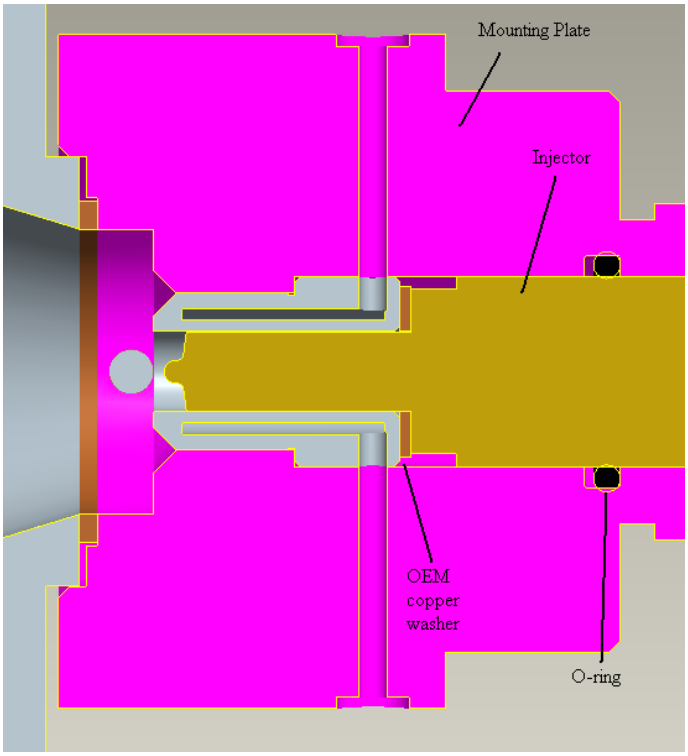

Figure 4.4: Final injector mounting configuration. The injector cooling jacket (Grey) was separately manufactured and then welded in place in the vee-shape produced by the chamfers.

4.2 Optical Fittings

The spray detection system required optical access. A previous project at the SAFL had remnant 10 mm diameter quartz windows, 10mm long which were used as the basis of the optical fittings. The initial optical housing designs are depicted in Figure 4.5 and would screw into the injector housing depicted in pink in Figure 4.4. The diode laser and photodiode had maximum operating temperatures of 40 and 100 ºC respectively and therefore the fittings were provided with a cooling jacket to modulate their temperatures.

This design made use of a unique threaded parts for the emitter and receiver, which thrusted against the quartz windows when tightened. The quartz windows had copper washers on both sides and it was thought that due to the high compressive strength of the quartz, the threaded parts could be tightened sufficiently to yield the copper washers and therefore effect a seal. However, it was found that the windows cracked when tightened, typically off the centre line of the windows and emanating from a localized point on the surface.

It was thought that the cracking was due to a stress concentration. The stress concentration may have been due to play in the thread, causing the thrusted part to push unevenly on the copper washer, or the window's seat and the window's face not being parallel with one another. In an attempt to remedy this, the thrusting copper washer was replaced with a fibre gasket, in the hope that its additional compliance would prevent the stress concentration. This helped to some extent, as the fitting could be tightened further, but the inside face (gas side) of the windows still cracked. Next, fibre washers were tried on both the inside and outside. This allowed the joint to be tightened down well, but the gasket leaked too much.

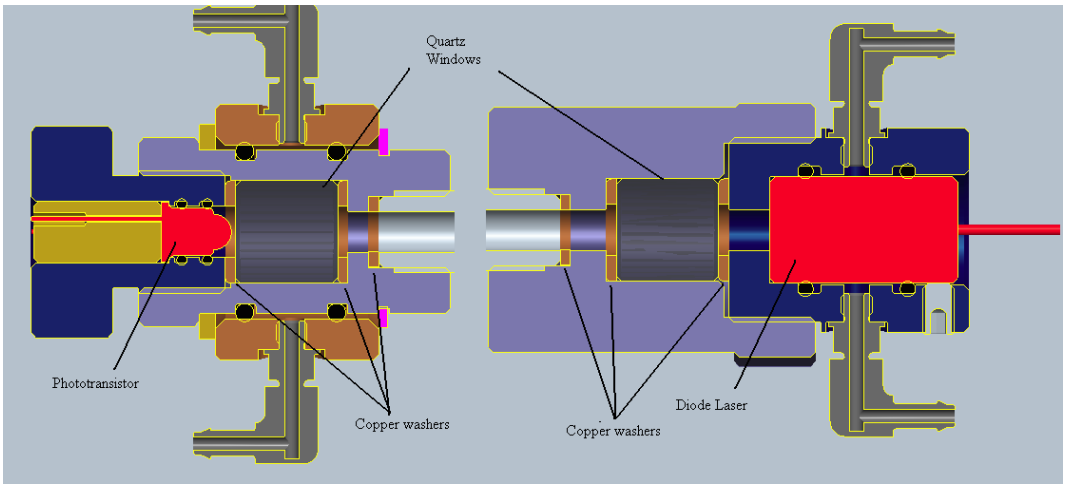

Figure 4.5: First optical receiver (left) and optical emitter (right) design

These trials led to a second sight glass holder design, as depicted in Figure 4.6. In

this design, the windows were held in a separately threaded part and sealed using a radially mounted Viton® o-ring. This design allowed for easy sealing of the windows, but had the limitation that the housing had to be cooled as the possibility of overheating the seals existed. Therefore a sleeve was designed to fit over the housing, such that coolant could be pumped between it and the housing. The quartz windows used in this design had a 12 mm diameter instead of the 10 mm diameter used for the previous iteration.

An additional benefit of this design was that it allowed the windows to be removed without stopping the coolant flow, as required in the previous design. This meant that if soot collected on the windows, they could be removed and cleaned as required. This sub-assembly was used on both the emitter and receiver side of the injector mounting and a suitable Teflon® guide was made for the receiver such that it could be press fitted into the window holder (orange.)

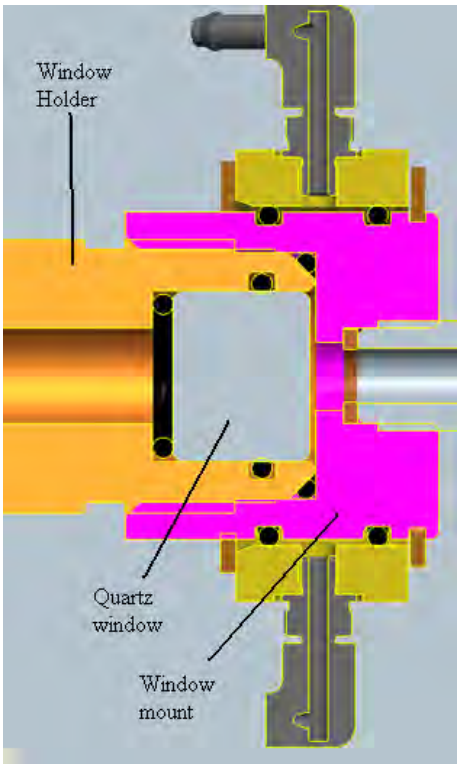

Figure 4.6: Second sight glass housing design.

4.3 Pressure Transducer Fitting

A Kistler 6121 piezoelectric pressure transducer was available for use with this project. The pressure transducer had no housing, so one was designed and manufactured as depicted in Figure 4.7. The pressure transducer was installed into a tee, also made in the course of this project, which allowed the fitment of another optical fitting with

a 7 mm aperture. This allowed optical access along the injector's axis, thereby allowing the auto-ignition/diffusion flame to be optically detected. While not one of the project's main objectives, it added functionality to the device which may be exploitable in a later project.

In this case a Honeywell 5620 optoschmitt detector was installed in the fitting. The detector responds to light with a wavelength of between 400-1100 nm and provides a digital output signal when the irradiance exceeds 0.25 mW/cm^2. The detector was unfortunately not uniformly sensitive to all wavelengths of light in the mentioned range and its relative sensitivity also changed with temperature. Similarly, the pressure transducer could also be sensitive to temperature and therefore the tee as well as the pressure transducer were water cooled.

Typically, fitment of a pressure transducer at the end of a long port is ill-advised [43] because the port can resonate adding cyclic pressure fluctuations to the measurement . However, in its original form, the IQT has the pressure transducer at the end of a long port. This already causes significant ringing to manifest as noted by [25, 24]. Since auto-ignition was of prime interest to this project, the ringing which may have occurred during combustion was not deemed to be an impediment and therefore the mounting of the pressure transducer in the manner shown was thought to be acceptable.

It has been noted by Lillo et al.[44] that auto-ignition is spatially variable and therefore there is a time delay between auto-ignition and the increase in pressure reaching the transducer. The flame detector therefore added another means to detect auto-ignition, provided that the reactions emit light in the required frequency with sufficient intensity.

An assembly drawing of the modified IQT and the various component drawings developed in this project can be found in Appendix E. Also shown is a photo of the rig as it was constructed.

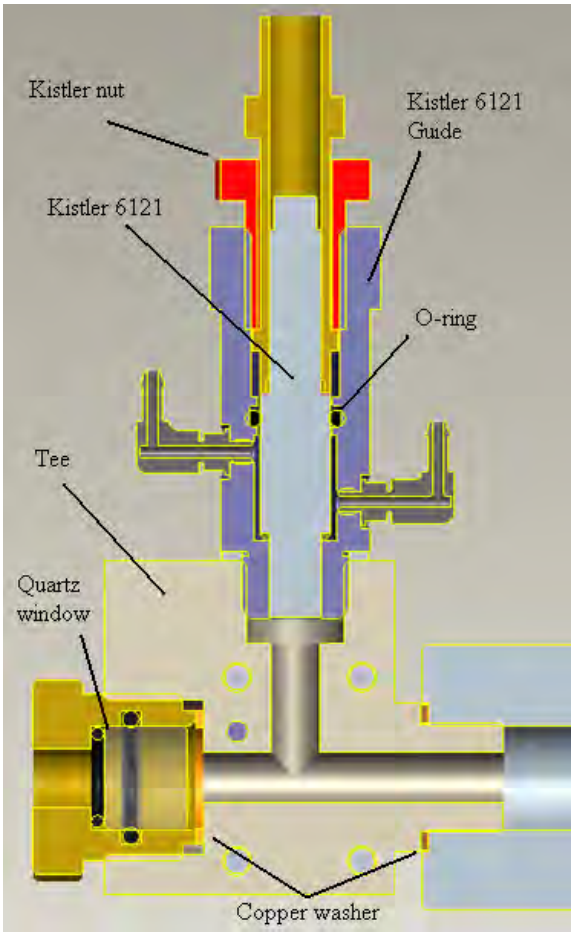

Figure 4.7: Pressure transducer tee. Window allows optical access along the injector's axis.

4.4 Gas and Coolant Flow Diagram

Various fluids were required for the system to operate and therefore suitable tubing/piping networks were developed. The gas and fuel system are depicted in Figure 4.8 while the coolant system is shown in Figure 4.9.

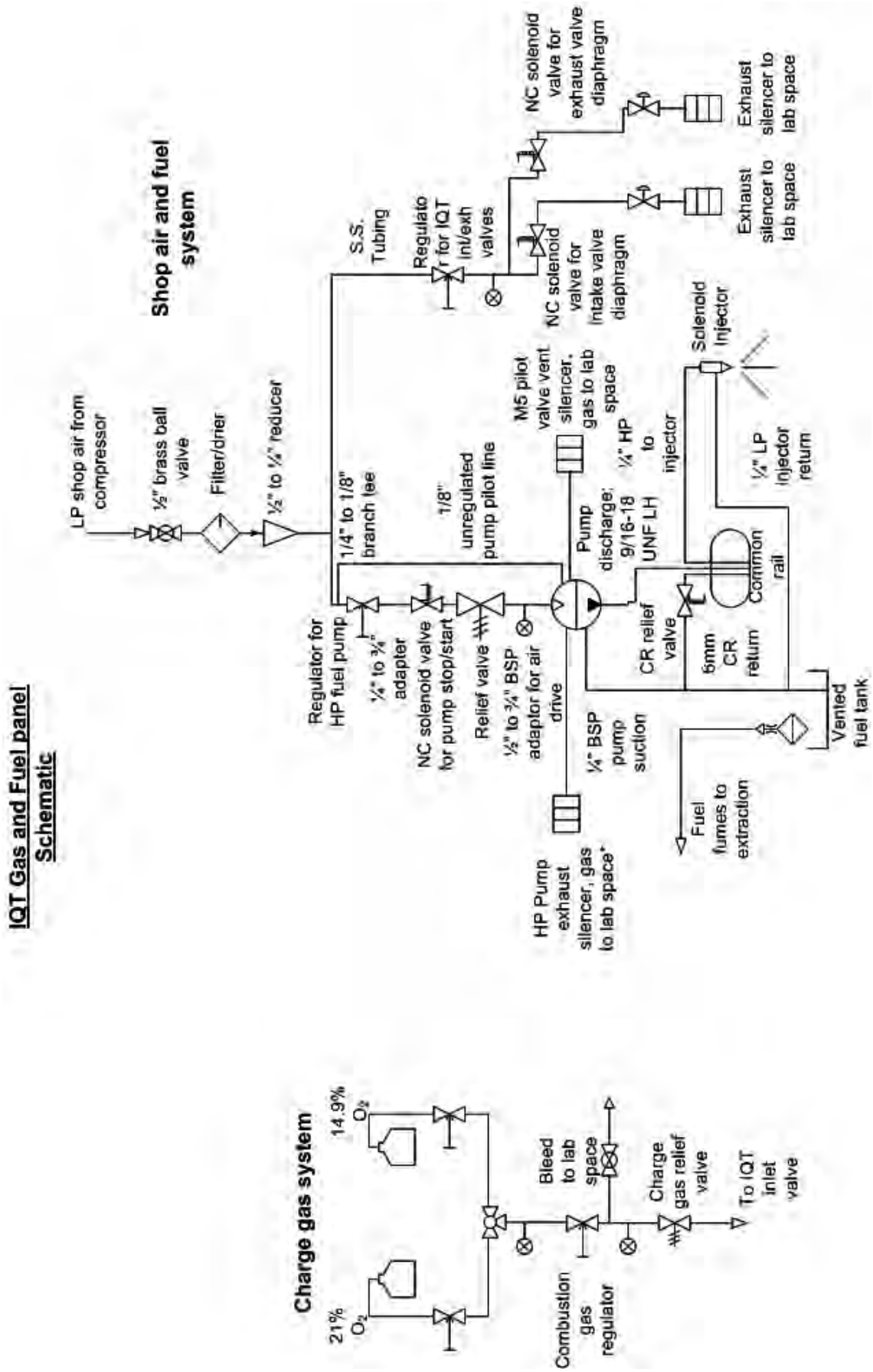

Figure 4.8: IQT gas and fuel schematic

A 50/50% mixture of ethylene glycol based engine coolant and distilled water were used as the cooling medium. The system featured a 50 W single phase centrifugal pump to circulate the coolant while a tube/fin heat exchanger with a 100 W centrifugal fan allowed the heat to be rejected to the lab space. The pump, fan and heat exchanger were fitted to the device's trolley while the gas equipment was fitted onto a panel which was then mounted onto a wall adjacent to where the rig was operated from.

The combustion chamber took approximately 3 hours to cool down. As a precaution, the coolant system was powered by an UPS so that if there was a power failure the critical components were still cooled.

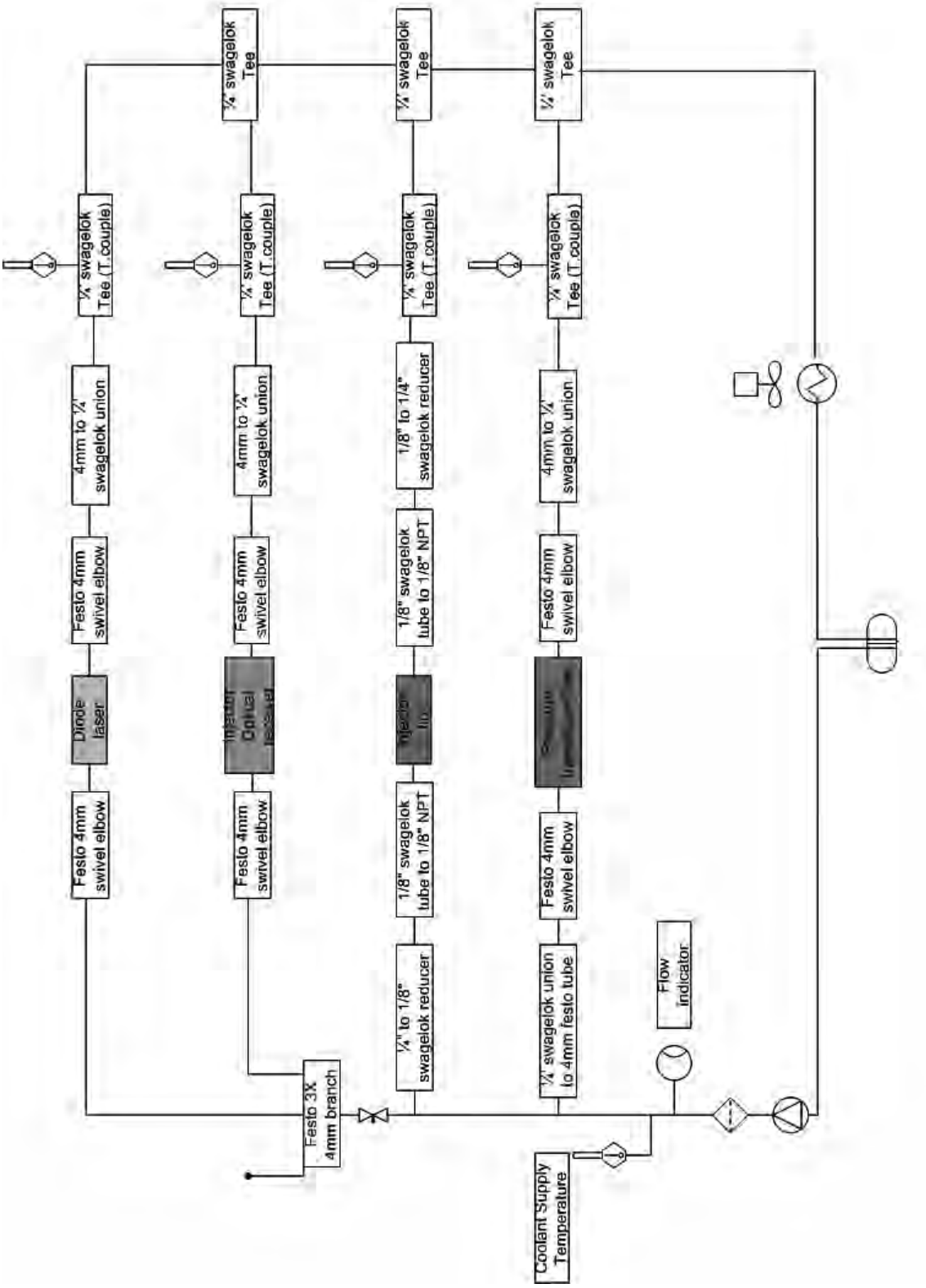

Figure 4.9: Coolant flow schematic

The combustion exhaust gases were piped to the outside of the building where they were expelled to the atmosphere.

Chapter 5

Electrical Design

A new electrical distribution box was developed in this project to power and control the components comprising the IQT. A completely new system was developed because much of the system envisaged differed significantly from the original device and therefore many new components needed to be added, requiring more space. Also, by leaving the original electrical cabinet intact, the possibility of returning the device to its original configuration remains.

5.1 Control System

The new electrical box housed a National Instruments (NI) CompactRIO 9012 Real-time controller with 8 slot chassis (NI 9112). The chassis incorporated a 40 MHz reconfigurable Field Programmable Gate Array (FPGA), which allowed synchronisation of measurements to a 25 nanosecond time scale and the chassis' 8 slots were filled with various National Instruments modules as indicated in Figure 5.1. The FPGA and the respective modules served as the interface between the higher level Real-time controller (RTC) and the various sensors and actuators, indicated in Figure 5.1 which the system was comprised of. The FPGA features fixed logic, which means it is capable of truly parallel processing, making it ideal for this application where multiple signals were measured simultaneously at high speed. The chassis connected to the Real-Time Controller via a PCI bus and the Real-Time controller connected to the host Windows based PC via an Ethernet cable. The Real-time controller was capable of performing floating point math and through its dedicated operating system it offered high reliability and confidence that operation would not be interrupted by other tasks, as could be the case when using a conventional Windows based PC system. Figure 5.1 indicates a schematic of the NI hardware.

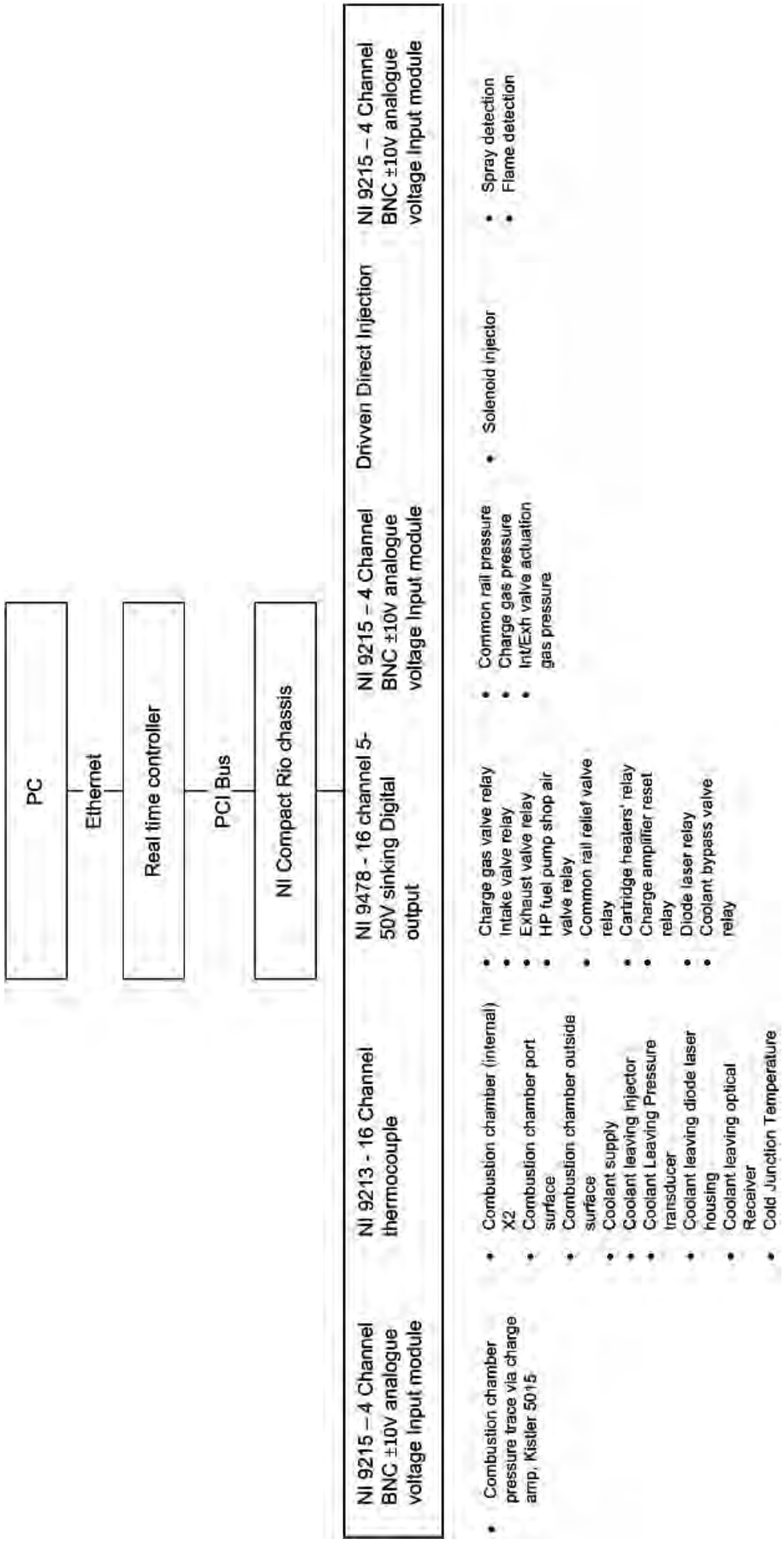

Figure 5.1: IQT control schematic

The National Instruments hardware was complemented by the Labview software. The software makes use of graphic based programming, where icons represent the various components of the system and data flow occurred via wires which were drawn between the respective components. Labview features a number of built in functions, ranging from simple arithmetic to high level filters and statistical functions. These standard functions, together with the ones added by the user, were used to develop so called virtual instruments (VIs). The virtual instrument model allowed sections of code to be combined into a stand alone routine, which could then be added to a higher level virtual instrument, thereby allowing the control system to built up from smaller sections of code. For this project three high level VIs were developed, one each for the FPGA, RTC and host PC respectively.

The FPGA interfaced with the modules and triggered the fuel injection and high speed measurements. It also took the low speed measurements such as the actuator pressure and temperature measurements. This data was transferred to the RTC in raw, fixed point data format, where it was converted to engineering units as required and sent via Ethernet to the host Windows based PC. The RTC VI also provided temperature control via a PID system for the combustion chambers heaters. The host PC performed the data logging function and also displayed the various measurements in a graphic user interface (GUI) as shown in Figure 5.2, so that the user could control and monitor the device's operation.

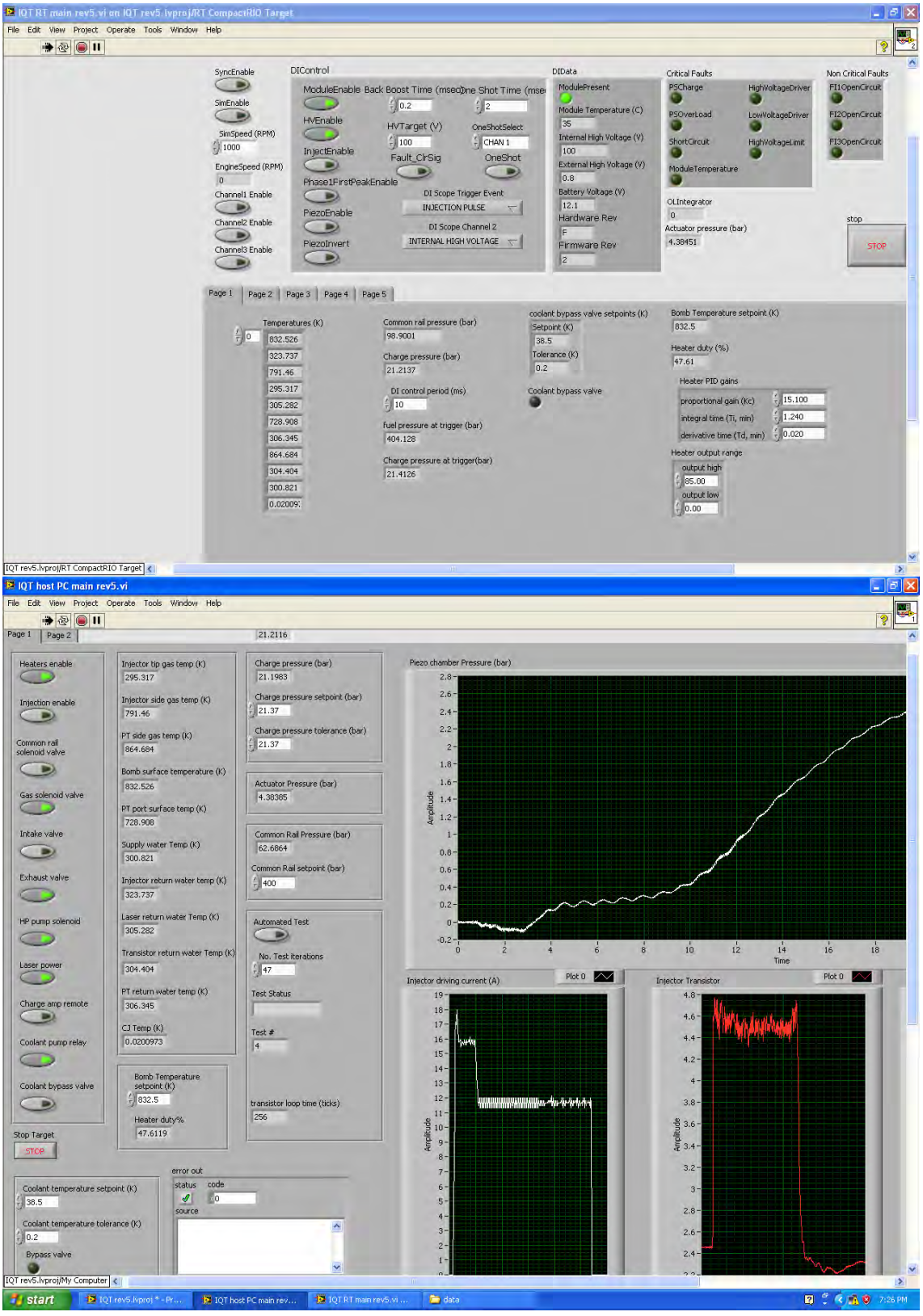

Figure 5.2: IQT Labview GUI. The top figure shows the real time controller and the bottom shows the host PC interface.

The host VI features both manual and automated control of the system. Each subsystem, such as the intake valve, could be manually actuated as required or an automated test can be initiated and the software will perform all steps necessary to complete it. Subsequent to a test, the data was processed using an Excel macro to arrive at the required DCN of the sample. With the new control system, the test conditions shown in Table 5.1 are possible.

The fuel and charge gas pressure were set by adjusting the relevant gas regulator. The control system monitored the pressures and if the charge gas pressure exceeded a specified maximum, the test would be stopped. Excessive fuel pressures were prevented by installing a relief valve in the HP pump's supply air line. The relief valve was sized so that even if the regulator pressure was set too high, the actual pump driving pressure would remain at a safe level, preventing the fuel rail and injector from being overloaded.

Additional information pertaining to the Labview code is shown in Appendix C.

Variable	Control Range
Combustion chamber surface temperature	Ambient - 865 K
Charge gas pressure	0-21.37 bar
Fuel pressure	0-1800 bar
Injection duration	0-5 ms

Table 5.1: Achievable variable ranges with new control system

5.2 Optical Circuit

The schematic of the circuitry required to control the optical components is depicted in Figure 5.3. The circuit comprised of three resistors which limited the current drawn by each component. At the start of each automated test, power was provided to the circuit via a relay and a 5 V power supply.

The diode laser shined onto the photodiode of the photo transistor. The photodiode converted the incident light into a photo-current, which provided the base current for the transistor. This caused the transistor to conduct and current flowed through *R2*, causing a voltage drop across *R2*, which is measured at *Vo1*. When fuel injection occurred the light intensity reaching the phototransistor decreased, due to light scattering by the fuel, which decreased the photo-current and hence the collector current of the transistor. This in turn resulted in a lower current through *R2* and the voltage at *Vo* increased. The change in voltage was used as an indication that injection had occurred.

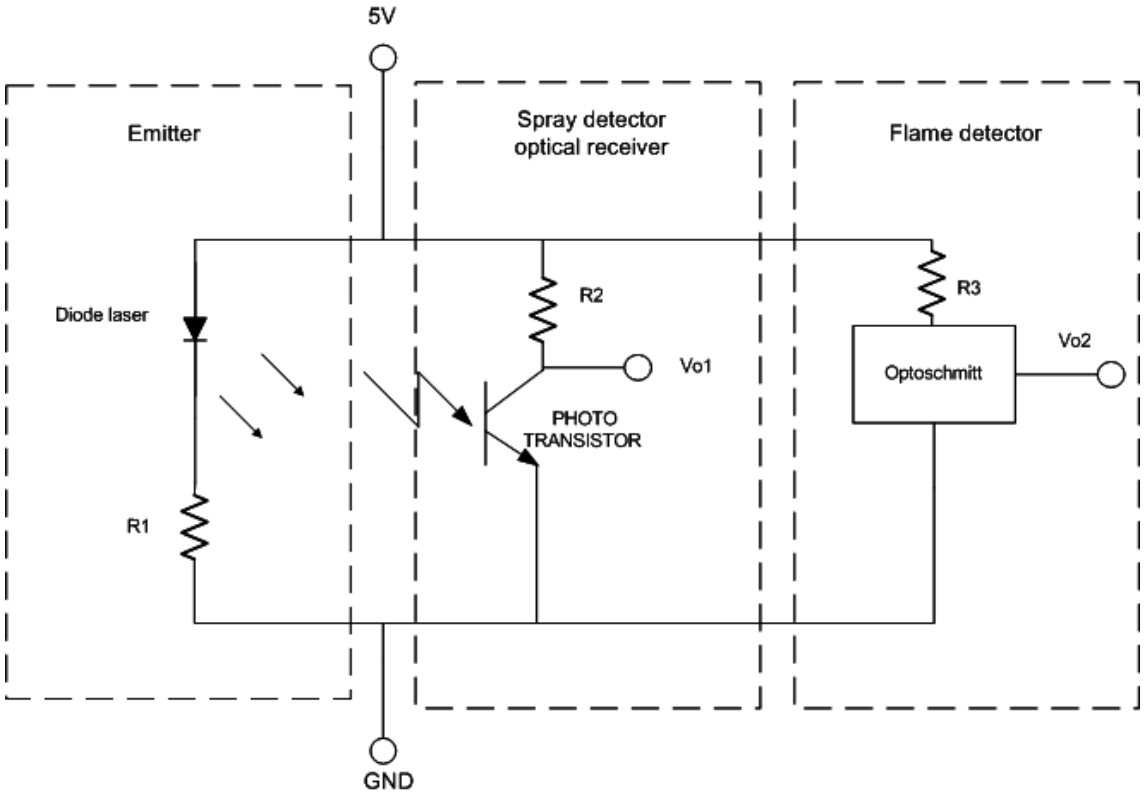

Figure 5.3: Circuit made to control sensors developed in this project

With respect to the flame detector, Figure 5.4 indicates a schematic of the Optoschmitt detector. The *Vcc* and *GND* terminals were connected to the 5 V and circuit ground as depicted in Figure 5.3. The photodiode is on the left of Figure 5.4. Normally the photodiode was not illuminated and does not conduct, which resulted in the amplifier seeing the *Vcc* voltage across its terminals. The amplifier greatly increased the magnitude of the voltage difference across its terminals and therefore its output saturated towards the supply voltage. The Schmitt trigger was supplied with the saturated voltage and emitted its own (positive) saturated voltage, which biased the transistor causing it to conduct. When the transistor conducted its collector voltage fell due to the voltage drop across the 10 kΩ resistor and *Vo* in Figure 5.4 registered the forward voltage of the transistor (typically 0.3 V).

However, when the fuel reacted and emitted light, the photodiode conducted, causing a current to flow and lowering the voltage across the amplifier's terminals. The Schmitt trigger provided noise isolation in that it would not switch output signals as long as the variation in the input signal did not exceed a certain magnitude called its hysteresis. The hysteresis in this context was a fixed quantity for each sensor, but it varies with manufacturing. For this sensor the hysteresis had a magnitude somewhere between 5-30% of the turn-on threshold irradiance of 0.25 mW/cm^2. If the change in illumination exceeded the hysteresis of the Schmitt trigger, it would switch to the negative saturated voltage (*GND*) and the transistor would not be bi-

ased. Therefore *Vo* registered the *Vcc* voltage because no current flowed through the 10 kΩ resistor. The Optoschmitt had a propagation delay of 2.5 μs at 40ºC, while its output was sampled by the CRIO every 6.4 μs, implying that it did not constrain the measurement.

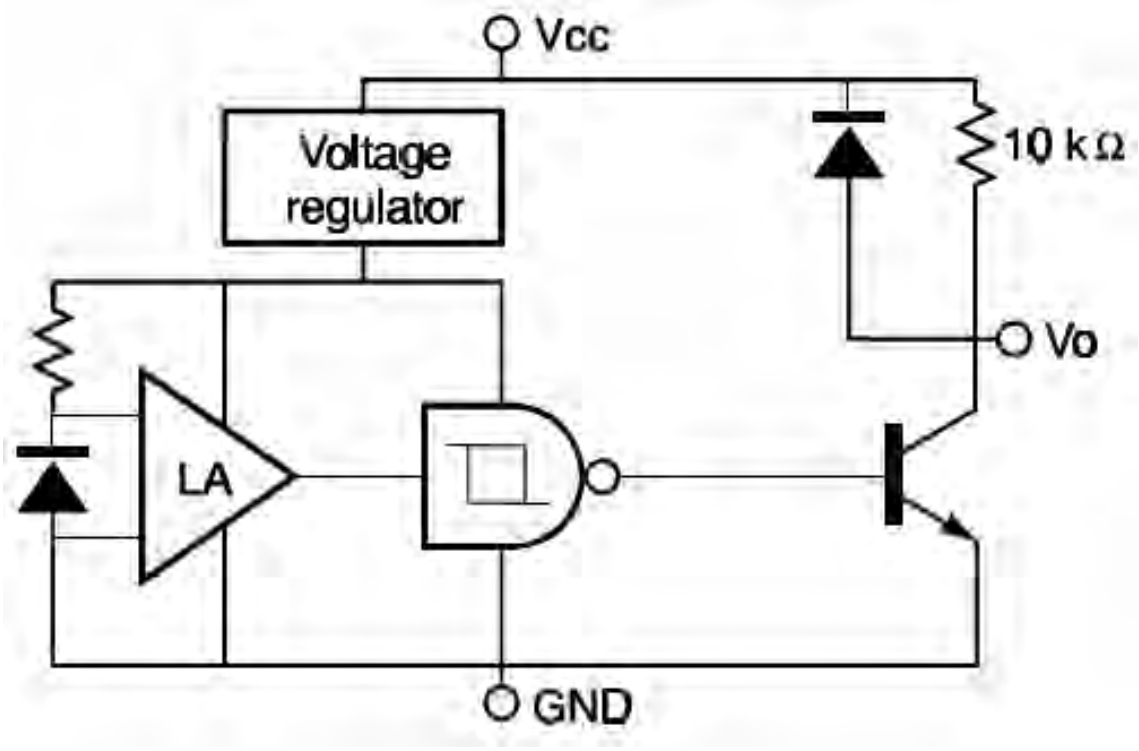

Figure 5.4: Circuit diagram of the Optoschmitt detector used as flame detector [45]

The hysteresis also worked in the opposite sense in that the Schmitt trigger would not bias the transistor until the ambient light decreased by an amount equal to its hysteresis. Therefore the flame detector not only indicated the start of luminous reactions but also provided some indication of how long they last above a certain threshold.

Chapter 6

Experimental Procedure

All of the tests presented were done in the following way:

The experimental procedure can be understood by referring to Figure 6.1. The coolant system was switched on by loading its uninterrupted power supply (UPS). The flow indicator behind the base unit was checked to see that the coolant was flowing. The combustion chamber surface temperature was set to the desired set-point and when it reaches the set-point a leak test was performed.

The leak test was performed by closing the exhaust valve, filling the combustion chamber with the charge gas and then closing the intake valve. The charge amplifier was set to “DC-Long” operating mode and the pressure decrease over a 20 second period was noted. In accordance with [4], if the leak rate was less than 3.5 KPa/s, with a starting pressure of 21.37 bar, the device was considered ready for testing.

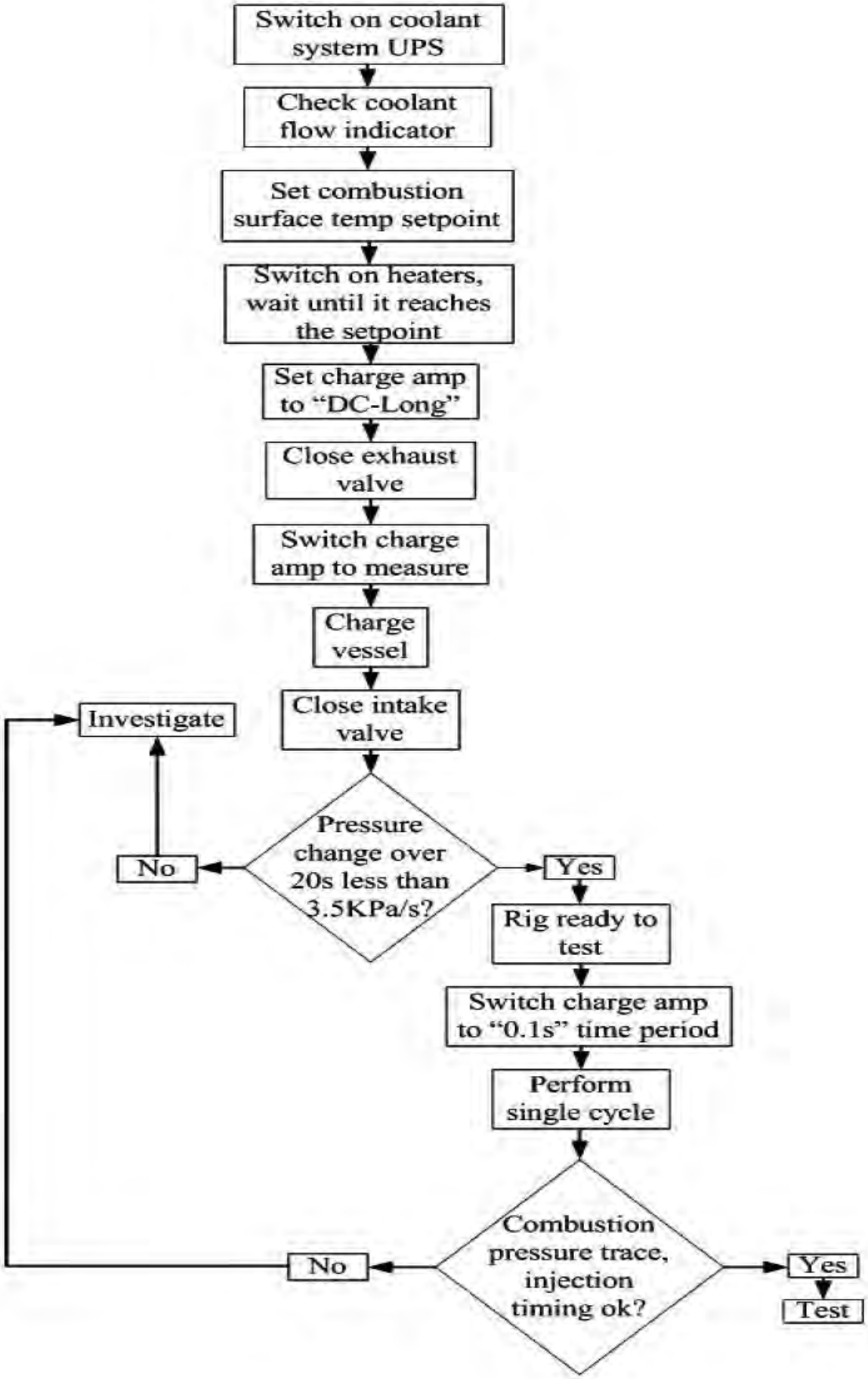

Figure 6.1: Experimental procedure used in this project.

If a fuel change was required, the HP pump suction and CR return line from the fuel reservoir were drained by opening and raising their ends so that the fuel drained back into the reservoir. The old fuel was discarded and the new sample was poured into the reservoir after it had been cleaned. The top port of the fuel rail was opened by loosening the clamping screw and after placing a rag at the bleed port, the HP pump was cycled until approximately 20 ml of the new fuel was displaced out of the open fuel rail port, ostensibly flushing the top part of the CR and the HP tube from the HP pump to the fuel rail. The port was then closed by tightening the clamping screw and the HP pump was run for a few minutes to mix and dilute the fuel remaining in the system. After this the combustion chamber was pressurized with the charge gas and five injections were manually performed to clear the injector. The combustion products were vented and the five injections were repeated three more times. The HP pump was again run for a few minutes to flush the remnants of the previous fuel out of the injector return line. The fuel in the reservoir was removed and the fuel swap thus far described was performed two more times. After this, the new fuel sample was considered to have removed/diluted the previous sample sufficiently well that its effect on the ignition delay could be considered negligible.

N-heptane was used to calibrate the device, as will be discussed in Section 8.6. It was found that at each calibration check, which often occured after other fuels were tested, good agreement between the n-heptane results occured. Therefore, despite the changes indicated in the aformentioned section, the flushing sequence described was considered to be effective.

A single automated cycle was performed to ensure that all of the components were working correctly and that the laser was correctly aligned. If all was well, a larger number of cycles, typically 47, was set and the automated test was initiated. Sporadic adjustments to the fuel and charge gas regulators were performed if they appeared to be drifting too far from the desired set point at the operators discretion.

On completion of the test, the GUI prompted the user to enter a name for the file with a standard Windows® save dialog box. Subsequent to this, the data was processed using a Microsoft Excel® macro. The macro calculated and collated all of the data for the test so that it can be reviewed by the user.

Savage [16] performed stoichiometric auto-ignition studies with the IQT using gasoline fuel samples. He found that 1 gas filling/purging cycle between tests was sufficient to remove all of the exhaust gas from the system. Therefore his purging process was used in this work.

Chapter 7

Experimental Measurement Uncertainties

Various measurements were taken during the course of each experimental cycle. The uncertainty of each measurement was estimated in this section so that the accuracy and repeatability of the DCN correlation could be determined and sources of DCN variation could be established. It has also been shown previously in Section 2.2 that the ignition delay was sensitive to a number of variables and therefore the accurate measurement and estimation of their respective uncertainties was of importance if the ignition delay data is used for more fundamental tasks such as validation of auto-ignition modeling for e.g. [23].

7.1 Temperature

The temperature measurements were performed with a NI 9213 module and $\frac{1}{8}$" shield diameter, K-type thermocouples. The module could be operated in a high speed or high resolution mode, with an increase in speed causing a decrease in accuracy [46]. The sampling rate was dependent on the number of channels used and in this instance it was limited to 1.5 Hz. All sources of uncertainty pertaining to the module were provided by NI, while NIST provided an indication of the polynomial uncertainty which was used in the conversion from voltage to temperature as well as for the inverse operation.

The temperatures were logged in degrees kelvin and hence must be converted back into volts so that the uncertainty could be determined. The total uncertainty in volts (excluding the thermocouple) can be expressed by [46]:

$$Module\,uncertainty = gain\,error + offset\,error + input\,noise + common\,mode\,voltage + cold\,junction\,uncertainty + polynomial\,accuracy \quad (7.1)$$

Table 7.1 provides an indication of the value of each respective uncertainty in Equation 7.1 when operating the module in high resolution mode. The afformentioned equation conflates uncertainty with measurment error. This is atypical, and therefore it would seem the value calculated considers both the measurement error and uncertainty combined.

Uncertainty	Value
Gain error	0.07%
Offset error	4 μV
input noise	200 nV
common mode voltage	0 V
Cold junction (CJ) compensation	0.8 K typical
polynomial accuracy	± 0.05 K

Table 7.1: NI 9213 uncertainty components[47]

The uncertainty contribution of the respective thermocouples must also be added to equation 7.1 to arrive at a final estimate of the uncertainty of each measurement. The two thermocouples used within the combustion chamber, labeled injector side and pressure transducer side gas temperature respectively, were checked against the melting point of water at sea level and found to give readings of 0.0 ºC and 0.3 ºC respectively. The brand of thermocouple used was not known but Omega, a thermocouple manufacturer estimate that their K-type thermocouples have an uncertainty of 2.2 ºC or 0.75%, whichever is larger, over the range of interest. As an indication of the calculated uncertainty, Table 7.2 shows the average temperatures for a test performed at 865.5 K set-point and the associated temperature uncertainty of the combined measurement chain for each measurement. The position of the high temperature thermocouples are shown in Figure 7.1. The low temperature i.e. coolant temperatures were on the return lines of the respective fittings.

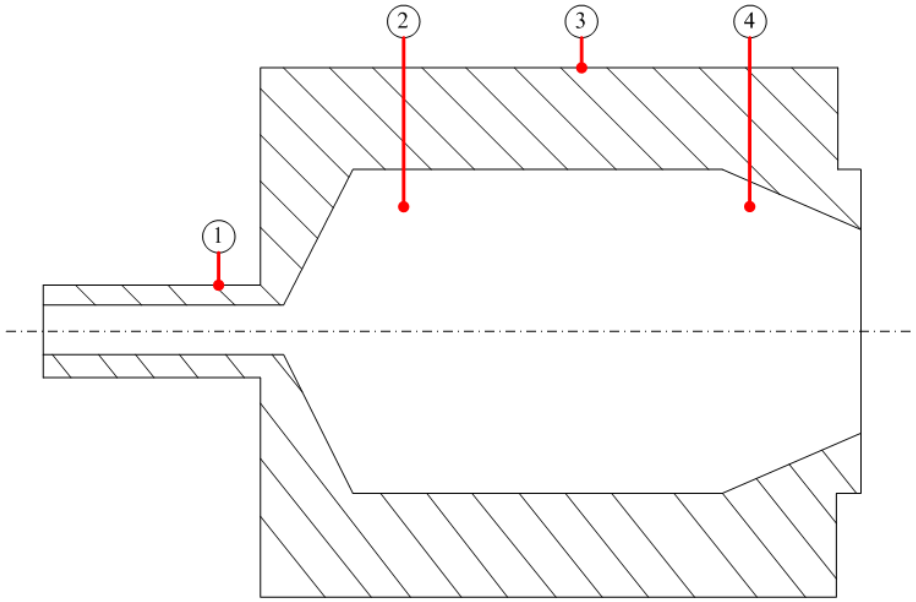

Figure 7.1: Position of the high temperature thermocouples relative to the combustion chamber.

Item	Average Temperature (K)	Calculated Module Uncertainty (± K)	Calculated Measurement Chain Uncertainty (± K)
Combustion Chamber surface	865.4	0.95	4.54
Injector coolant return	326.6	0.81	2.34
Injector side gas	819.0	0.93	4.20
Laser coolant return	307.6	0.81	2.34
PT port surface	758.8	0.9	3.75
Pressure transducer coolant return	307.8	0.81	2.34
PT side gas temperature	894.8	0.96	4.76
Spray transistor coolant return	305.8	0.81	2.34
Coolant supply	302.0	0.81	2.34

Table 7.2: Calculated NI 9213 module uncertainties for a test performed at a set-point temperature of 865.5 K (PRF 25 and 14.9% O_2). The measurement chain error combines both the module error with the thermocouple error.

The NI 9213 module's calibration was checked using a Fluke 741B process calibrator. The calibrator outputs a voltage equal to the temperature specified by the user, for a K-type thermocouple. The results of the calibration are shown in Figure 7.2 for the high temperatures and Figure 7.3 for the low temperatures respectively. It was apparent that the measurement error was lower for the high temperature channels when compared with those of the lower temperatures. This may be due to the relatively larger signal to noise ratio of the high temperature measurements when compared to the low temperatures, which were nearer to the cold junction (CJ) temperature and therefore have outputs which were smaller in magnitude.

In each respective figure, the temperature error accross channels should ideally be the same because the calibrator and module have different CJ temperatures. In comparison to the calculated uncertainty, it was clear that the cold junction temperature had the dominant effect on the module error across all channels, because its contribution was a large fraction of the total calculated module uncertainty. The module only had 1 CJ and therefore there may have been a temperature gradient between it and the respective channels of the module which may have contributed to the variation in the measured errors between different channels as depicted.

It was also apparent in Table 7.1, that the thermocouple accuracy was the major source of uncertainty in the respective temperature measurements if one compares the measurement chain uncertainty with the module uncertainty. The consequence of these measurement uncertainties and errors will be considered in the context of the ID data in Chapter 10.2.

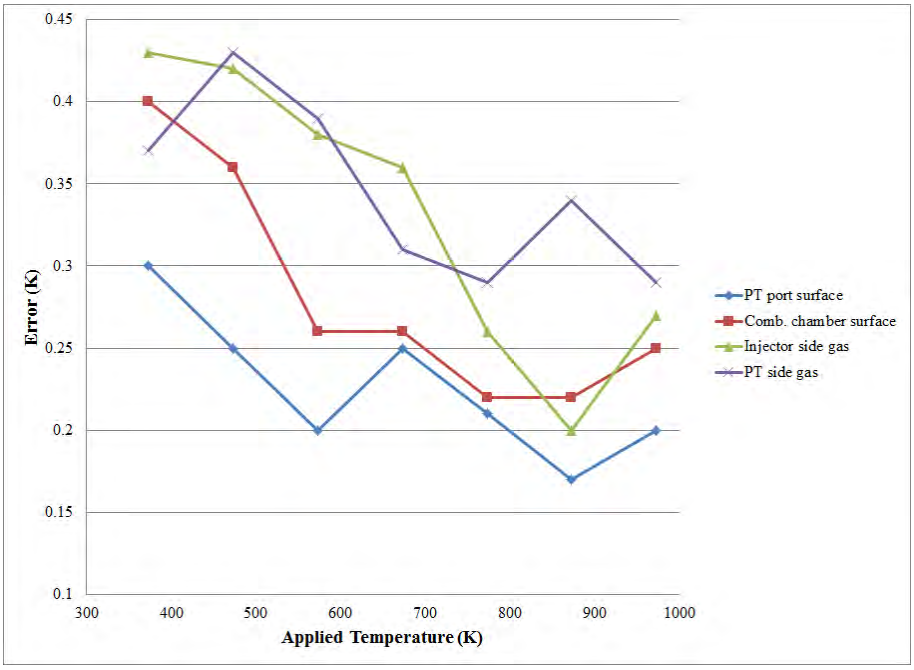

Figure 7.2: NI 9213 module calibration check on 23 of May 2014. Results for channels used for high temperature measurements. Lines between data points were added to improve readability

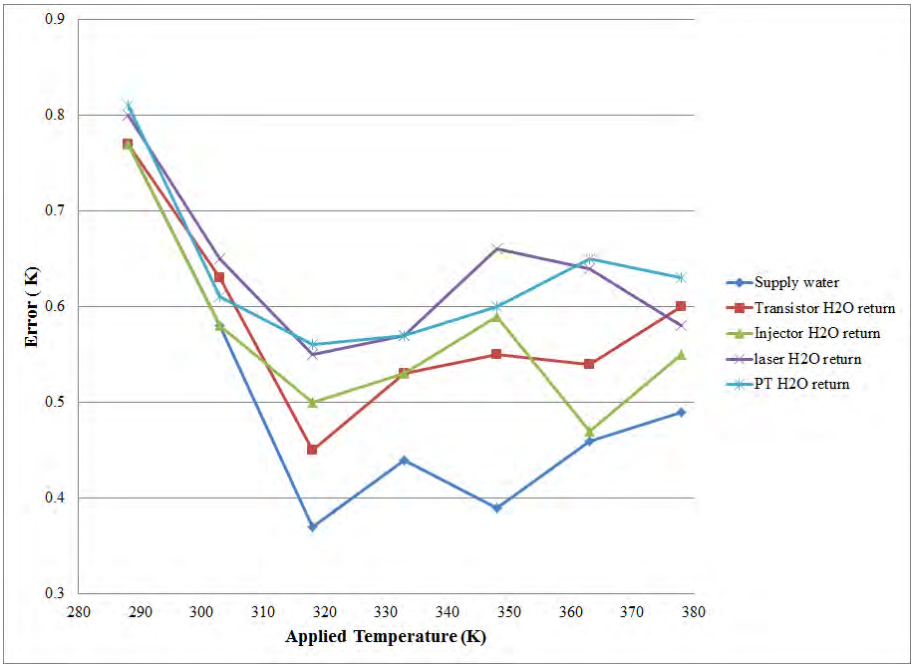

Figure 7.3: NI 9213 module calibration check on 23 of May 2014. Results for channels used for low temperature measurements. Lines between data points were added to improve readability

7.2 Pressure

The quasi static pressure measurements were performed using a NI 9215 module. The module's uncertainty is indicated by Equation 7.2 [48].

$$Module\,error = 0.02\% \times (gain) + 0.014\% \times (Full\,Range) + Noise\,Uncertainty \quad (7.2)$$

As before, there was a conflation of error and uncertainty in Equation 7.2. Equation 7.2 was valid for a module temperature of 298 ± 5 K and a full range of 10.4 V. The coefficients in Equation 7.2 changed at a rate of 10 ppm/K and 60 μV/K respectively if the module's temperature exceeded the aforementioned range. The module did not have its own temperature measurement and therefore the CJ temperature of the thermocouple module was assumed to be indicative of its temperature because both modules were in the CompactRIO's chassis. The CJ temperature was also logged for each cycle of a test to ensure that it was stable and was typically found to be 307 K. The respective pressures were logged in units of bar and therefore were converted back into a voltage in order for the uncertainty to be determined. An example calculation is shown in Appendix D. Neither the actuator, used for the intake and exhaust valve diaphragms, nor the charge gas pressure sensor had any labels on their bodies to identify them and as such the precision information could not be defined. In order to check their operation, each transducer was tested by making use of a Druck DPI 620 pressure calibrator. The calibrator allowed pressure to be applied to the sensors and the associated voltage output to be measured. This process was completed at a number of pressures and the relationship between pressure and output voltage was determined as depicted in Figure 7.4. The conversion equations for the pressure sensors are indicated in Table 7.3 as well as the associated uncertainty due to the module for typical values which occurred during testing at the aforementioned typical cold junction temperature.

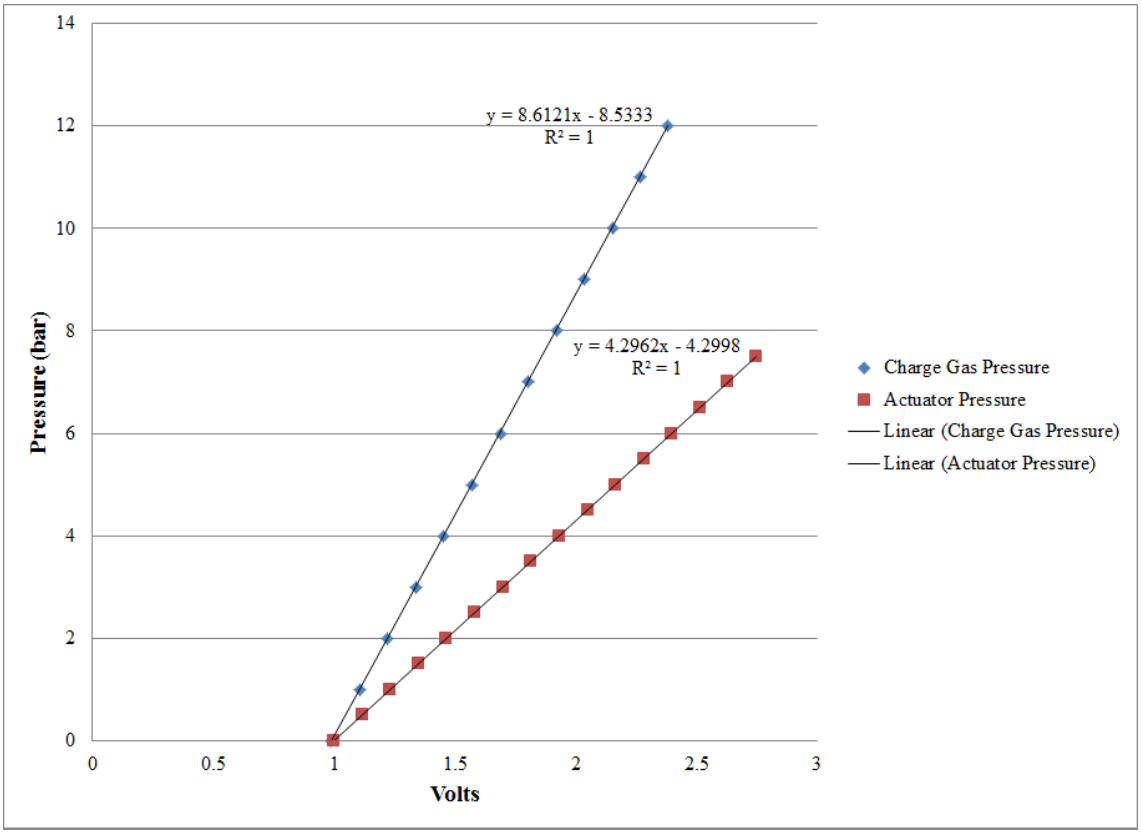

Figure 7.4: Actuator and Charge gas calibration results 05 June 2013

Item	Typical value (bar)	conversion equation (bar/V)	Voltage	Pressure Uncertainty ± (bar)
Actuator Pressure	4.40	4.2962V-4.2998	2.025	0.027
Charge Gas Pressure	21.37	8.6121V-8.5333	3.479	0.029
Fuel Pressure	400	450V-231.5	1.403	0.953

Table 7.3: Quasi-static pressures as a function of sensor output voltages and associated NI 9215 uncertainties

At best the uncertainty of the charge pressure sensor must be the same as that of the Druck calibrator, which had an uncertainty of 0.025% of its 100 bar full scale. Based on this, the sensor's uncertainty was estimated to be at least ± 0.025 bar. Therefore the combined charge pressure measurement chain uncertainty was estimated to be at least ± 0.038 bar, when combining the module and Druck calibrator uncertainty together in the same manner as is done in Appendix D. Of special importance was that ASTM D6890 [4] specified a charge gas pressure tolerance of ± 0.07 bar under test conditions and therefore it has been tentatively shown that measurements to this tolerance were possible. It has been shown previously in Section 2.2.1 that the ignition delay was sensitive to the charge pressure and therefore minimizing its variation was expected to assist in achieving high precision ignition delay data.

With respect to the fuel pressure, a Bosch® 0 281 002 504 sensor was used and fits onto the end of the fuel rail. It has a "sensitivity accuracy" of 1.5% of its 1800 bar full scale [49] . This means the sensor alone had an uncertainty ± 27 bar and therefore a combined measurement uncertainty of ± 27.02 bar when considering the module uncertainty as well. Since most tests were performed at 200 and 400 bar fuel pressure respectively, this represents a relatively large uncertainty. This detrimentally effects the usefullness of the data from an ignition delay modelling perspective and is something that should be addressed in future studies.

7.3 Reagent Composition

240 ml of each PRF blend was required for flushing and testing. The PRFs were measured using 100 ± 0.5 ml measuring cylinders and therefore at least three measurements were required for each PRF blend. When the blend called for constituent volumes of fuel with non-integer values, an electronic pipette was used in conjunction with the measuring cylinders. It had microlitre precision and therefore contributed negligibly to the blend accuracy. Since the number of volume measurements required for each PRF blend varied, there was an uncertainty in the volume of each constituent PRF as well as on the total volume of fuel blended. The resulting PRF CN uncertainty is depicted in Table 7.4.

CN	Uncertainty, CN
100	0
78.75	0.40
57.5	0.36
36.25	0.23
30	0.23
25	0.23
15	0

Table 7.4: PRF CN blend uncertainties

The high cetane blends were the most sensitive to the blending uncertainty because PRF 100 had a stronger influence than PRF 15 on the resulting blend CN.

It has been mentioned in [4, 2, 10] that diesel fuels are sensitive to the U.V. light emitted by fluorescent lighting and sunlight. The light can potentially alter the CN of the fuel in a "short" period of time. When stored, the fuel was kept in cool, dark areas. However, during mixing and treating it was exposed to fluorescent lighting for uncontrolled lengths of time, potentially changing the CN characteristics of the fuel. The consequence of the CN uncertainty to the ID uncertainty is further discussed in Section 10.4.

Chapter 8

Comissioning Experimental Results and Discussion

The majority of DCN tests shown in this and subsequent sections occurred at four conditions, namely:

1. 818 K front thermocouple temperature, 21.37 bar, 21% O_2 in N_2 concentration charge gas, 2ms electronic injection at 400 bar fuel pressure. This condition is most representative of the nominal IQT operating point as was discussed in Section 2.1 . It is referred to as the "High temperature, 21% O_2 condition." The 2 ms injection duration, which is relatively long, was chosen to ensure that possible variability in the injector flow rate during the injector opening phase contributes only a negligible amount to the total quantity of fuel injected.
2. 818 K front thermocouple temperature, 21.37 bar, 14.9% O_2 in N_2 concentration charge gas, 2ms electronic injection at 400 bar fuel pressure. It is referred to as the "High temperature, 14.9% O_2 condition."
3. 788 K front thermocouple temperature, 21.37 bar, 21% O_2 in N_2 concentration charge gas, 2ms electronic injection at 400 bar fuel pressure. It is referred to as the "Low temperature, 21% O_2 condition."
4. 788 K front thermocouple temperature, 21.37 bar, 14.9% O_2 in N_2concentration charge gas, 2ms electronic injection at 400 bar fuel pressure. It is referred to as the "Low temperature, 14.9% O_2 condition."

8.1 Combustion Chamber Temperature Distribution

The ASTM method [4] for the IQT performs 47 cycles of which the last 32 cycles are used for the DCN determination. Figure 8.1 indicates the front and back temperatures measured just prior to injection for each cycle of a 47 cycle test within the IQT's

combustion chamber corresponding to the low temperature set-point. The temperature within the combustion chamber increased during the initial cycles and then stabilised. It was found that the ignition delay deviations measured in this work decreased if the deviation was calculated based on the last 32 cycles instead of the entire 47, indicating the importance of establishing equilibrium within the combustion chamber if accurate ignition delays are sought.

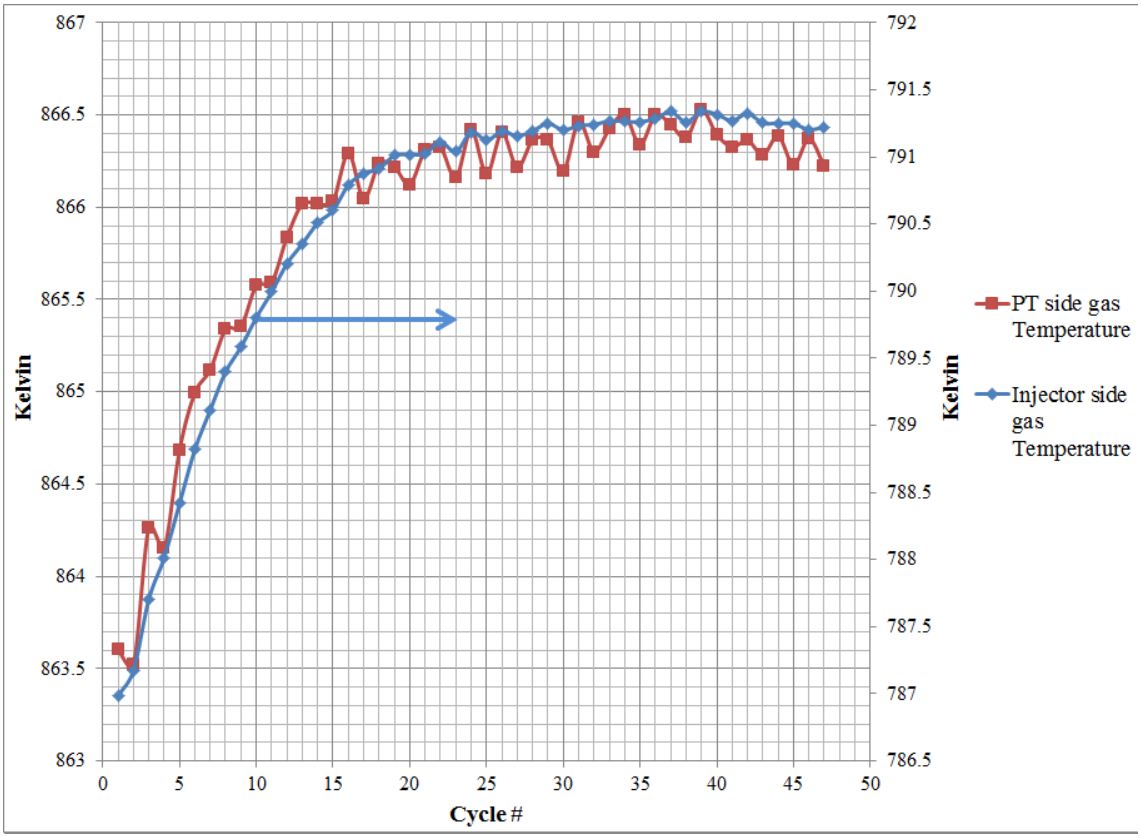

Figure 8.1: Comparison of cyclic injector and pressure transducer side gas temperatures prior to injection for a 835.5 K temperature set-point.

The figure also shows that the temperature maldistribution through the combustion chamber had increased due to the modifications made to the IQT in this project. It was discussed in Section 2.1, that the original temperature difference between the two thermocouples was approximately 56 K. At the indicated condition, it was 74 K and at the higher temperature condition, corresponding to the nominal IQT test temperature used in this work, it was found to be 80 K. Since fuel penetration varies with composition, the difference in temperature could have resulted in ID results of certain fuels differing if their penetration was markedly different from the PRFs such as n-heptane.

8.2 Coolant Temperature Control

In order to control the coolant temperature a three way solenoid actuated valve was also installed into the coolant system to allow the coolant to bypass the heat exchanger. However, the low coolant flow rate and relatively large reservoir and tubing volume meant that the system had considerable inertia. This meant that the coolant temperature could only be controlled within ± 2.5 K range, with a control period that was short relative to the test duration. Since the coolant temperature would alter the fuel temperature in the injector, the temperature variation was thought to be counterproductive to ignition delay stability and therefore this control system was not used. Instead the coolant temperature was left to float relative to the ambient temperature, with the ambient temperature controlled via an air-conditioner. This resulted in the coolant supply temperature varying less than ± 0.5 K during a test.

8.3 Fuel Spray Detection

The definition of ignition delay varies in the literature, depending on what the aim of the work is. In this project, the start of auto-ignition was taken from the point when the spray detector indicated that fuel injection had occurred. An example of this can be seen in Figure 8.2. It was found that there was at least 0.3 ms from the start of the software triggering sequence until the point when the change in spray detection signal was large relative to the initial value prior to fuel injection. Therefore, the initial points were averaged to find the mean output voltage prior to injection in order to mitigate the effects of noise and the start of the auto-ignition delay period was taken from the point when the voltage measured exceeded the mean value in addition to the maximum value which had occurred in that initial period. For the test depicted, the spray detection time averaged 0.3073 ms with a standard deviation of ± 0.007 ms. The figure also indicates that the actual injection duration was longer (~2.6 ms) than the 2 ms electronic injection duration specified. This disparity is common as was discussed in Section 2.3.

Tentatively, the figure also suggests that the injection rate was quite stable for this injection duration and that the injector opened and closed quickly. In comparison, Figure 8.3 shows the results of Musculus et al. [50] , who compared the injector needle lift, the laser attenuation and mass flow rate of single hole injector. The figure shows that when the laser signal remains constant, the injector mass flow rate can also be considered constant. They discuss that a potential limitation of the needle lift sensor for the same task is that there is still significant flow while the injector is closing implying that during the opening phase, uncertainty exists about when meaningful fuel flow has begun.

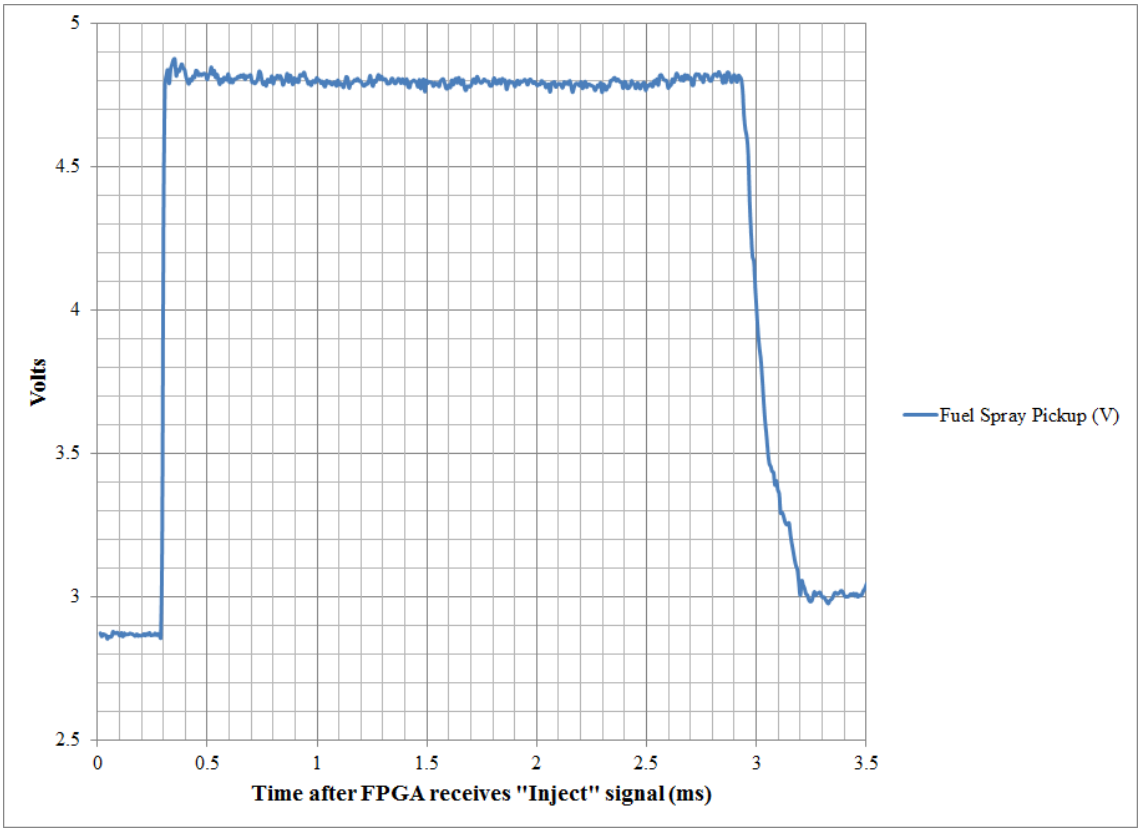

Figure 8.2: Spray detection for n-heptane.788 K front temperature, 21.37 bar synair, 2 ms (electronic) injection duration at 400 bar fuel pressure

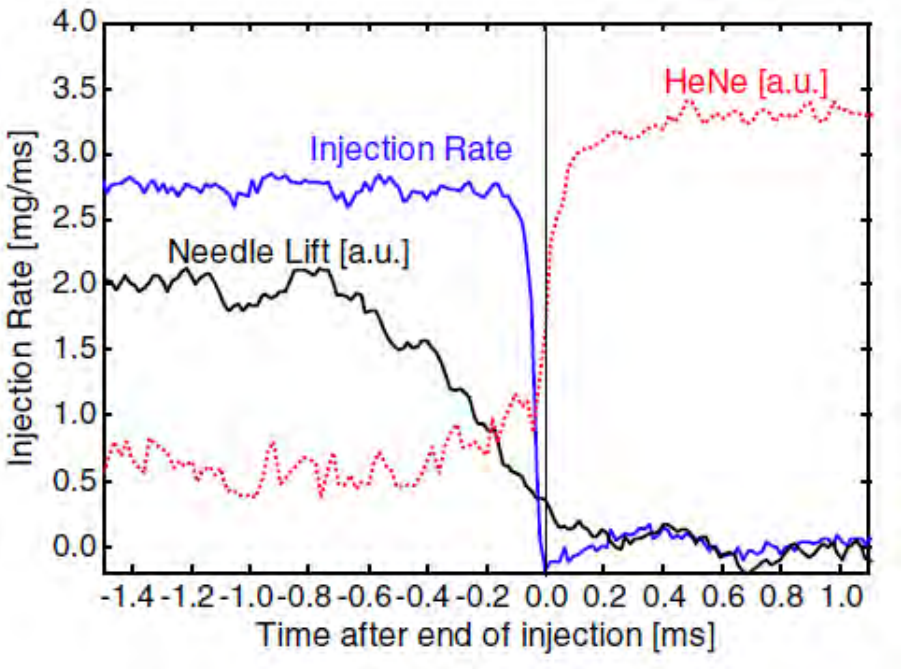

Figure 8.3: Injection rate shape results of Musculus et al. [50]

The combustion chamber pressure and the spray detection were sampled every 6.4 μs respectively. It was not known where in each 6.4 μs period the required change in signal actually occurred and therefore when combined there was an additional uncertainty of 9.05 μs on each ignition delay due to the sampling rate used. This uncertainty was present in every cycle of every test and therefore it would have a varied effect on the repeatability of the ignition delay measurement, depending on how its magnitude compared with the mean ignition delay measurements.

8.4 End of Ignition Delay Detection

A combustion pressure rise value was sought to define the end of the ignition delay period. This was particularly challenging because the pressure traces varied significantly between cycles of a test and indeed between fuels.

Figure 8.4 indicates the combustion pressure of the 32nd (last) cycle of each PRF blend tested at 788 K, 21% O_2 condition. It is evident that the combustion pressure form varies with CN and that the variation is non-consistent. What is especially noticeable is the change from PRF 25 to 36.25, where the latter undergoes a distinct, rapid premixed combustion phase and the former reacts slowly, with a gradual change from cool to hot flame chemistry, surmised by the change in gradient at approximately 8 ms after the start of the measurement. This change in form has been noted by Rabl et al. [26] who found that the burn duration for PRFs varied with CN, under conditions similar to those tested here as well as under engine-like thermodynamic conditions albeit with quiescent charge gas.

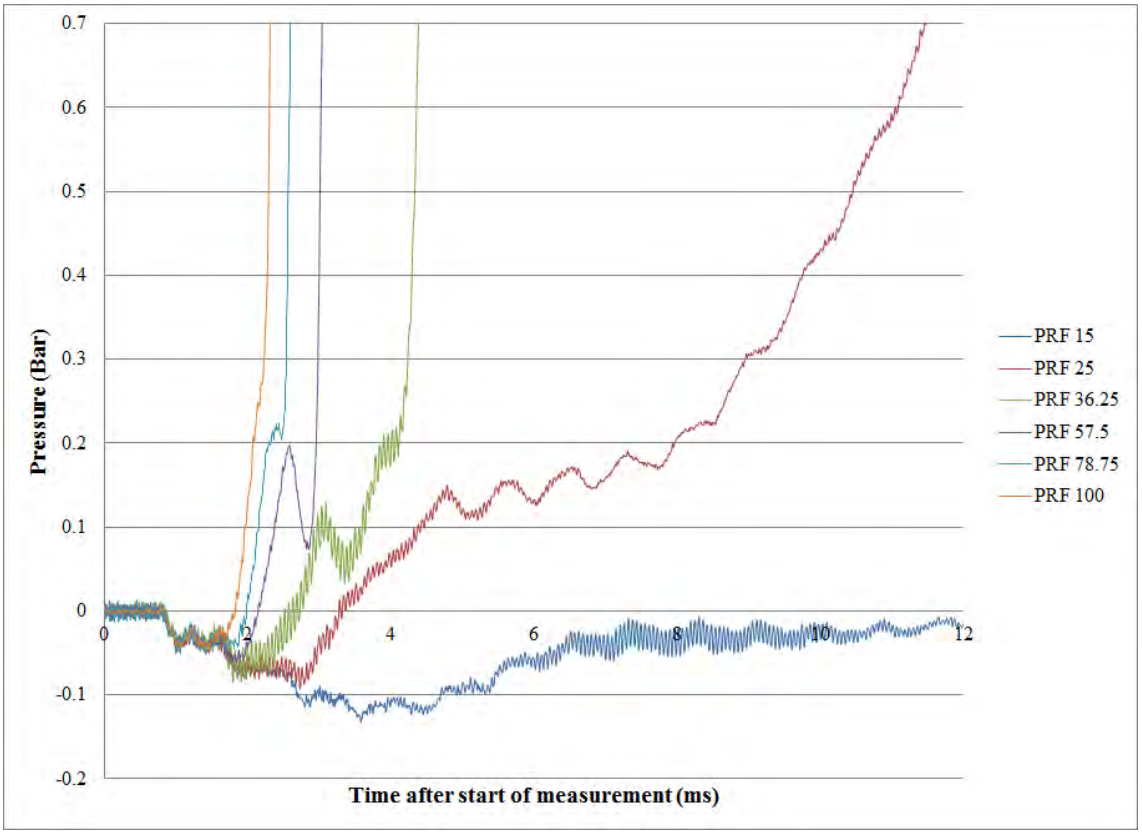

Figure 8.4: Variation in combustion pressure form with changing CN. 788 K front temperature, 21.37 bar synair, 2 ms (electronic) injection duration at 400 bar fuel pressure

Figure 8.5 indicates the sequential combustion pressure data points logged for the 32 cycles which comprised a PRF 25 and PRF 100 test respectively. PRF 15 was not used for comparison because at the conditions indicated in the figure it hardly reacted, as shown in Figure 8.4 and the manner in which it reacted was not representative of the higher cetane fuel blends as was shown in 8.4. Figure 8.5 shows the piezoelectric combustion pressure measurements' standard deviation for the 32 cycles comprising a test by themselves, as well as the combined quasi-static charge gas and combustion pressure measurements. Also shown is the combined sensor pressure trace for the last cycle of the test so that the variability can be seen in context. This figure allows the variation due to combustion phenomena to be separated from the charge gas precision and also indicates the relative effect of noise on the pressure traces. It shows that for PRF 25 the dynamic-only pressure form and magnitude were quite similar to the combined form and that the piezoelectric sensor's noise was a major contributor to the total variability between cycles until well after the cool flame. It was also noticeable for PRF 25, that the post cool flame ignition delay was variable in duration and that the agreement between the cycles worsened quickly on average after the cool flame, as indicated in the figure.

However, for PRF 100, the charge pressure variation was relatively large in comparison to the piezoelectric noise as indicated by the initial offset between the graphs, but once again the form between the dynamic and combined signals are congruent. Both the PRF 25 and the PRF 100 graphs indicate that the standard deviation increases as evaporation commenced and it was apparent that the agreement was worse than earlier in the cycle as the combustion pressure crossed the initial charge pressure. This may once again be due to noise, but also indicates that a large enough number of cycles have experienced the start of the cool flame so as to increase the magnitude of the standard deviation, while some still have not.

The previous points indicate that going forward, the initial charge pressure could be excluded from the analysis because it contributed to the standard deviation between cycles, thereby concealing the actual fuel effects, which would worsen the ID variability calculated. Additionally, the combined form was similar to the dynamic-only form and therefore the charge pressure will not drastically alter when the end of the ID was defined, provided it was defined by a change of state that was relative to the initial pressure returned by the dynamic-only measurements.

Figure 8.4 shows that when the combustion chamber pressure was below the initial charge pressure, the various fuel blends tended to have near coincident pressures, due to the similarities in the thermophysical properties of the PRF blend constituents. If one considers the pressure trace turning point as the beginning of exothermicity, subsequent to the evaporation phase, as the end of ignition delay, it is apparent that the ID would be 2.8 ms and 1.5 ms approximately for PRF 25 and PRF 100 respectively. This would result in a very steep CN/ID correlation and therefore poor DCN precision if the repeatability was determined based on the gradient of this correlation.

Alternatively, Allard et al.[1] made use of the pressure recovery point to define the end of the ignition delay period, which was the point when the pressure crossed its initial value prior to fuel injection. At first glance of the aforementioned figures, it would appear that this is a poor choice due to the relatively large variation in readings between cycles comprising a test at this point. However, the gradient of the pressure trace is relatively steep here and therefore despite the relatively large difference in pressure values, it can be expected for this change in pressure to occur quickly and therefore the ID temporal variation may not be as conspicuously large. This ID definition and others will therefore be considered in Section 9.

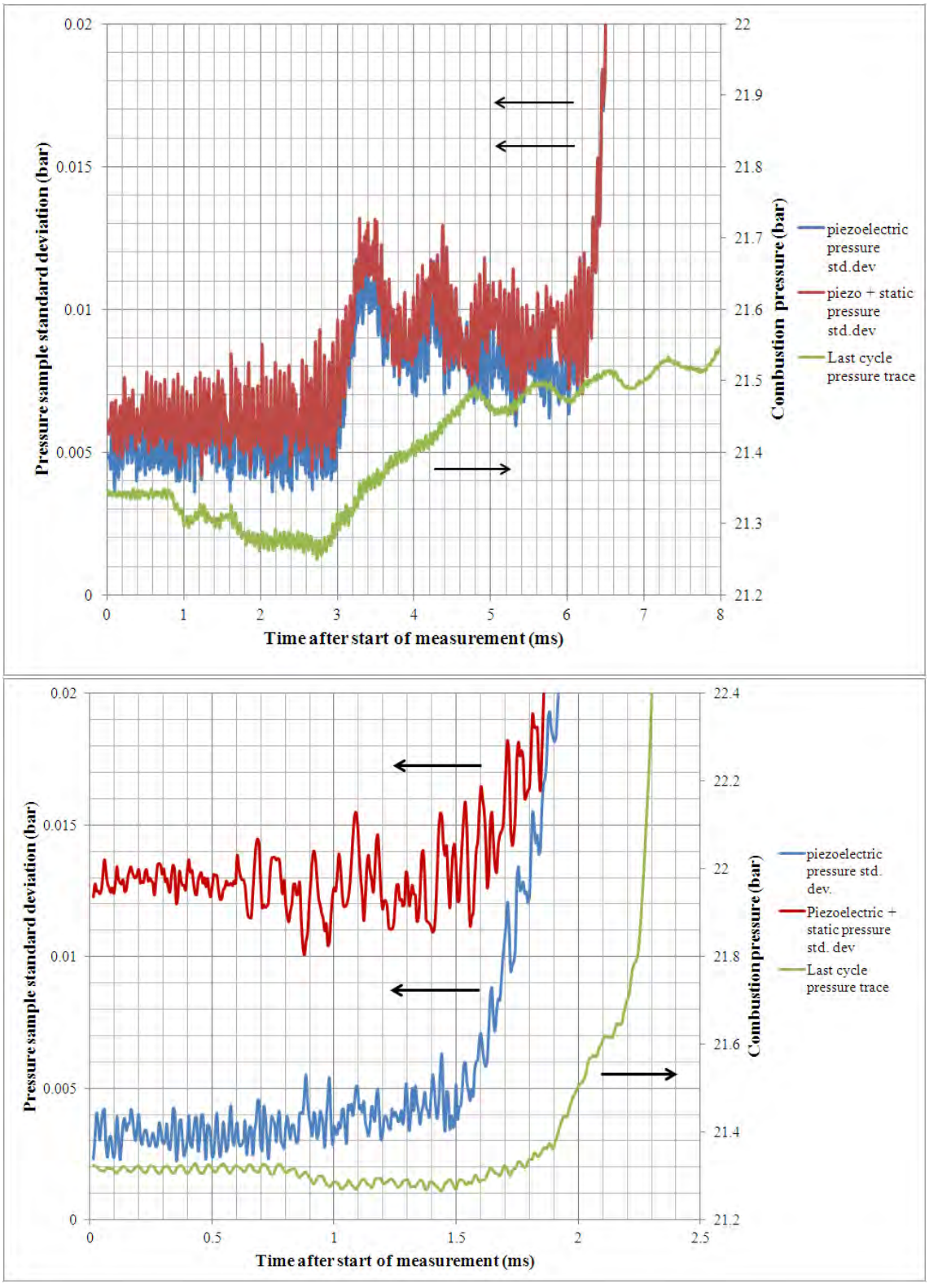

Figure 8.5: Comparison of piezoelectric combustion pressure measurement sample standard deviation and the combined piezoelectric and charge gas deviation for PRF 25 (top) and PRF 100 (bottom) at 788 K, 21.37 bar and 21% O_2 condition.

The optical ignition delay was defined as the time taken from the start of injection,

as discussed previously, to the point when the optical signal output changed from low to a high output as depicted in Figure 8.6. The figure shows that the signal typically went from low to high in one measurement period and therefore the flame detection could be considered as having a temporal resolution equal to the 6.4 μs measurement resolution. During data processing, the flame detector signal was checked for when it exceeded 0.5 V, which was reliably above the 0.3 V no-signal value corresponding to the optoschmitt's transistor forward voltage.

The ignition delay data from the flame detector typically had lower precision than that of the pressure based ignition delay. This was potentially due to two things:

1. The position of the sensor at the end of the IQT's port, and its narrow optical acceptance angle (± 15º at 10% sensitivity) meant that the auto-ignition kernel(s) had to be located on the injector's axis for it to be picked up punctually. The on-axis position is typically the richest part of the spray [51], and may not coincide with the typical spatial position of the first auto-ignition kernals. Lillo et al. [44] performed a study to triangulate the position of auto-ignition using multiple pressure transducers and then temporally corrected the pressure measurements, based on its distance from the sensors accounting for the speed of sound of the gas. They found that at temperature conditions similar to that of the IQT, but at a higher pressure, the cool flame activity tended to make the position and timing of auto-ignition more variable than those tests performed at higher temperatures and found that the potential for multiple auto-ignition kernels to occur simultaneously was present. Additionally, they found that early in the ignition phase the kernels could be detected via optical methods while they were not yet discernible by pressure based methods. If the optical sensor was able to detect these smaller auto-ignition zones and these zones are more variable, it is likely that the deduced optical ignition delays would also have higher variability. It may also be possible that the sensor triggered on the cool flame, which has previously been shown to have variable duration and timing.

2. The flame detector had variable sensitivity to the incident light's wavelength. Therefore if the combination of wavelength and intensity was not correct, the sensor would not trigger, or it would trigger erratically.

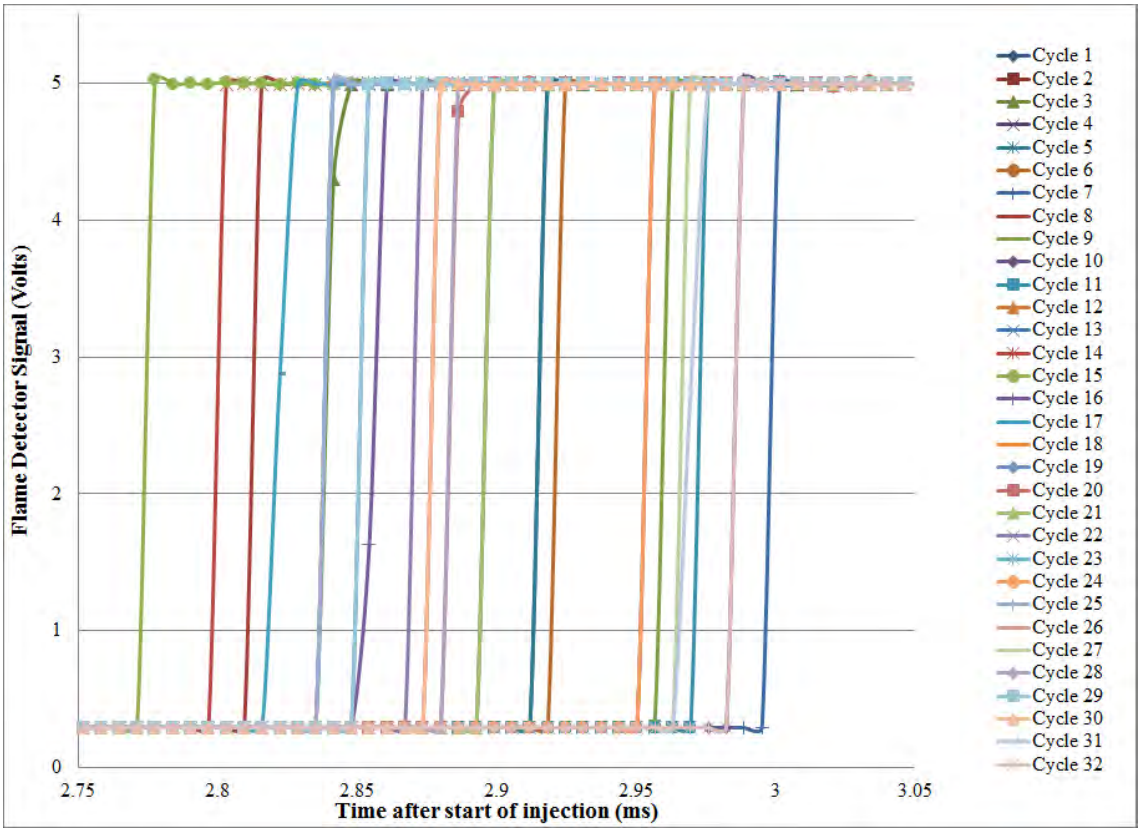

Figure 8.6: Flame detector signal of n-heptane. 788 K front temperature, 21.37 bar synair, 2 ms injection duration at 400 bar fuel pressure

8.5 Injector Sticking

During testing the injector's needle stuck on many occasions, preventing fuel from being injected. The injector was removed from the combustion chamber so that it could be set up to inject into a beaker using EN 590. It was found that the EN 590 was able to free the injector needle, albeit sometimes only after a few days of the fuel being left in the system. Initially during the testing of solvents, it was surmised that the injector sticking could be related to the poor lubricity of the solvents and therefore all subsequent tests were performed with a 300 ppm addition of an ester based lubricity additive. Fukumoto et al. [52] found that a GTL diesel, with composition indicative of PRFs, achieved an acceptable Wear Scar Diameter [6] with 100 ppm of ester based lubricity additive, so the 300 ppm was deemed to be conservative.

Since the injector continued to stick after the adoption of the lubricity additive it would seem that the issue may be related to formation of deposits within the injector, due to the high temperature that the injector tip was continuously exposed to. The hot soak was particularly severe in the IQT because fuel injection occurred relatively infrequently and there was no cool gas moving over the injector as would cyclically

occur in an engine. The formation of deposits is not yet confirmed, because the injector has not been disassembled, nor has it been confirmed that the EN 590 used has a detergency additive. It was also noticed that the injector sticking could occasionally be remedied in a few minutes if the solvent was removed and the EN 590 was put in the fuel system, which suggests that it may still be a lubricity issue.

8.6 Temperature Calibration

ASTM D6890 [4] recommends recalibrating the system after significant mechanical work has been performed. This is done by adjusting the temperature set point such that n-heptane achieves a standardised ignition delay of 3.78 ms. Given the problems with the injector, it was removed frequently and it was found after the last rebuild that the temperature distribution within the combustion chamber had changed. This was most likely due to a shift in the insulation surrounding the combustion chamber. Since the ignition delay is highly temperature sensitive, this posed a problem. Additionally, the method by which the ignition delay would be defined had not been absolutely chosen and therefore calibrating based on n-heptane's ignition delay alone was also problematic.

As a compromise, the temperature set-point was adjusted so that the internal combustion chamber temperatures were representative of what was achieved previously as far as possible, since a correlation analysis indicated that the ignition delay was most sensitive to these temperatures and the set-point was adjusted so that the ignition delay between previous n-heptane results and those after the rebuild were within one standard deviation of one another based on 1.38 bar pressure rise. The 1.38 bar pressure rise was based on the work of Zheng et al. [24], who found that there was a 1.38 bar decrease in pressure due to evaporation when testing n-heptane in the IQT and therefore this "amount" of heat release was required for the pressure to reach the recovery point. The result of this attempt at calibration are shown in Table 8.1 and the new temperatures are shown in Table 8.2.

Low Temperature	Initial	Final
Ignition delay (ms)	3.091	3.134
standard deviation (ms)	0.031	0.046
High Temperature	Initial	Final
Ignition delay (ms)	2.544	2.578
standard deviation (ms)	0.021	0.033

Table 8.1: Ignition delay calibration at the low and high temperature set-points for n-heptane.

Temperature	Initial (K)	Final (K)
Low set-point	835.5	832.5
Front-Low set-point	788.6	789.0
Back- Low set-point	866.0	860.0
High set point	865.5	868.5
Front-High set-point	816.6	821.0
Back-High set-point	896.6	896.7

Table 8.2: Change in Temperature conditions after rebuilding and calibration.

The consequence of calibration is that the data is less useful in its absolute form, because the critical dependence of ignition delay on temperature has been manipulated in an attempt to achieve a standardised ignition delay instead of an absolute one.

Chapter 9

Correlation Experimental Results and Discussion

This section presents and describes the major experimental results collected during the testing phase of this project. The aim of these experiments was to redevelop the correlation between CN and ID by testing diesel PRFs, surrogates and full boiling range fuels.

The PRF fuels and solvents were sourced from Sigma Aldrich and had a nominal purity of 99%, except for heptamethylnonane which had a purity of 98%. The batch of fuel used for each PRF blend as well as the 21% O_2 (synair) batch for the corresponding tests are shown in Appendix A.1. The tests performed at 14.9% O_2 concentration all used the same bottle of gas. It was discussed in Section 8.6 that a temperature calibration was attempted. Therefore some of the tests occurred at a revised temperature in line with the calibration.

ASTM D613 [2] only indicates the CN precision for fuels in between 40 and 56 CN. This means that while fuels out of this range can be rated, their precision is typically based on far fewer tests than for fuels within the specified range. Additionally, for the GTL diesel sample used, only a DCN (80) using ASTM D6890 was available as indicated by its specifications in Appendix A.2. Therefore the CN used when developing the correlation must be viewed with circumspection for the aforementioned fuels.

9.1 Condition 1: High Temperature, 21% O_2

It has already been mentioned that [4] makes use of the pressure recovery method to define the ID period. In comparison,[10] and [11] make use of 0.2 bar pressure rise to define the ID, while [11] makes additional use of the time taken to reach half of the maximum combustion pressure for correlating DCN with ID. The correlation in

[11] uses the half maximum pressure rise to improve distinction between higher CN fuels, by making use of the change in burn rate with CN as indicated by [26].

The DCN correlation was based on equation 9.1, which has the same form as original device for the full DCN range [4].

$$DCN = A(ID - B)^C + D \tag{9.1}$$

Where:

A,B,C and D are constants and "ID" is the ignition delay in milliseconds.

In an attempt to find an optimised pressure rise value to define the end of the ignition delay period, the ignition delays were parametrically determined for combustion chamber pressure rises in the range of 0.2 to 2.4 bar, while simultaneously determining the sample standard deviation for each pressure rise value of the 32 cycles comprising a test. The range was based on inspection of the pressure traces. It was perceived that for PRF 100, the traces were coincident after the cool flame, which caused a pressure rise of about 0.2 bar, and it became variable when the pressure exceeded 2.3 bar. This range was divided by 800 to get the pressure increment that would be used to calculate the ID mean and sample standard deviation. The range was divided by 800 because this represented the number of data points between the pressure range of 0.2 to 2.3 bar and theref It was based on PRF 25, where there are approximately 800 data points in the pressure range from 0.2 to 2.3 bar. The division by 800 allows the pressure trace to be analysed at its temporal measurement resolution and therefore gives the best ID resolution achieveable.

This method was limited, because it was simply based on when the combustion pressure exceeded the aforementioned pressure rise, namely its cut-off value. The combustion pressure measurements oscillated as was depicted in Figure 8.5 and therefore this method missed out on values which are in the troughs of the combustion pressure oscillations as depicted in Figure 9.1. However, the temporal agreement will not be good near the turning point of a trough anyway, because the pressure gradient is not steep there and therefore it will take a longer time when cycles are compared, for all cycles to rise to a certain value. In other words, when the pressure gradient is high, the time difference for a certain pressure change is short and better temporal agreement is likely.

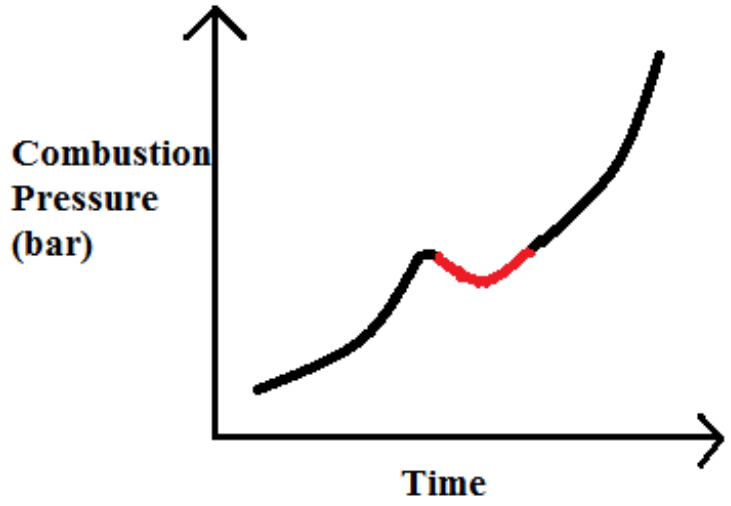

Figure 9.1: Limitation of pressure cut-off method for ignition delay optimisation. Area in red not tested for suitability

The DCN standard deviation was determined by calculating the derivative of the DCN correlation, as depicted in Equation 9.1, at each ID point and multiplying that by the ID standard deviation. It was assumed that if the ID variation was small, the error associated with assuming the bilateral tolerance to be symmetric and linear would also be small. The resulting coefficients are shown in Appendix B.1 The sum of the DCN correlation errors squared and the standard deviation error squared for this condition at the aforementioned range of cut-off pressures is shown in Figure 9.3. The figure indicates that both the correlation and standard deviation total errors are approximately stable over a wide range of cut-off pressures and the DCN error has a minimum value near 0.22 bar.

At first glance the DCN correlation error was thought to be the most important of the two properties to minimize, because if it is not accurate, the precision was meaningless. However, the figure indicates that the minimum correlation error occurs at approximately 0.22 bar, but the corresponding standard deviation error at this point is relatively large. With this in mind, it was decided to use the point where the combined error was lowest, at the modest expense of a slightly worse DCN correlation error. At this test condition, the minimum combined error occurs at a cut-off pressure of 0.255 bar and the resulting correlation between DCN and ID can be seen in Figure 9.2. The figure shows that the gradient of the DCN correlation is steep for the high DCN fuels and is in comparision is almost flat for the low DCN fuels.

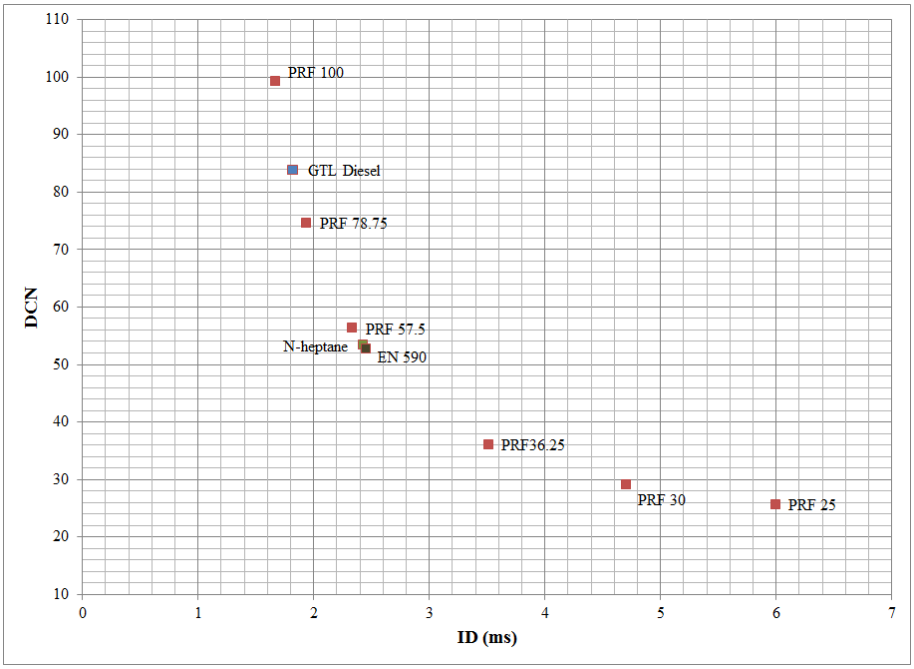

Figure 9.2: DCN of indicated fuels and their associated mean IDs at the high temperature, 21 % O_2 condition.

The correlation between DCN and CN and the asociated standard deviation are depicted in Figure 9.4.

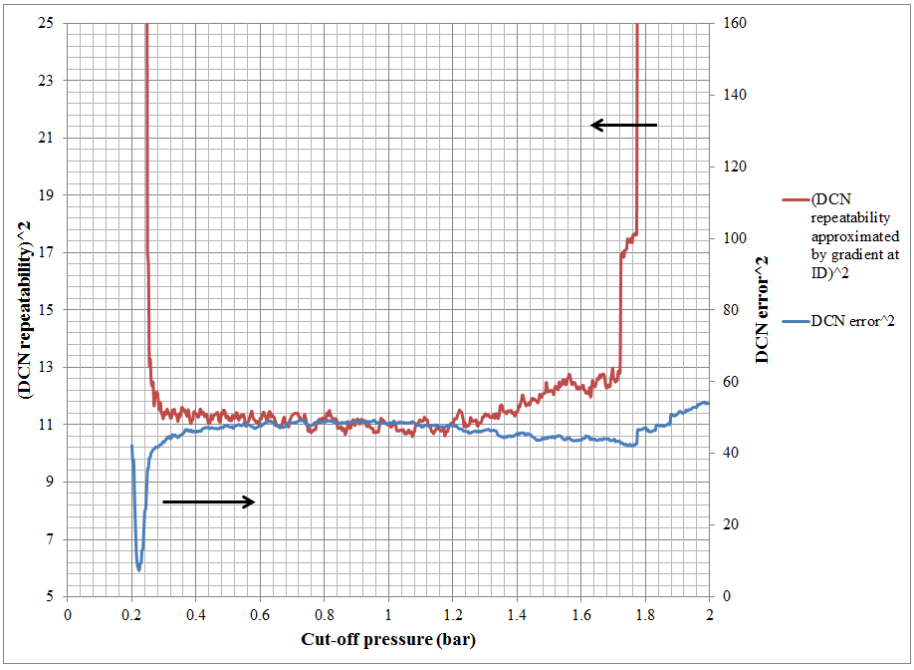

Figure 9.3: DCN correlation error and associated total standard deviation error for varying cut-off pressures. High temperature and synair conditions

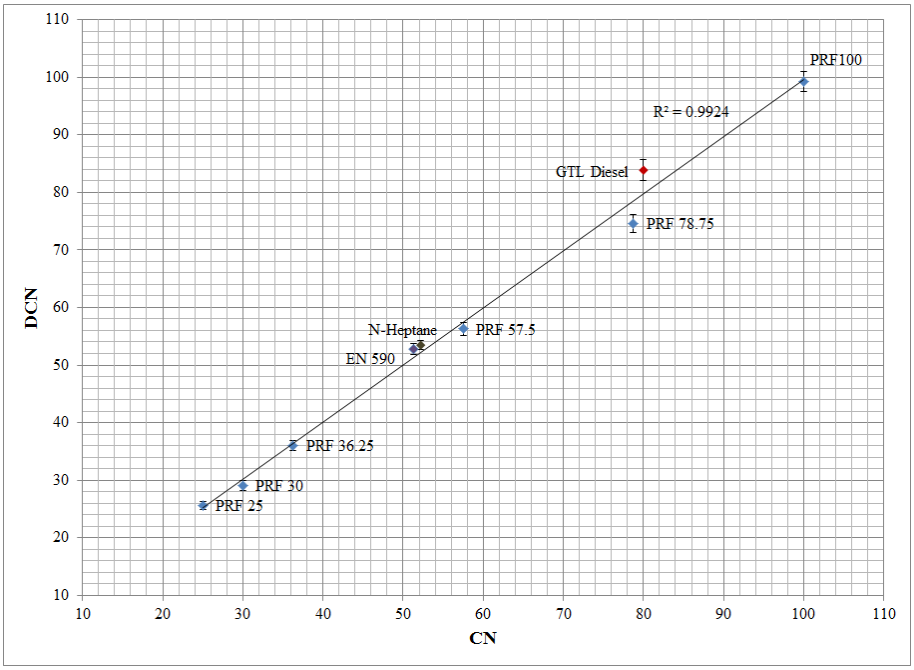

Figure 9.4: Optimized correlation between DCN and CN for high temperature, synair condition. Also shown are the DCN sample standard deviations at each point.

Figure 9.4 shows that the agreement between the DCN and CN is good across the range considered. PRF 78.75 has the largest DCN error of -4.1, while GTL diesel, has the 2nd largest error of +3.8. This suggests that the GTL diesel is pulling the PRF 78.75's DCN down, because both fuels would fit better if the GTL diesel's CN used for the fit was higher. However, A CN for GTL diesel was not available and therefore a DCN value was used instead. A fundamental issue of the D613 test is that it does not provide precision for fuels exceeding a CN of 56 and therefore a better way of dealing with the GTL is not available.

This condition was most representative of the nominal IQT operating point and it is interesting to note the difference in ignition delay of n-heptane between this work and the original device. In this work an ignition delay of 2.42 ms was determined while the original device returned 3.78 ms[4] which is a relatively large difference. This was despite the original device indicating the end of the ignition delay period at the pressure recovery point, while this work indicated it later in the heat release.

The major differences between the two devices are the different injectors and a corresponding difference in injection pressure and quantity of fuel injected. Bogin et al. [25] indicates that the original injection pressure was approximately 225 bar while these tests were done at 400bar. Also, the the original device injected 72 mg of fuel[25] while in this work it was an order of magnitude lower, based on extrapolations made using the total heat release.

Figure 9.5 indicates the difference in pressure traces averaged over the 32 cycles

of tests performed at 200 and 400 bar injection pressure respectively for n-heptane at the same test conditions described for this section. As expected the maximum pressure rise for the 200 bar case was reduced, because a lower amount of fuel was injected for the set injection duration. However, it was apparent that the reduced fuel pressure increased the ignition delay and it was therefore directionally possible that the difference in injector was the major source of variation between the two devices.

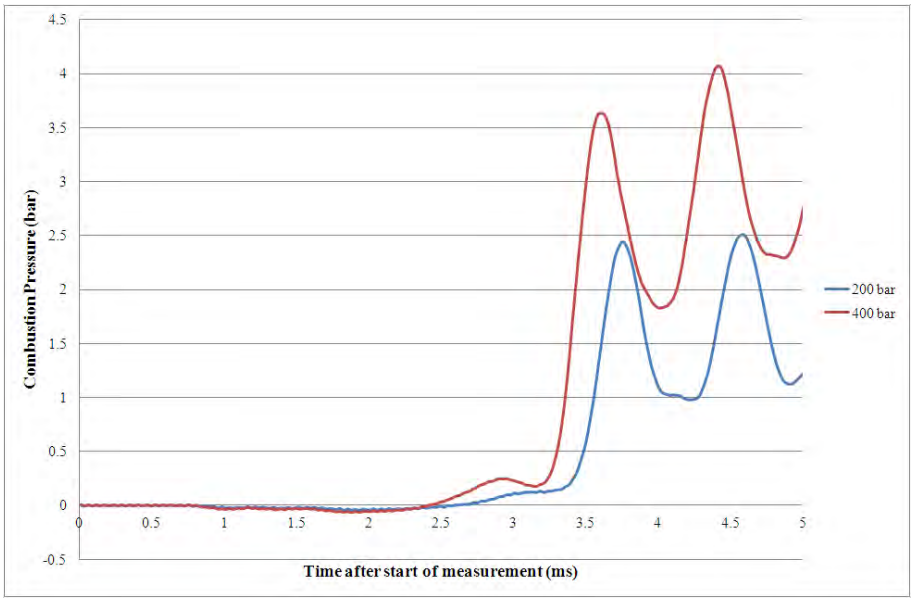

Figure 9.5: Pressure trace for n-heptane at 200 and 400 bar injection pressure with 2 ms electronic injection duration.

It was mentioned in Section 8.4 that the original IQT makes use of the pressure recovery point to define the end of the ignition delay period. The goodness of fit of the correlation developed using this method is shown in Figure 9.6. It indicates that this method offers worse correlation than the pressure cut-off method, especially for the high CN fuels, which don't seem to have monotonically varying cool flames based on the the large standard deviations indicated for the fuels with CN of 78.75 and above. Additionally, the IDs span the range of 2.823 to 1.181 ms across the CN range of 25 to 100. Therefore this method has a much steeper DCN/ID gradient and therefore the DCN precision is also worse for all of the fuels except PRF 25.

Based on the poorer fit, it was decided to rather make use of the pressure cut-off method for considering the IDs at the other conditions tested.

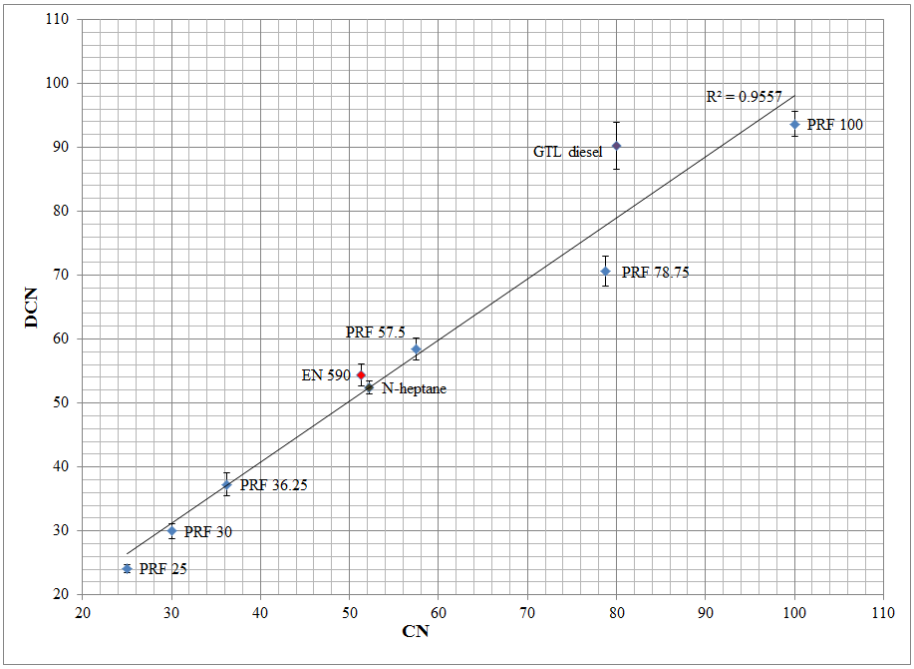

Figure 9.6: Pressure recovery based DCN correlation comparison with associated CN at high temperature, 21% O_2 conditions.

Figure 9.7 indicates the correlation developed based on the flame detector measurements. Reliable flame measurements were only achievable with fuels of CN equal to or greater than 36.25.

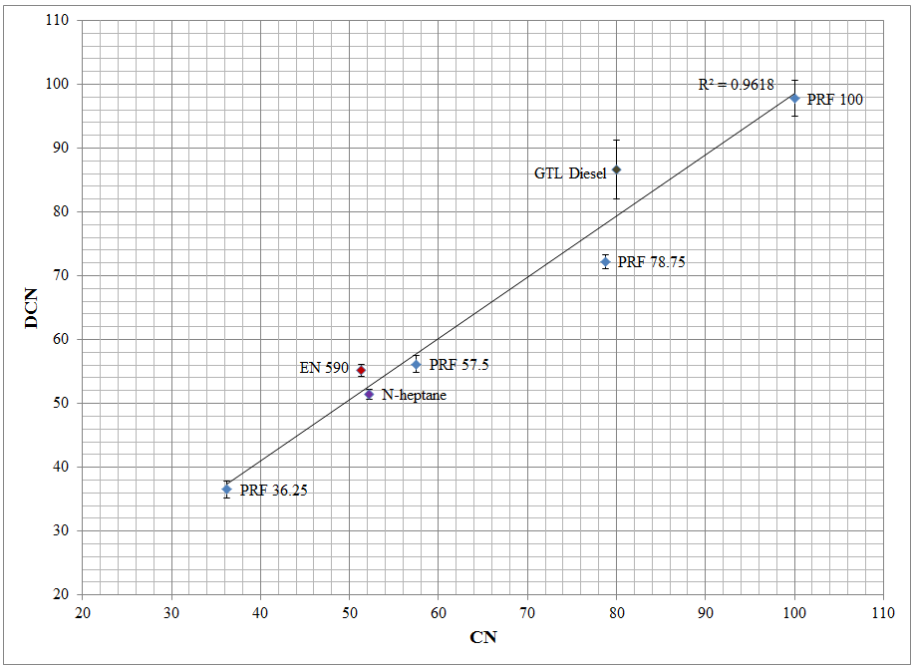

Figure 9.7: Flame detector based DCN correlation at high temperature 21% O_2 concentration.

The flame detector outputs a digital signal and therefore the end of the ignition delay period was not subject to optimisation. Of interest was the timing of the flame detection relative to the pressure measurement because this provides some indication of whether the flame detector responded to the cool or hot flame chemistry at this condition. Figure 9.8 indicates a pressure trace averaged over the 32 cycles of an EN 590 test at this condition. The figure indicates that the flame detector responded very early in the hot flame heat release period, shortly after the turning point in the pressure trace, suggesting that it was a good indicator of the end of the hot flame auto-ignition delay. However, the flame detector repeatability was typically worse than that achieved using the pressure based method, because it triggered after the cool flame which was shown in Section 8.4 to have potentially the worst synchronisation between cycles. This means that, while it was phenomenologically the most appropriate point for defining the end of the hot flame ignition delay, its relatively poor repeatability means that the correlation was not as accurate as the optimised pressure based one.

Additionally, the correlation depicted in Figure 9.7 could only reliably detect auto-ignition down to a CN of 36.25, where the end of injection occurred approximately 1 ms before auto-ignition was detected. The sensor is sensitive to a broad range of light wavelengths and therefore may have triggered on any of a number, or indeed combination, of chemiluminescent species. Singh et al [53] discuss that there are a variety of broadband chemiluminescent sources which are associated with each phase of auto-ignition and that the second stage of ignition is predominantly associated with emissions from OH,CH and CO radicals in the light wavelength range of 360-560 nm. OH luminescence is substantial when the local equivalence ratio is in the range of $0.5< \varphi <1.2$, outside of which the luminescent intensity may drop by at least an order of magnitude.

Siebers [54] made use of OH luminosity at 310 nm to surmise flame lift off length at near stoichiometric conditions. Musculus et al. [55] have shown that, using a detailed chemical kinetic model at 800 K, 50 bar conditions with premixed n-heptane at $\varphi = 0.7$ conditions, significant OH forms late in the 2nd ignition delay period. Directionally, conditions that result in lower local equivalence ratios, would emit a critical level of irradiance later into the hot flame ignition and given the high fall-off rate of luminescence with equivalence ratio, once this condition is reached, any additional increase in mixing may not produce a sufficiently strong optical signal to be detected with this sensor. Therefore given that the system cannot reliably register an optical signal for PRF 30 and below, it seems reasonable that the fuel air mixture has sufficient time to mix to conditions that are too lean to form enough OH incandescence and therefore no luminosity detection occurs. Musculus et al. [55] indicate that the other aforementioned CO, CH radicals are still present at lean conditions and therefore it seems that the sensor responds most favourably to OH. However, the datasheet

for the sensor does not specifically indicate that it can measure light of wavelengths as low as 310 nm, indicating sensitivity to 400 nm only.

The other potential source of irradiance was from soot. In the conventional direct injection diesel model of Dec [56], soot forms in the fuel rich region between the point of flame lift to the boundary of the diffusion flame where it is consumed. Since the time between the end of injection and auto-ignition is seemingly short, fuel rich regions may still have been present where soot may form and irradiate light. These emissions are well within the sensors sensitivity range [57] and are often very bright which would make triggering the sensor possible if they are present at this point in the combustion process. However, at this point in the pressure trace the temperature is still relatively low, and therefore it is somewhat doubtful that soot has formed, but it is after the start of the hot flame and is therefore still a possibility.

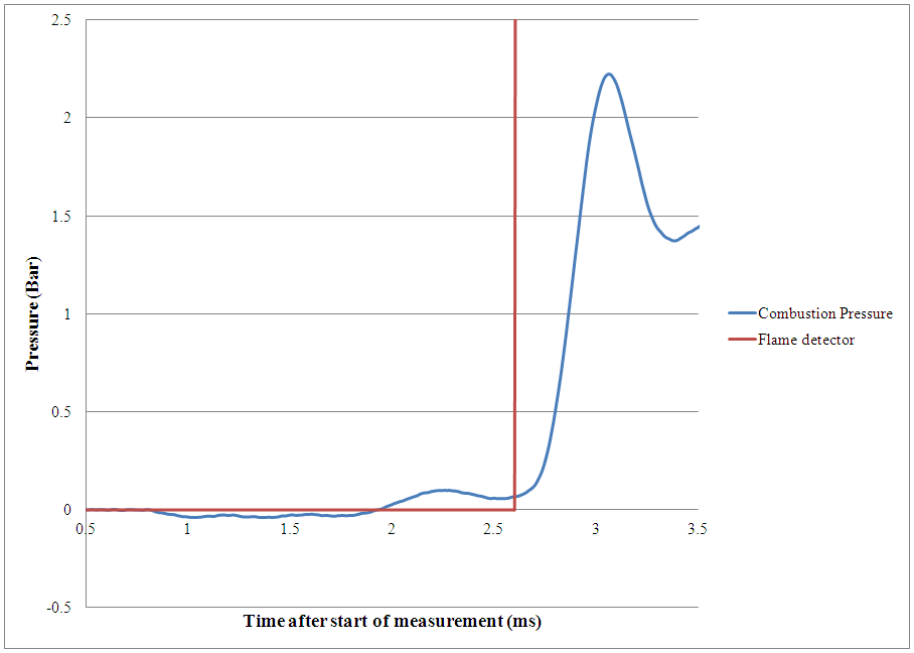

Figure 9.8: EN 590 optical detection timing relative to pressure trace. Both traces averaged over 32 cycles at high temperature 21% O_2 condition

9.2 Condition 2: High Temperature, 14.9% O_2

Figure 9.9 indicates the correlation between DCN and CN at the high temperature, reduced oxygen concentration condition. The best fit, based on the combined correlation and precision error minimum, occurred at a pressure of 0.267 bar, in contrast to the 0.255 bar at the 21% O_2 condition. The goodness of fit was the same as was found at the 21% O_2 concentration.

It was apparent after studying Figure 9.10, that the reduction in oxygen concentration had the desired effect of decreasing the DCN/ID correlation gradient, thereby in-

creasing the correlation's sensitivity with respect to CN in agreement with literature [14]. This was of most potential benefit in the mid CN range where the ID difference between n-heptane and EN 590 had increased. However, both correlations return an error for n-heptane indicating that its CN should be higher. For these correlations a CN of 52.2 was used for n-heptane based on the value produced by Yates et al. [13] of 52.2 ± 4.3. However, Yates et al. [12] initially report a CN of 56, while Naik et al. [23] reports 54.4, a number taken from NREL's [58] cetane number compendium. It may therefore be beneficial to let the n-heptane CN float within its repeatability limits to improve the correlations' fits while optimising them.

Of further interest is that GTL, PRF 78.75, EN 590 and PRF 25 all return a lower DCN correlation and standard deviation error at the 14.9% O_2 condition. Additionally, GTL diesel and PRF 78.75 exhibited the same trend as Condition 1, where GTL diesel returned a higher DCN rating than expected and PRF 78.75 a lower one. However, the DCN error of GTL diesel has changed from +3.9 to +2.8 with only a minor change for PRF 78.75. The reader is reminded that the GTL diesel CN was actually a DCN value. N-heptane was found to be more sensitive to the oxygen concentration than EN 590, with the DCN difference between them increasing from 0.7 to 4.1.

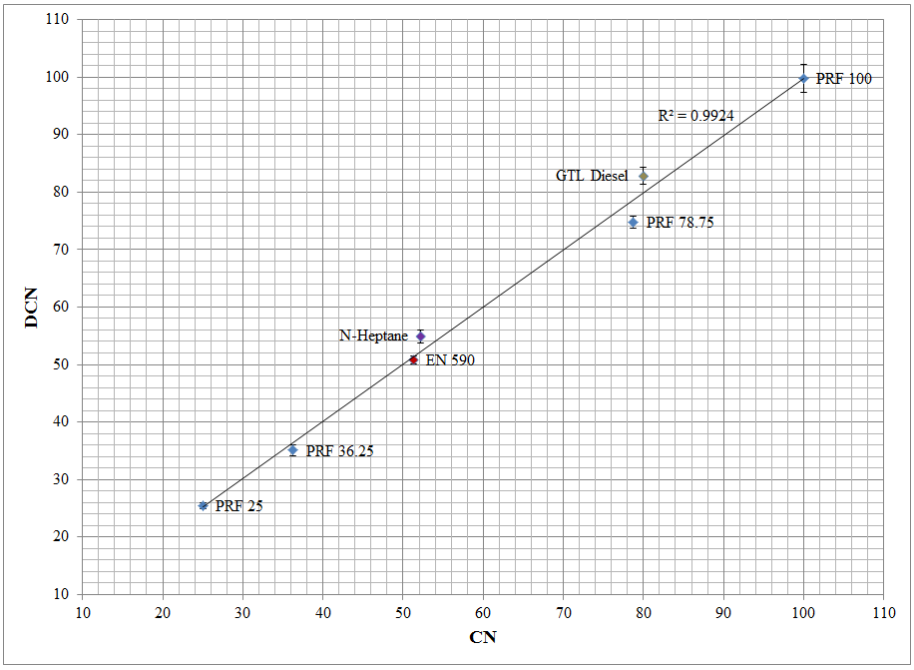

Figure 9.9: Fit between DCN and CN for high temperature, 14.9% O_2 condition as well as DCN sample standard deviation at each point.

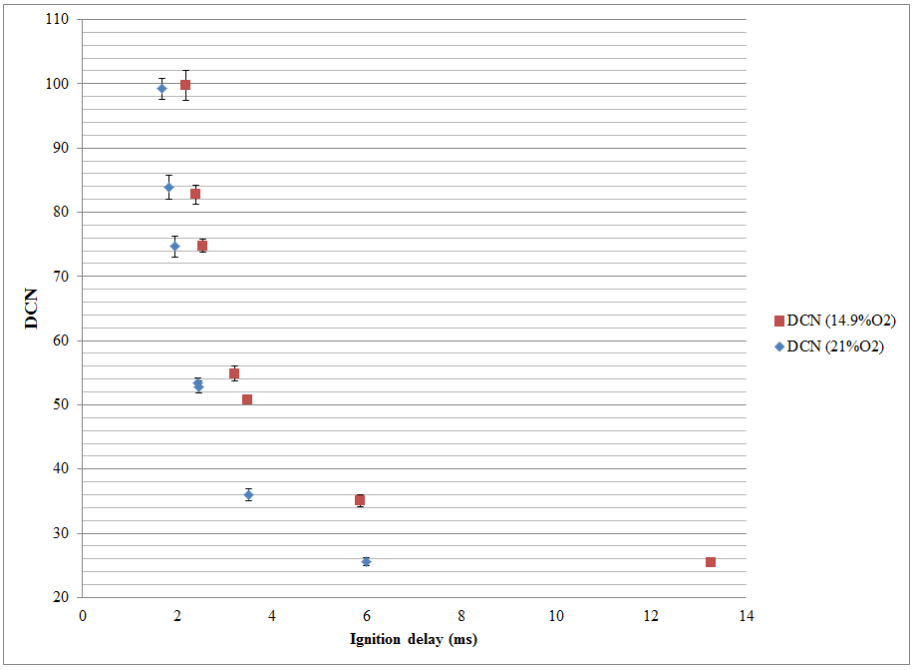

Figure 9.10: Comparison between high temperature DCN results

With respect to the flame detector based correlation, only fuels with a CN equal to or greater than EN 590 showed a result. The flame detector correlation was therefore based on fewer fuels and it was found to be more accurate for PRF 100, GTL diesel, PRF 78.75 and EN 590 but less so for n-heptane when compared with the 21% O_2 condition. The 21% O_2 condition's correlation error was dominated by GTL diesel and PRF 78.75, with a respective error of +6.7 and -6.5.

The reduction of fuels that produce an optically detectable emission was directionally consistent with the reasoning described in Section 9.1, where the increased ignition delay resulted in more time for fuel/air mixing, lowering the local equivalence ratio and thereby decreasing the amount of OH or soot produced. This decreased the intensity of the light emissions and prevented suitable optical detection.

9.3 Condition 3: Low Temperature, 21% O_2

The largest number of fuels were tested at this condition, totaling 10. Figure 9.11 indicates the ignition delay for fuels with CN of 50 and above, as the cut-off pressure defining the end of the ignition delay period is changed between 0.2 and 1.5 bar. The range was chosen based on the slowest igniting PRF 25 cycle to ensure that the ignition delays were compared at each measurement time step in the range, at the temporal resolution of the pressure measurement increment.

At this condition, it was apparent that at low cut-off pressures the cool flame remnant activity did not produce monotonically varying pressure traces for each fuel based on

their respective CN. For example, n-heptane initially has a shorter ignition delay than PRF 57.5 despite its CN being lower. Later in the ignition process, when the hot flame was dominant, its response relative to PRF 57.5 was more regular, but it's ID was still longer than EN 590 despite it having a higher CN.

The figure indicates that GTL only returned a shorter ignition delay relative to PRF 78.75 in the initial period, contrary to the expectation that it would be shorter throughout the range due to its higher CN. The behavior of GTL was peculiar because in terms of composition, GTL is highly saturated [59] and n-paraffinic [52] and therefore should behave in a manner similar to the high CN PRFs as was shown previously in Figure 9.4.

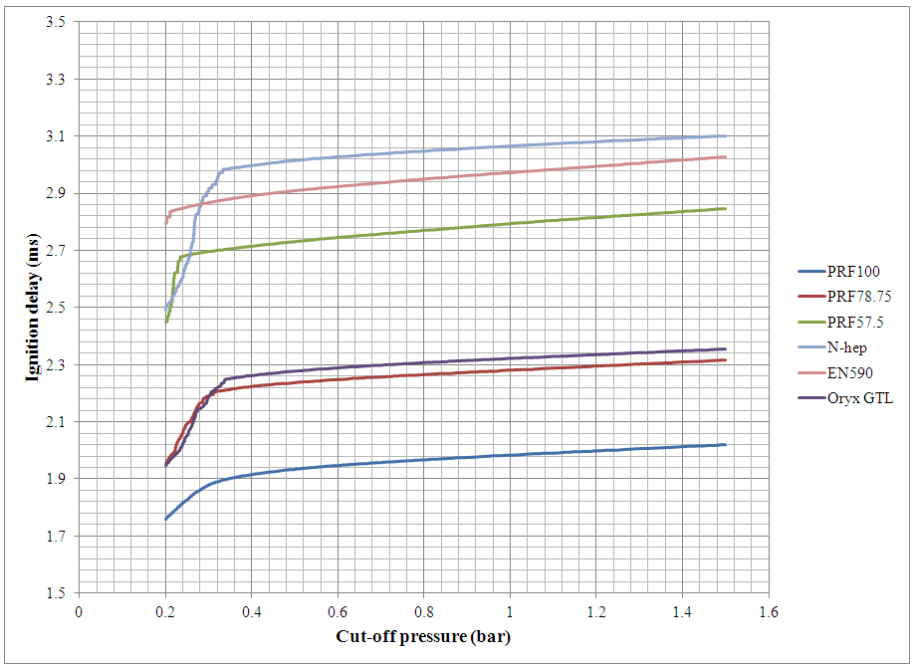

Figure 9.11: Ignition delay of fuels with CN higher than 50 at low temperature, 21% O_2 conditions.

The response of GTL may be potentially attributed to the fact that it was tested at the revised, 832.5 K temperature set-point in comparison to the PRF 78.75 that was tested at 835.5 K, in line with the attempted calibration discussed in Section 8.6. Additionally it may be attributed to a difference in evaporation time scales between the high and low temperature conditions. At the higher temperature, the higher CN, lower volatility fractions of the GTL diesel may evaporate fast enough to participate in the auto-ignition phase.

Figure 9.12 shows that at this condition the correlation error and standard deviation error are competing variables in the range where the DCN error was a minimum. It also shows that after the initial phase, the respective errors stabilise as was shown before, implying a similarity in 2nd stage ignition and subsequent combustion form.

Therefore the correlation was developed at a cut-off pressure of 1.14 bar, where the combined error was minimised, because the penalty in terms of DCN accuracy was relatively small.

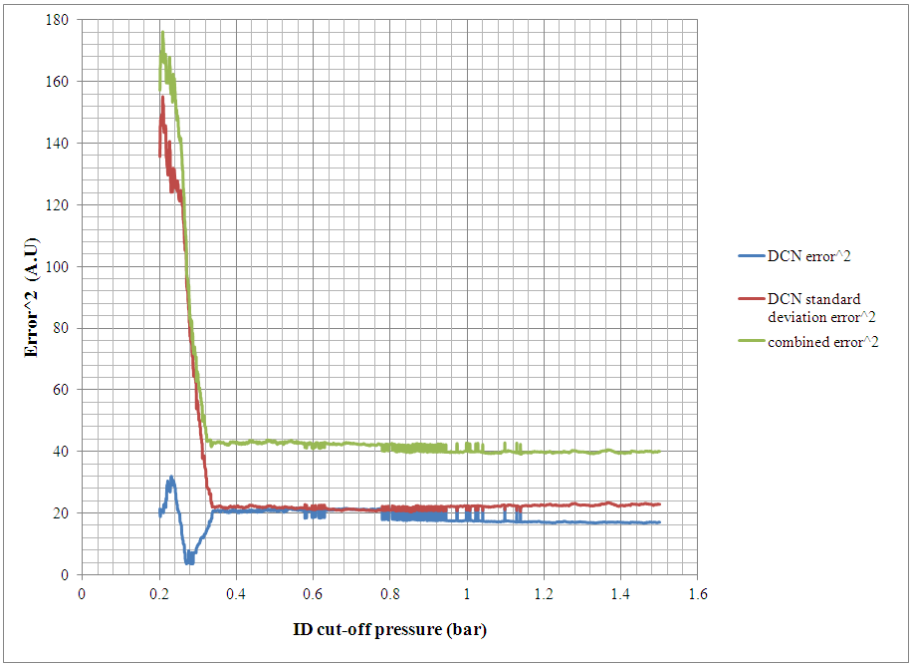

Figure 9.12: DCN correlation and standard deviation error at varying cut-off pressures defining the end of the ignition delay phase.

Figure 9.13 indicates the DCN correlation fit at this condition. The peculiar response of GTL means that the correlation at this condition was better when compared to the high temperature condition, where both PRF 78.75 and GTL diesel were tested at the same temperature after calibration, as was previously shown in Figure 9.3. However, the expected trends with respect to ID, given their CN, was not observed because GTL diesel returns a DCN of 77.3 in comparison to PRF 78.75 which returns a DCN of 79.5. This correlation returns the best fit with the highest number of fuels tested.

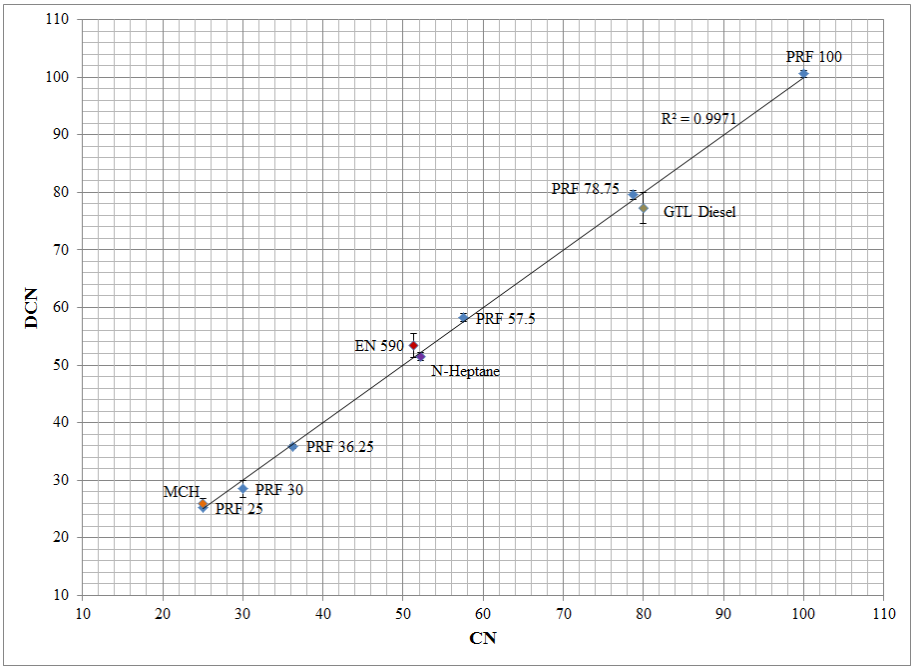

Figure 9.13: Comparison of DCN and CN at low temperature, 21% O_2 conditions

The luminosity based correlation covers the CN range from 36.25 to 100, much like the high temperature based correlation, and its agreement with the respective fuel CN is indicated in Figure 9.14. The response of GTL diesel using the optical sensor was much closer to the specified CN, with a DCN of 80.7, while PRF 78.75 returns a DCN of 79.8, which was directionally correct. The longest ignition delay that could be detected optically at this condition is 4.388 ms, while at the high temperature condition it was 3.752 ms and at 14.9% O_2 it was 4.204 ms. For the high temperature 21% O_2 condition, PRF 30 had 8 cycles that produced an optical emission with a mean ignition delay of 5.208 ms. It seemed that given the similarity in ambient density and with nominally fixed fuel injection pressure and duration, that somewhere in the range between 4.388 and 5.208 ms there was an induction period required for the fuel to mix well enough to not exhibit auto-ignition with significant quantities of luminous emissions.

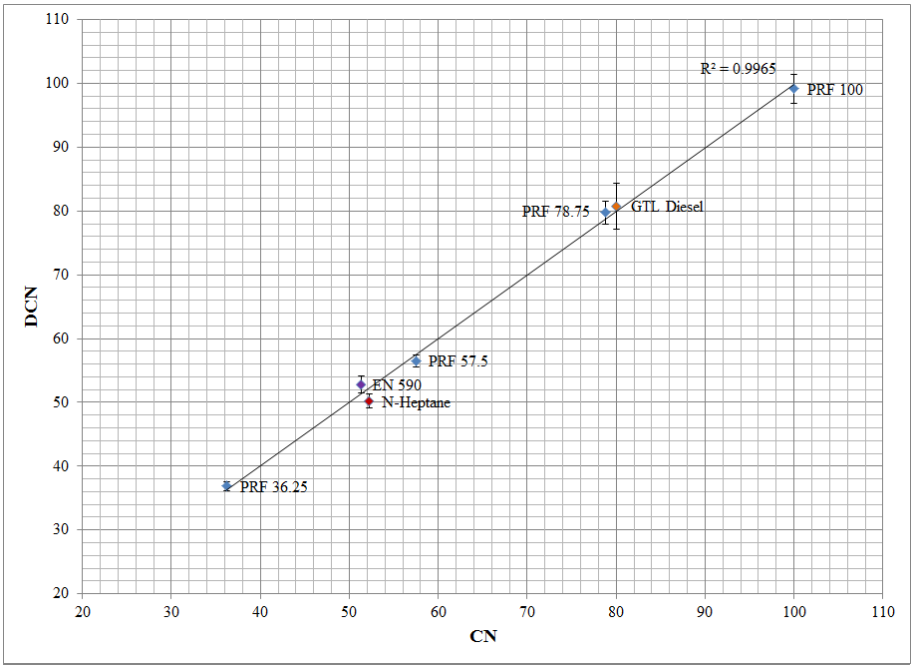

Figure 9.14: Correlation between DCN and CN for optical detector at low temperature 21% O_2 condition.

9.4 Condition 4: Low Temperature 14.9% O_2

The ignition delays were optimised in the range between 0.2 to 1.2 bar as described in the previous sections. The range was chosen based on PRF 36.25's slowest heat release cycle because it was the lowest CN fuel which showed a reaction at this condition. At this condition, the cycle to cycle variation of PRF 36.25 was large subsequent to the cool flame and therefore a relatively low cut-off pressure range of 0.2 to 1.2 bar was chosen. After a pressure of approximately 1.2 bar, the disparity between the cycles only increased and an acceptable correlation could not result. The best correlation fit was found at a cut-off pressure of 0.522 bar and Figure 9.15 compares the results of this condition with those at the low temperature, 21% O_2 concentration condition. Figure 9.15 indicates that the accuracy and precision are competing parameters between the correlations, with the 14.9% O_2 condition being more accurate, while the 21% O_2 condition returns better repeatability for most fuels. The poorer repeatability of the 14.9% O_2 condition is most evident with the three high CN fuels, which indicate larger DCN standard deviations for two of the three fuels when compared with the 21% O_2 condition. The data is represented in full in Appendix 9.4.

At the low temperature, 14.9% O_2 condition, the response of GTL to PRF 78.75 was more typical than achieved at 21% O_2, but the correlation still over-estimated its DCN. The fuel property data for GTL, as shown in Appendix A.2, indicated that approximately 40% of the fuel by mass was at a carbon number higher than C16. This

meant that while it may have a higher CN overall, the CN of its front end may not be as high as the PRF 78.75 and therefore it does not have the shorter ignition delay as expected at the 21% O_2 condition. When the fuel has more time to evaporate at this lower oxygen concentration, the GTL has shorter ignition delays as expected and allows for a better fit.

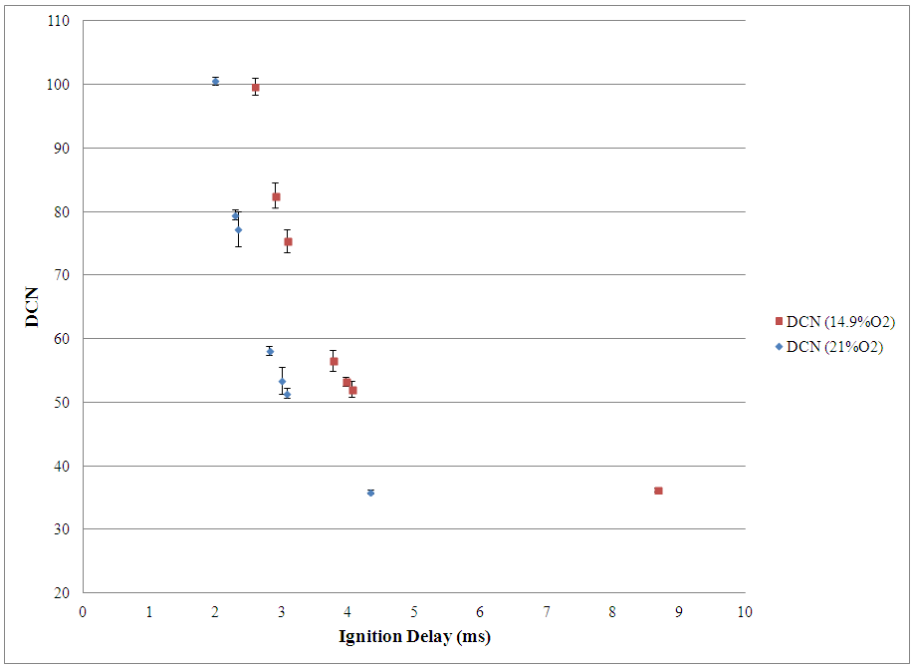

Figure 9.15: Comparison of DCN results for low temperature condition at the two respective oxygen concentrations.

The optical correlation at this condition had responses from the same number of fuels as at the high temperature condition, and once again the longest ignition delay for which an optical emission could be detected was 4.79 ms of PRF 36.25. This adds credence to the notion that there was a minimum mixing time after which optical emissions were too low for detection.

A summary of all of the ignition delay data as well as the optimised coefficients can be found in Appendix B.2 through B.5.

Chapter 10

General Discussion

10.1 End of Ignition Delay

The optimised ignition delays described in the experimental results section typically occured at the end of the 2nd stage of ID. If one were instead to consider the end of the first stage ID, by using the pressure trace turning point during the evaporation phase as the indicator of exothermicity, very different results would occur. At the high temperature, 21% O_2 condition PRF 100 would return a mean CFID of 1.068 ms with a standard deviation of 0.098 ms, while PRF 25 would return a CFID of 1.959 ms with a standard deviation of 0.057 ms. This would result in a very steep DCN/ID correlation and the resulting DCN precision would be relatively poor when compared with the results used at the hot flame.

10.2 Influence of Temperature Set-point and Control on Ignition Delay Measurements

Figure 10.1 compares the pressure based IDs for the low and high temperature, 21% O_2 conditions for all of the fuels common to both tests, except PRF 25, at the same cut-off pressure of 1.14 bar. This allows the relative response of each fuel due to 30 K nominal difference in temperature to be inferred. The figure indicates that the temperature difference had a proportional 20.3% effect on all the fuels indicated, with a high degree of linearity across the fuel CN and composition range, except for PRF 25 which showed a lower response to temperature in comparison to the other fuels. This is mostly due to the relatively low heat release rate of PRF 25 and therefore the associated low pressure rise and delay to reach the cut-off pressure.

It was shown in Figure 2.3 that over a wide range, n-heptane has a non-linear response to temperature, but at approximately 800 K the ignition delay sensitiv-

ity to temperature is reduced. Figure 10.1 generalises this result to all of the fuels indicated in the figure and shows the value of testing within this region of the ID/temperature map. If one considers that the internal gas temperatures had standard deviations of approximately 0.3 K during a test, interpolation between the two temperatures tested at would suggest a 0.68% change in ignition delay time per degree temperature change. The ignition delay standard deviations exceeded 0.52% of the mean for all fuels, at all conditions used. This suggests that the temperature control was sufficient because a temperature change of 0.74 K would be necessary for the temperature alone to cause the minimum required variation, based on the aforementioned interpolation. However, it does indicate the strong influence temperature control has on the resulting data.

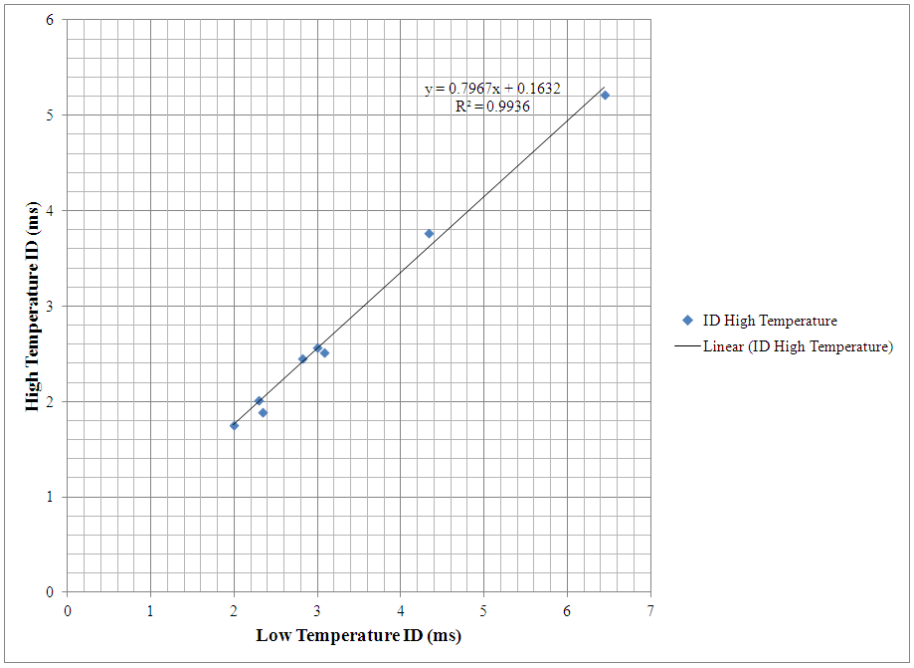

Figure 10.1: Comparison of High and Low Temperature 21% O_2 Ignition delays.

10.3 Effect of Oxygen Concentration on ID

The effect of oxygen concentration on the resulting DCN correlations at the low temperature was shown in Section 9.4 and is replicated in Figure 10.2, this time indicating the effect on the ignition delay instead. It is apparent that when using the same 0.522 bar cutoff pressure for the 21% O_2 condition as the 14.9% O_2 condition, that the oxygen concentration does not have a linear effect on ID between the two conditions, based on the relatively poor fit of the trend line indicated in the figure. It was also apparent that the change in oxygen concentration had the strongest effect on n-heptane, as highlighted in the figure, which lies well above the trend-line. This may be attributed to its higher volatility which would result in a leaner mixture when it

auto-ignites at the 14.9% O_2 condition. Also highlighted is the response of PRF 100, which at the reduced oxygen condition undergoes a much larger and more distinct cool flame than occured at the 21% O_2 condition. The hot flame subsequent to cool flame is more variable and this causes more variability in the resulting ID worsening the correlation between the two conditions. The consequence of this is that the oxygen concentration of the charge gas must be tightly controlled to achieve accurate correlations. It also suggests that using oxygen/nitrogen gas mixtures, which was done in this project may be unwise, because accurate and repeatable blending may be difficult to achieve.

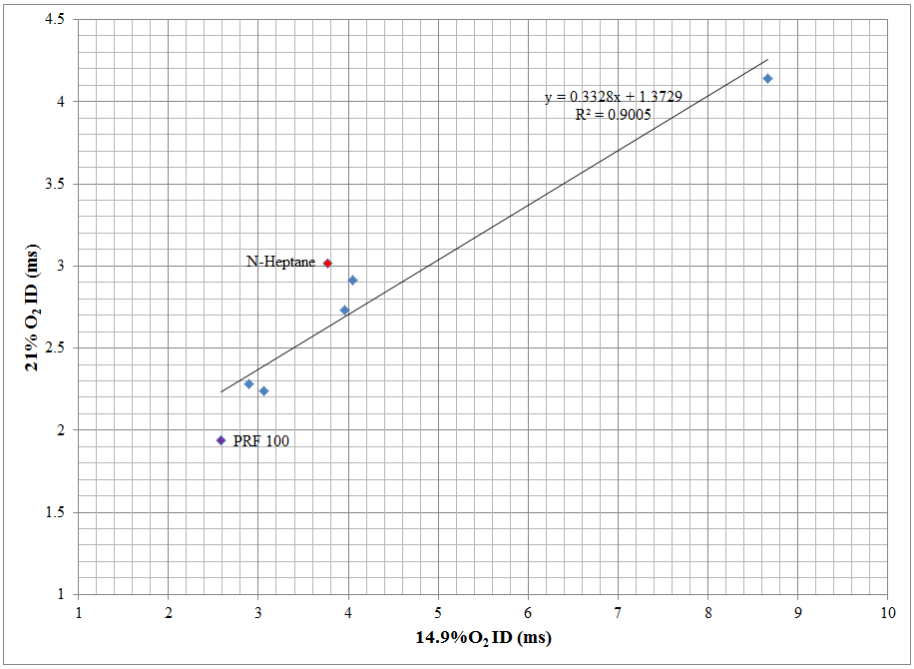

Figure 10.2: Comparison of 21% and 14.9% O_2 concentration IDs at low temperature

10.4 Effect of Blending Uncertainty on DCN Correlation Accuracy

It was shown in section 7.3 that the PRF blends have a CN uncertainty due to the blending method used. The magnitude of the blending CN uncertainty compared with DCN error for the low temperature 21% O_2 condition is shown in Table 10.1. The table indicates that the blending uncertainty represents a significant fraction of the DCN error for this condition and that improved blending accuracy may result in a better DCN correlation.

PRF	DCN error	Blend uncertainty ±
100	0.59	0
78.75	0.78	0.40
57.5	0.69	0.36
36.25	-0.34	0.23
30	-1.49	0.23
25	0.17	0.23

Table 10.1: DCN error at low temperature 21% O_2 condition as well as the associated blending uncertainty

10.5 Effect of Fuel Composition on DCN Correlation Fit

Table 10.2 indicates the DCN correlation fit if only the PRFs are used for the low temperature, 21% O_2 condition at an optimised cut-off pressure of 0.911 bar. The correlation form used has four variables and therefore this correlation, based on six fuels, is overdetermined. The Table shows that the PRFs can be correlated very accurately, considering the blending uncertainties mentioned in the previous section.

It is apparent that the different fuel classes respond in a varied manner to the fixed test conditions as alluded to in Section 2.1. This is inferred based on the relatively good agreement that the PRF-only fuels are able to achieve over the CN range of 25-100 when compared to the correlation presented in the afformentioned section. However, despite the often large difference in things such as volatility, in the case of n-heptane, it still possible to correlate CN with ID well. It also indicates the importance of developing a correlation with a variety of fuels because the non-PRF fuels return less accurate results if the PRF-only correlation is used for determining DCN.

PRF	DCN error
100	0.14
78.75	-0.38
57.5	0.27
36.25	0.32
30	-0.68
25	0.33

Table 10.2: DCN correlation error when only PRFs are considered at the low temperature, 21% O_2 condition.

Chapter 11

Conclusions

An IQT was modified to incorporate a common rail diesel injector and the control system was redeveloped to allow flexible control of the device. The system operated as required, however due to problems with the injector, only a limited number of tests could be performed. The major findings of the experimental regimen are the following:

1. The ignition delay of a wide variety of middle distillate and diesel surrogate fuels can be adequately correlated with a single equation based on the respective fuel's ignition delay. The ability to correlate the ID with the CN indicates that the respective fuel's chemistry is the most dominant aspect influencing their ID, with the physical evaporation related effects only playing a minor, secondary role.

2. A CN of 80 was ascribed to GTL diesel for the purposes of correlation development as mentioned in Section 9.1. The data strongly suggests that this rating is too low, based on its response relative to PRF 78.75. This conclusion has been noted in literature by Yates et al. [13]. They tested a different GTL diesel batch from the same refinery, and found a DCN of 77.3 using ASTM D6890. However, when analysed using an ignition delay and CFR engine model they revised the rating to 86.9. In comparison, the four conditions used in this work returned DCNs of 83.9, 82.8, 77.3 and 82.6 respectively.

3. It was found in this work that the duration of the cool flame, particularly for low CN fuels, was variable and therefore the subsequent hot flame was poorly synchronised between the cycles comprising a test, resulting in poor ID precision. This conclusion was also noted by Henien [60] , when testing low CN fuels in the CFR cetane engine.

4. Reduction of the charge gas oxygen concentration decreased the DCN/ID gradient, as implied by literature. This sporadically caused an improvement in

DCN precision, but with only 1 test performed at each condition, this result is tenuous. The reduction of oxygen concentration also exacerbated the cool flame which had detrimental effects as previously discussed.

5. The ASTM method for the IQT only covers the DCN range from 33 to 64. The ability to correlate fuels over a wide range with reasonable accuracy suggests that improving the injector fuel mixing characteristics may be beneficial for increasing the range over which the device can be used. However, this concept is limited by the precision of the defining method, ASTM D613, and may suggest that a DCN correlation independent of the D613 CN should be developed.

Chapter 12

Recommendations

The aim of this project was to develop a flexible fuels research apparatus that could be used to study diesel auto-ignition and use it to redevelop the correlation between DCN and ignition delay. The following suggestions may improve the device and its output relative to what was achieved in this work:

1. The injector was a constant source of problems. It should be disassembled and checked for corrosion, deposition and perhaps viewed under a microscope to see if there are signs of wear on the needle. If it shows sign of damage, it should be replaced and all subsequent tests should be performed with a lubricity or detergency additive as standard.

2. The tests performed in this work must be repeated many times so that the standard deviation of the respective ignition delay mean can be determined. In this work, the DCN repeatability was based on 1 test, however the various ASTM methods mentioned for DCN determination make use of multiple tests for each fuel to determine the mean ID's repeatability for estimating the DCN confidence interval.

3. The gasket used to seal between the injector housing and the combustion chamber is likely to conduct more heat than the original device, and is therefore thought to be the major source of the greater temperature gradient measured in this work. A different gasket material should be considered, such as Klinger K1000, which has much lower conductivity, while simultaneously being able to operate at the required temperature and pressure.

4. The fuel flushing sequence is quite slow. Through adequate placing of additional valves, this process can be automated and made to be much faster.

5. The original device made use of a much shorter cycle time. The effect of cycle time was not substantially considered in this work and is worthy of consideration.

6. The sequencing of the fuel pump relative to the point when injection occurs was sporadically out of synchronisation. This could be improved by placing a sensor in the pump to monitor its stroke and only inject when its piston is away from the ends of its stroke. The piston has a vented guide on the top of the pump that could be easily exploited in this fashion. Alternatively, the Labview code could be amended to check the fuel pressure at the beginning of each injection, and repeat cycles where the fuel pressure exceeds a specified tolerance.

7. The laser diode used for the injection timing was supported in a temporary holder. This moved sporadically and required realignment. A more permanent bracket would improve ease of use as well as slightly improve ID accuracy.

8. The peak combustion pressures in this work were modest relative to the original device's peak pressures. Tests should be performed to assess the effects of charge pressure variation on the ignition delay in order to determine if improved correlation may occur at higher charge pressures.

Bibliography

[1] Luc N. Allard, Gary D. Webster, Thomas W. Ryan III, Dale Ott, and Craig W. Fairbridge. Diesel Fuel Ignition Quality As Determined In The Ignition Quality Tester. *SAE Technical Paper*, 961182, 1996.

[2] ASTM D613-13. Standard Test Method for Cetane Number of Diesel Fuel Oil. *ASTM International*.

[3] Luc N. Allard, Gary D. Webster, Thomas W Ryan Iii, Andrew C. Matheaus, Gary Baker, Andrew Beregszaszy, Harry Read, Kate Mortimer, Garry Jones, and Thomas W. Ryan III. Diesel Fuel Ignition Quality as Determined in the Ignition Quality Tester (IQT) - Part IV. *SAE Technical Paper*, 2001-01-35, 2001.

[4] ASTM D6890-13b. Standard Test Method for Determination of Ignition Delay and Derived Cetane Number (DCN) of Diesel Fuel Oils by Combustion in a Constant. *ASTM International*.

[5] John B. Heywood. Knock Fundamentals. In *Internal Combustion Engine Fundamentals*, chapter 9, pages 463–467. McGraw-Hill, 1988.

[6] SANS 342 : Automotive Diesel Fuel, 2006.

[7] ASTM D4737-10. Standard Test Method for Calculated Cetane Index by Four Variable Equation. *ASTM International*.

[8] ASTM D976. Standard Test Method for Calculated Cetane Index of Distillate Fuels. *ASTM International*.

[9] Noel Bezaire, Kapila Wadumesthrige, K.Y. Simon Ng, and Steven O. Salley. Limitations of the use of cetane index for alternative compression ignition engine fuels. *Fuel*, 89(12):3807–3813, December 2010. ISSN 00162361.

[10] ASTM D7170-14. Standard Test Method for Determination of Derived Cetane Number (DCN) of Diesel Fuel Oils - Fixed Range Injection Period , Constant Volume Combustion Chamber Method. *ASTM International*.

[11] ASTM D7668-14a. Standard Test Method for Determination of Derived Cetane Number (DCN) of Diesel Fuel Oils-Ignition Delay and Combustion Delay Using a Constant Volume Combustion Chamber Method. *ASTM International*.

[12] Andy D. B. Yates, Carl L. Viljoen, and André Swarts. Understanding the Relation Between Cetane Number and Combustion Bomb Ignition Delay Measurements. *SAE Technical Paper*, 2004-01-20, 2004.

[13] Andy D. B. Yates, Carl Viljoen, and Owen Metcalf. An Accurate Determination of the Cetane Number Value of GTL Diesel. *SAE International*, 2007-01-00, January 2007.

[14] Luc N. Allard, Norman J. Hole, Gary D. Webster, Andrew Beregszaszy, Craig W. Fairbridge, Jean Cooley, K. Mitchell, E. Keith Richardson, G. Elliot, Nigel, and J. Rickeard, David. Diesel Fuel Ignition Quality as Determined in the Ignition Quality Tester-Part II. *SAE Technical Paper*, 971636, 1997.

[15] Owen J Metcalf, André Swarts, and Andy Yates. A Study of the Ignition-Delay Character of n-Heptane in the IQT Combustion Bomb Using CFD Modelling. *SAE Technical Paper*, 2007-01-00, 2007.

[16] Nicholas Savage. The use of a modified IQT apparatus and detailed chemical kinetic model to investigate the atmospheric auto-ignition characteristics of model fuels. MSc. Thesis University of Cape Town, 2009.

[17] John B. Heywood. Ignition Delay. In *Internal Combustion Engine Fundamentals*, chapter 10, pages 539–562. 1988.

[18] Gareth Floweday. *Two Contrasting Approaches to Auto-Ignition Modelling for HCCI Engines*. PhD thesis, University of Cape Town, 2010.

[19] Hamza M. Abo El Ella, J. E. D. Gauthier, and G. D. Webster. Study on the Effects of Nozzle Fuel Spray Pattern on Cetane Number Measurment as Determined in the Ignition Quality Tester (IQT). *SAE Technical Paper*, 2008-01-15, 2008.

[20] Luc N. Allard, Gary D. Webster, Thomas W. Ryan III, Gary Baker, Andrew Beregszaszy, Craig W. Fairbridge, Alfred Ecker, and Josef Rath. Analysis of the Ignition Behaviour of the ASTM D-613 Primary Reference Fuels and Full Boiling Range Diesel Fuels in the Ignition Quality Tester (IQT) - Part III. *SAE Technical Paper*, 1999-01-35, 1999.

[21] D. L Siebers. Scaling liquid-phase fuel penetration in diesel sprays based on mixing-limited vaporization. *SAE Technical Paper*, 1999-01-05, 1999.

[22] G E Bogin, A M Dean, A Defilippo, J Y Chen, and G Chin. Modeling the Fuel Spray and Combustion Process of the Ignition Quality Tester with KIVA-3V. In *Fall meeting of the Western States Section of the Combustion Institute*, 2009.

[23] Chitralkumar V. Naik, Karthik Puduppakkam, Ellen Meeks, and Long Liang. Ignition Quality Tester Guided Improvements to Reaction Mechanisms for n -Alkanes: n -Heptane to n -Hexadecane. *SAE International*, 2012-01-01, April 2012.

[24] Ziliang Zheng, Tamer Badawy, Naeim Henein, and Eric Sattler. Investigation of Physical and Chemical Delay Periods of Different Fuels in the Ignition Quality Tester. *Journal of Engineering for Gas Turbines and Power*, 135(6):061501–1, May 2013. ISSN 0742-4795.

[25] G. E. Bogin Jr., A. M. Dean, M. A. Ratcliff, J. Luecke, and B. T. Zigler. Expanding the experimental capabilities of the ignition quality tester for autoigniting fuels. *SAE International Journal of Fuels and Lubricants*, 3(1):353–367, 2010.

[26] S. Rabl, T.J. Davies, A.P. McDougall, and R.F. Cracknell. Understanding the relationship between ignition delay and burn duration in a constant volume vessel at diesel engine conditions. *Proceedings of the Combustion Institute*, 35(3):2967–2974, June 2015. ISSN 15407489.

[27] J. V. Pastor, J. M. García-Oliver, J. G. Nerva, and B. Giménez. Fuel effect on the liquid-phase penetration of an evaporating spray under transient diesel-like conditions. *Fuel*, 90(11):3369–3381, November 2011. ISSN 00162361.

[28] Advanced Engine Technologies. Procedures Manual: Ignition Quality Tester for Diesel Fuel Cetane Number Evaluation, 2002.

[29] D.L. Siebers. Liquid-phase fuel penetration in diesel sprays. *SAE Technical Paper*, 980809, 1998.

[30] Brenainn A. Cross. An Investigation into the Effects of Diesel Fuel Properties on the Injection Characteristics of a Common Rail Injection System. MSc. Thesis University of Cape Town, 2012.

[31] Bernard Fryskowski and Janusz Waldemar Mazur. A Method for Distributor Fuel Injection Pump and Injectors Diagnostics in Diesel Engines. *SAE Technical Paper*, 2004-01-00, 2004.

[32] Kistler. Engine Pressure Measurement for Research and Development, 2010. URL `www.kistler.com/medias/sys_master/.../100-460e-12.10.pdf`.

[33] AVL. Pressure Sensors for Combustion Analysis. URL `https://www.avl.com/c/document_library/get_file?uuid=5c7f1865-39d4-47f6-86c8-e98fd55e28e8&groupId=10138`.

[34] J. Dernotte, C. Hespel, F. Foucher, S. Houillé, and C. Mounaïm-Rousselle. Influence of physical fuel properties on the injection rate in a Diesel injector. *Fuel*, 96:153–160, June 2012. ISSN 00162361.

[35] James P Szybist and André L Boehman. Behavior of a Diesel Injection System with Biodiesel Fuel. *SAE Technical Paper*, 2003-01-10, 2003.

[36] Geoff Miller. Development of a Constant-Volume Combustion Apparatus for Fuels Research. MSc. Thesis University of Cape Town, 2007.

[37] Maximator GmbH. Air driven high pressure pumps up to 7000 bar, 2014. URL http://www.maximator.de/assets/mime/f5018004b8e65d6b33d5707eca218ea3/MAXIMATOR-High-Pressure-Pumps-08-2014.pdf.

[38] Jingyu Zhu, Olawole Abiola Kuti, and Keiya Nishida. Effects of Injection Pressure and Ambient Gas Density on Fuel - Ambient Gas Mixing and Combustion Characteristics of D . I . Diesel Spray. *SAE International*, 2011-01-18, 2011.

[39] Teledyne ISCO. Precision Syringe Pumps, 2011. URL http://www.isco.com/WebProductFiles/Product_Literature/105/D-Series_Pumps_Brochure.pdf.

[40] Agilent Technologies. Infinite Power Range of the Agilent 1290 Infinity LC, 2015. URL http://www.chem.agilent.com/en-US/products-services/Instruments-Systems/Liquid-Chromatography/1290-Infinity-Binary-LC-System/Pages/powerrange.aspx.

[41] Lyle M. Pickett. Engine Combustion Network: " "Spray-A" and "Spray-B" Operating Condition, 2014. URL http://www.sandia.gov/ecn/cvdata/dsearch/frameset.php?nam=1.

[42] SABS Standards Division. *SANS 347: Categorization and conformity assessment criteria for all pressure equipment*. 2012.

[43] J.P. Holman. Pressure Measurement - Dynamic Response Considerations. In *Experimental Methods for Engineers*, chapter 6.2, pages 258–259. McGraw-Hill, seventh ed edition, 2001.

[44] Peter M. Lillo, Lyle M. Pickett, Helena Persson, Oivind Andersson, and Sanghoon Kook. Diesel Spray Ignition Detection and Spatial/Temporal Correction. *SAE Int. J. Engines*, 5(3):1330–1346, April 2012.

[45] Honeywell. SD5620/SD5630 Optoschmitt Detector. URL http://sensing.honeywell.com/index.php?ci_id=39238&la_id=1&name=SD5620-001.

[46] Unknown. NI 9213 Operating Instructions and Specifications, 2009. URL http://www.ni.com/pdf/manuals/374916a.pdf.

[47] National Instruments. 9213 Operating Instructions and Specifications, 2009. URL http://www.ni.com/pdf/manuals/374916a.pdf.

[48] National Instruments. 9215 Operating Instructions and Specifications, 2011. URL http://www.ni.com/pdf/manuals/373779f.pdf.

[49] Robert Bosch Gmbh. Bosch Pressure Sensors.

[50] Mark P B Musculus, Thierry Lachaux, Lyle M Pickett, and Cherian A Idicheria. End-of-injection over-mixing and unburned hydrocarbon Emissions in Low-Temperature- Combustion Diesel Engines. *SAE Technical Paper Series*, 2007-01-09, 2007.

[51] L M Pickett, J Manin, C L Genzale, D L Siebers, M P B Musculus, and C a Idicheria. Relationship Between Diesel Fuel Spray Vapor Penetration/Dispersion and Local Fuel Mixture Fraction. *SAE International Journal of Engines*, 4(1):764–799, April 2011.

[52] Masahiro Fukumoto. Experimental Investigation of Lubricity Improvement of Gas-to-liquid (GTL) Fuels with Additives for Low Sulphur Diesel Fuel. *SAE International*, 2003-01-19, 2014.

[53] Satbir Singh, Mark P.B. Musculus, and Rolf D. Reitz. Mixing and flame structures inferred from OH-PLIF for conventional and low-temperature diesel engine combustion. *Combustion and Flame*, 156(10):1898–1908, October 2009. ISSN 00102180.

[54] D.L. Siebers and Brian Higgins. Flame lift-off on direct-injection diesel sprays under quiescent conditions. *SAE Technical Paper*, 2001-01-05, 2001.

[55] Mark P B Musculus, Paul C. Miles, and Lyle M. Pickett. Conceptual models for partially premixed low-temperature diesel combustion. *Progress in Energy and Combustion Science*, 39(2-3):246–283, April 2013. ISSN 03601285.

[56] J.E. Dec. A Conceptual Model of DI Diesel Combustion Based on Laser-Sheet Imaging. *SAE Technical Paper*, 970873, 1997.

[57] Brian Higgins, Dennis Siebers, and Allen Aradi. Diesel-Spray Ignition and Premixed-Burn Behavior. *SAE Technical Paper*, 2000-01-09, 2000.

[58] Michael J Murphy, Joshua D Taylor, and Robert L Mccormick. Compendium of Experimental Cetane Number Data. NREL/SR-54(September), 2004.

[59] Paul Schaberg and Mark Wattrus. Comparative Emissions Performance of Blends of GTL Diesel and FAME. *SAE Technical Paper*, 2014-01-27, 2014.

[60] Naeim A Henein. Cetane Scale : Function , Problems and Possible Solutions. *SAE Technical Paper*, 870584, 1987.

Appendix A

Fuel Properties

A.1 Solvent Details

The PRFs and synair lots for each test are indicated in the following tables. The low temperature 21% O_2 tests were done first and then a second blend of those fuels was produced for all subsequent tests at that CN i.e. for the fuels indicated in Table A.1, two blends were produced. For each set of PRF tests, all of the PRF 100 and PRF 15 were treated with the lubricity additive before blending and hence the additive content should be the same for each set of tests.

Fuel	Hexadecane Lot #	Heptamethylnonane Lot #	Synair batch #
PRF 100	STBD 5779V	N/A	140901/01
PRF 78.75	STBD 5779V	STBD 5642V	140901/01
PRF 57.5	STBD 5779V	STBD 5642V	140901/01
PRF 36.25	STBD 5779V	STBD 5642V	140901/01

Fuel	Lot #	Synair batch #
N-heptane	STBD 5823V	140901/01
Methylcyclohexane	STBB 3822V	140901/01
EN590	1	140901/01

Table A.1: Initial reagents and corresponding lot/batch numbers

The PRF blends indicated in Table A.2were used for the high temperature and 14.9% O_2 conditions as well as the low temperature 21% O_2 conditions if they were not initially tested. They too were treated before blending to ensure the same amount of lubricity additive across all of the blends.

Fuel	Hexadecane Lot #	Heptamethylnonane Lot #	Synair batch #
PRF 100	STBD 5779V	N/A	140829/02
PRF 78.75	STBD 5779V	STBF 0890V	140930/02
PRF 57.5	STBD 5779V	STBF 0890V	140829/02
PRF 36.25	STBD 5779V	STBF 0890V	140930/02
PRF30	STBD 5779V	STBF 0890V	140829/02
PRF25	STBD 5779V	STBF 0890V	140829/02

Fuel	Lot #	Synair batch #
N-heptane	STBD 5823V	140901/01
EN590	1	140829/02
GTL Diesel	1	140930/02

Table A.2: Final Reagent batch/lot numbers

As was required, at the change of a gas bottle or the rebuilding of the device, the IQT was calibrated with n-heptane at the low temperature, 21% O_2 condition. The results of the various calibrations are indicated in Table A.3. Only after the final rebuild of the device, did the temperature gradient change enough to warrant changing the set-points as was discussed in Section 8.6.

Test #	Date	ID (ms)	ID std.dev (ms)	Fuel Lot #	Synair batch #
1	30/09	3.091	0.031	STBD 5823V	140901/01
2	06/10	3.124	0.034	STBD 8507V	140901/01
3	06/10	3.1307	0.0359	STBD 8507V	140901/01
4	15/10	3.0479	0.0275	STBD 8507V	140829/02
5	16/10	3.079	0.0297	STBD 8507V	140829/02
6	04/12	3.134	0.046	STBD 8507V	140930/02

Table A.3: N-heptane calibration results at low temperature, 21% O_2 conditions

A.2 Full Boiling Range Fuel Properties

The following table indicates the fuel properties of the full boiling range diesel fuels used in this work. The data was produced by an external laboratory and the author had no hand in producing it.

Properties of Diesel Fuels

Property	Units	Method	EN590 Diesel	GTL Diesel
Appearance	Rating	CALTEX CMM 76	1	Pass
Colour	Rating	ASTM D1500	1	< 0.5
Density at 15 °C	kg/l	ASTM D4052	0.8317	0.7698
Density at 20 °C	kg/l		0.8283	0.7654
Distillation		ASTM D86		
IBP	°C		158.4	150.6
0.05	°C		181	173.9
0.1	°C		189.6	184.3
0.2	°C		207.6	201.8
0.3	°C		225.4	223.1
0.4	°C		243.9	243.9
0.5	°C		258.7	262.8
0.6	°C		272.7	280.8
0.7	°C		287.1	298.7
0.8	°C		303.7	317.3
0.9	°C		326.1	338.6
0.95	°C		344.7	352.4
FBP	°C		357.4	356.7
Copper Corrosion		ASTM D130	1A	1b
Total Sulphur	mg/kg	ASTM D5453	4	1
Nitrogen Content	mg/kg	ASTM D 4629	<0.01	
Water Content	mg/kg	IP438	60	<250
Acid Number/Total Acids	mg KOH/g	ASTM D664	0.022	
Bromine number	gBr/100g	ASTM D1159	0.77	0.8
Kinematic Viscosity at 40 °C	cSt	ASTM D445	2.35	2.2
Flash point	°C	ASTM D93	60	57
Derived Cetane Number	Rating	ASTM D6890 (Mod)	51.3	80
Cetane Number	Rating	ASTM D613	51.3	
Cetane Index	Rating	ASTM D4737	50	
Cloud point	°C	ASTM D2500	-7	-5
CFPP	°C	IP309	-23	-7
Pour point	°C	ASTM D97	-27	-9
Carbon residue	mass %	ASTM D4530	<0.01	0.01
Ash content	mass %	ASTM D482	<0.01	< 0.01
Lubricity (HFRR)	um	CEC F06-A-96	405	542
SL BOCLE	g	ASTM D6078	Not Reported	
Oxidation stability	mg/100 mL	ASTM D2274	0.4	0.2
Total contaminants	mg/kg	IP440	1	

Property	Units	Method	EN590 Diesel	GTL Diesel
Mononuclear Aromatics	mass %	IP391	Not Reported	<0.01
Polynuclear (2+3) Aromatics	mass %		Not Reported	<0.01
Total Aromatics	mass %		18.23	<0.01
Aromatics	vol. %	ASTM D1319	Not Reported	
Olefins	vol. %	ASTM D1319		
Carbon Content	mass %	ASTM D5291	86.45	84.57
Hydrogen Content	mass %		13.55	15.43
Atomic H/C Ratio		Calculation	1.87	2.17
Atomic O/C Ratio				
C/H Mass Ratio			6.38	
Gross Heat of Combustion	MJ/kg	ASTM D 4809	45.82	47.26
Net Heat of Combustion	MJ/kg		42.94	43.99
Net Heat of Combustion	MJ/l		35.71	33.67
Net Heat of Combustion	Btu/lb		Not Reported	
Oxygen Content	mass %	ASTM D5291	Not Reported	
Conductivity	pS/m	ASTM D2624	110	
Water & Sediment	vol. %	ASTM D2709	<0.01	
Zinc Content (ICP-ES)	mg/kg	IP 501	Not Reported	
Zinc Content (ICP-ES)	mg/kg	IP 501 MOD		

Appendix B

DCN Correlation Data

B.1 Optimised Pressure Based Coefficients

Condition	A	B	C	D
High Temp, 21% O_2	66.13	0.82	-1.29	17.72
High Temp, 14.9% O_2	54.94	1.59	-0.77	17.19
Low Temp, 21% O_2	723.14	-0.31	-2.69	24.25
Low Temp, 14.9% O_2	41702516	-4.25	-6.96	35.55

B.2 Condition 1 Data

Fuel	CN	Optimised mean ID (ms)	pressure ID std.dev (ms)	DCN	DCN std.dev	Optical mean (ms)	optical std.dev (ms)
PRF 100	100	1.669	0.0134	99.24	1.66	1.508	0.014
GTL diesel	(80)	1.818	0.021	83.86	1.82	1.582	0.040
PRF 78.75	78.75	1.941	0.024	74.65	1.57	1.771	0.021
PRF 57.5	57.5	2.336	0.032	56.26	1.05	2.239	0.057
N-heptane	52.2	2.427	0.026	53.47	0.76	2.473	0.045
EN 590	51.3	2.451	0.033	52.78	0.92	2.283	0.042
PRF 36.25	36.25	3.516	0.101	36.03	0.89	3.752	0.159
PRF 30	30	4.708	0.227	29.12	0.86	N/A	N/A
PRF 25	25	5.996	0.348	25.59	0.69	N/A	N/A

B.3 Condition 2 Data

Fuel	CN	Optimised mean ID (ms)	pressure ID std.dev (ms)	DCN	DCN std.dev	Optical mean (ms)	optical std.dev (ms)
PRF 100	100	2.181	0.023	99.76	2.39	2.540	0.048
GTL diesel	(80)	2.386	0.953	82.76	1.46	2.847	0.051
PRF 78.75	78.75	2.531	0.023	74.77	1.04	3.018	0.073
N-heptane	52.2	3.478	0.280	54.89	1.17	3.884	0.158
EN 590	51.3	3.219	0.059	50.82	0.66	4.202	0.265
PRF 36.25	36.25	5.861	0.023	35.08	0.91	N/A	N/A
PRF 25	25	13.268	0.05	25.42	0.48	N/A	N/A

B.4 Condition 3 Data

Fuel	CN	Optimised mean ID (ms)	pressure ID std.dev (ms)	DCN	DCN std.dev	Optical mean (ms)	optical std.dev (ms)
PRF 100	100	1.995	0.022	100.59	1.92	1.774	2.306
GTL diesel	(80)	2.331	0.068	77.27	2.73	2.024	3.595
PRF 78.75	78.75	2.290	0.019	79.53	1.08	2.040	1.815
PRF 57.5	57.5	2.808	0.023	58.19	0.67	2.608	1.005
N-heptane	52.2	3.075	0.031	51.47	0.68	2.757	1.356
EN590	51.3	2.989	0.037	53.42	0.88	2.883	1.139
PRF36.25	36.25	4.331	0.151	35.91	1.02	4.388	0.668
PRF30	30	6.440	0.432	28.51	0.73	N/A	N/A
PRF25	25	11.59	2.846	25.17	0.60	N/A	N/A
MCH	25	9.200	0.717	25.94	0.34	N/A	N/A

B.5 Condition 4 Data

Fuel	CN	Optimised mean ID (ms)	pressure ID std.dev (ms)	DCN	DCN std.dev	Optical mean (ms)	optical std.dev (ms)
PRF100	100	2.583	0.017	99.70	1.27	2.929	0.039
GTL diesel	(80)	2.895	0.031	82.57	1.96	3.407	0.063
PRF78.75	78.75	3.067	0.036	75.40	1.85	3.589	0.079
PRF57.5	57.5	3.966	0.057	53.33	0.74	4.651	0.215
N-heptane	52.2	3.770	0.069	56.59	1.61	4.482	0.219
EN 590	51.3	4.051	0.080	52.09	1.25	4.790	0.265
PRF 36.25	36.25	8.671	1.438	36.31	0.35	N/A	N/A

Appendix C

Labview Code

The various Labview VIs operate on a state machine principle. In a state machine, the code moves from one group of code to the next after completing various tasks and satisfying the necessary criteria.

C.1 FPGA VI

On the FPGA, there is one main loop that starts when the VI is deployed. It begins by initialising the various parameters, such as the valves, to safe states, and then it moves into the measurement loop where it remains until it is stopped. When the command to stop is received, it moves out of the measurement state and once again ensures the system is in a benign state before stopping code execution.

The FPGA code takes the measured raw data and converts it to fixed point numbers which are indicated on its front panel. During operation, the host VI and RT are able to read and write values to the FPGA's front panel and this therefore serves as the medium of communication between the three VIs.

The measurement state features five loops, of which four run continuously. The final loop takes the high speed pressure and voltage measurements, and waits until the "single shot" command on the FPGA changes to true before it commences, indicating that fuel injection is imminent. This high speed loop iterates 4095 times, to take the necessary measurements and transfers the data into a buffer. The buffer then transfers this data to the host for further processing and storage. This loop then returns to the "waiting state," ready for the next injection. The loop duration is measured for each iteration and is also stored in the buffer. The sum of the loop durations are added during post processing to infer the injection and ID timing.

The measurement speed is dependent on the modules used (NI 9215) and the number of channels (1 and 2 respectively) used per module [48] . Since three measurements

are required namely the pressure trace, spray detection and flame detector, the loop iterates at 156.25 kHz.

Of the other loops, two take continuous measurements from the low speed sensors including the thermocouples and various pressure sensors. With respect to the pressure measurements and the associated voltage measurements, the precision information indicated in Section 7 is based on an average of 100 cycles. Therefore the averaging is done the FPGA before making it available on the front panel. The thermocouple measurements are made available to the front panel in voltage form and are converted to temperature on the RTC.

The injector control loop is a generic loop that comes standard with the Drivven direct injection module. It is devised to make implementing fuel injection on an engine easy, but it also conveniently features a single shot feature which is used in this project. This loop controls the current and duration that the injector is powered for and features inputs which allow the various phases of injector control to be individually altered. The various parameters required to control the injector peak and hold time are coded into the system and are used as default. The only variable the user may wish to alter is the injection duration, which is done via the RT interface. A schematic of the FPGA code is shown in Figure C.1.

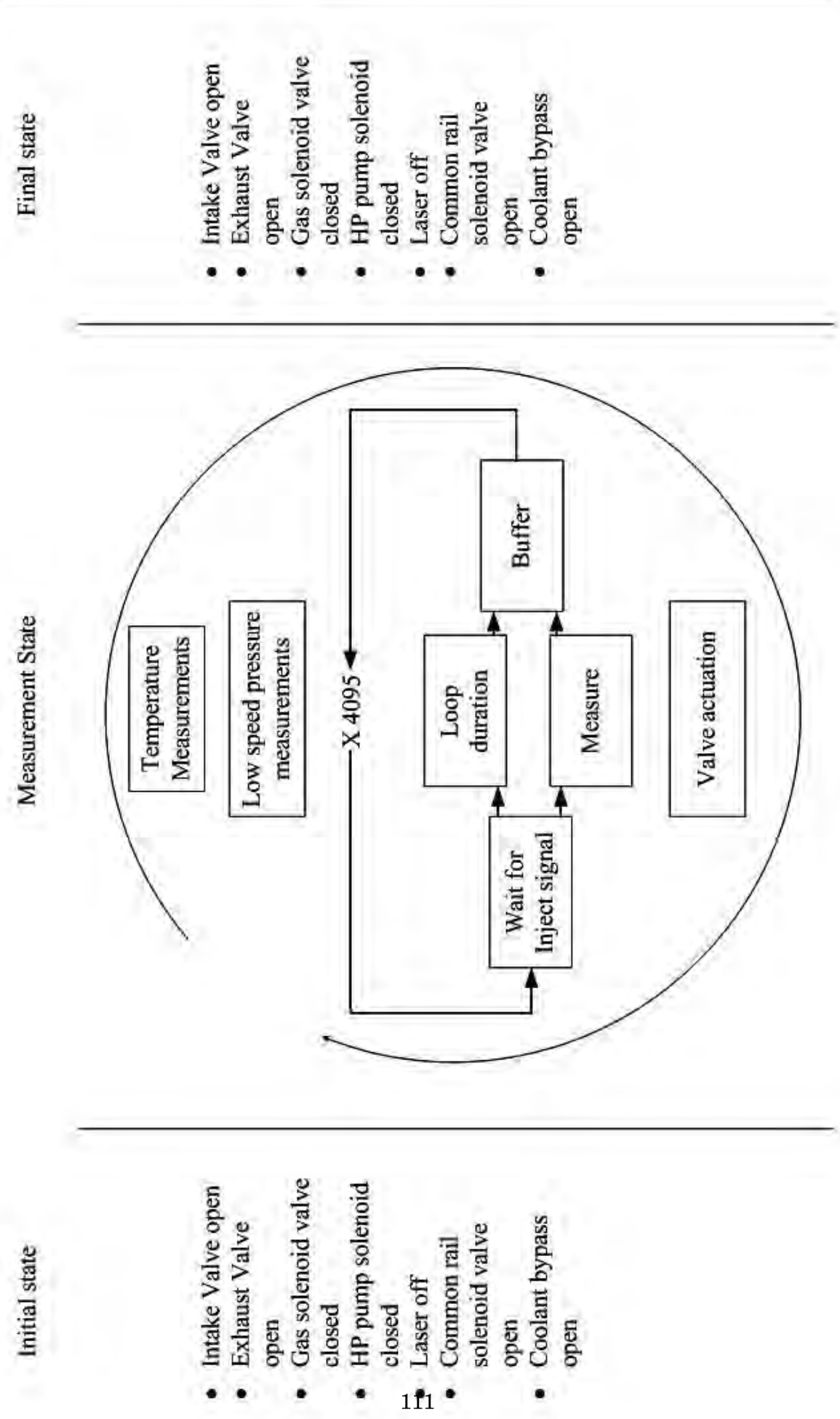

Figure C.1: IQT FPGA schematic

C.2 Real Time controller VI

Much like the FPGA, the RTC also makes use of a state machine design. It too specifies and intilialises the various sub-systems to benign values first, then moves into a measuring/operating mode and when stopped moves to a final state where it once again returns the system to default values. This VI has a main loop with 6 sub loops. The six loops do the following:

- Receive the valve states from the host PC and send to the FPGA .
- Receive temperature data in raw, voltage form and convert it to a temperature in kelvin. It then sends this data to the host PC for viewing and logging, as well as displays them on the RTC front panel. The conversion occurs in a timed loop with a duration of 660 ms, which is the fastest the 9213 thermocouple module can sample at the defined precision, as specified in Section 7. The temperature data is also used for the PID heater control. The loop makes use of PID gains that are initialised when the VI starts. The PID loop reads the set point temperature from the host PC and controls the duration that a solid state relay is on for in order to achieve the desired set point. The PID gains and set point can also be adjusted on the host PC if desired. The PID loop controls the combustion chamber surface temperature, as was done with the original device.
- Receive pressure measurements from FPGA and convert them from voltage into engineering units (bar). These measurements are displayed on the RTC front panel and also sent to the host.
- Direct injection control. The peak and hold current targets and durations are specified. Default values are loaded when the RTC initialises and the same values are used throughout the testing phase of this project. The injection duration can be changed on the RTC front panel as desired by the user.
- Injector triggering - When the host VI indicates that injection should occur, the triggering sequence enables the direct injection module, powers its high voltage power supply and enables injection. A command is then sent to the FPGA which is used to trigger injection and start the high speed data logging as previously discussed in Section C.1.

C.3 Host VI

The host VI also makes use of a state machine architecture. It comprises of one main loop with two sub loops. The first loop reads all of the low speed measurements and displays them on the GUI. This may take the form of graphs for the surface

temperature or display blocks for other measurements.During an automated test, the 2nd loop changes the valve states as required and this is passed through the system as previously discussed. When an automated test is not in progress, the user can also manually actuate the actuators by clicking on the appropriate button. This loop also sends the valve states to the RTC. Finally, it compares the temperature measurements with pre-programmed maxima for each thermocouple. If a measured temperature exceeds any of these maxima, the user is warned and all of the code execution is stopped. This switches off the heaters, but leaves the coolant supply on.

The common rail pressure was subject to noise and therefore it is filtered by using a built in low pass filter. It was found during testing that the filter's response was too slow and therefore the fuel pressure measurement just before injection was logged without filtering as well as with filtering.

The 2nd loop controls the automated test. Its functions are best understood with the aid of Figure C.2. At the start of an automated test, the user specifies temperature and pressure tolerances which are checked prior to injection. The user also specifies the number of cycles to be performed for that test. Typically 47 were performed in this project.

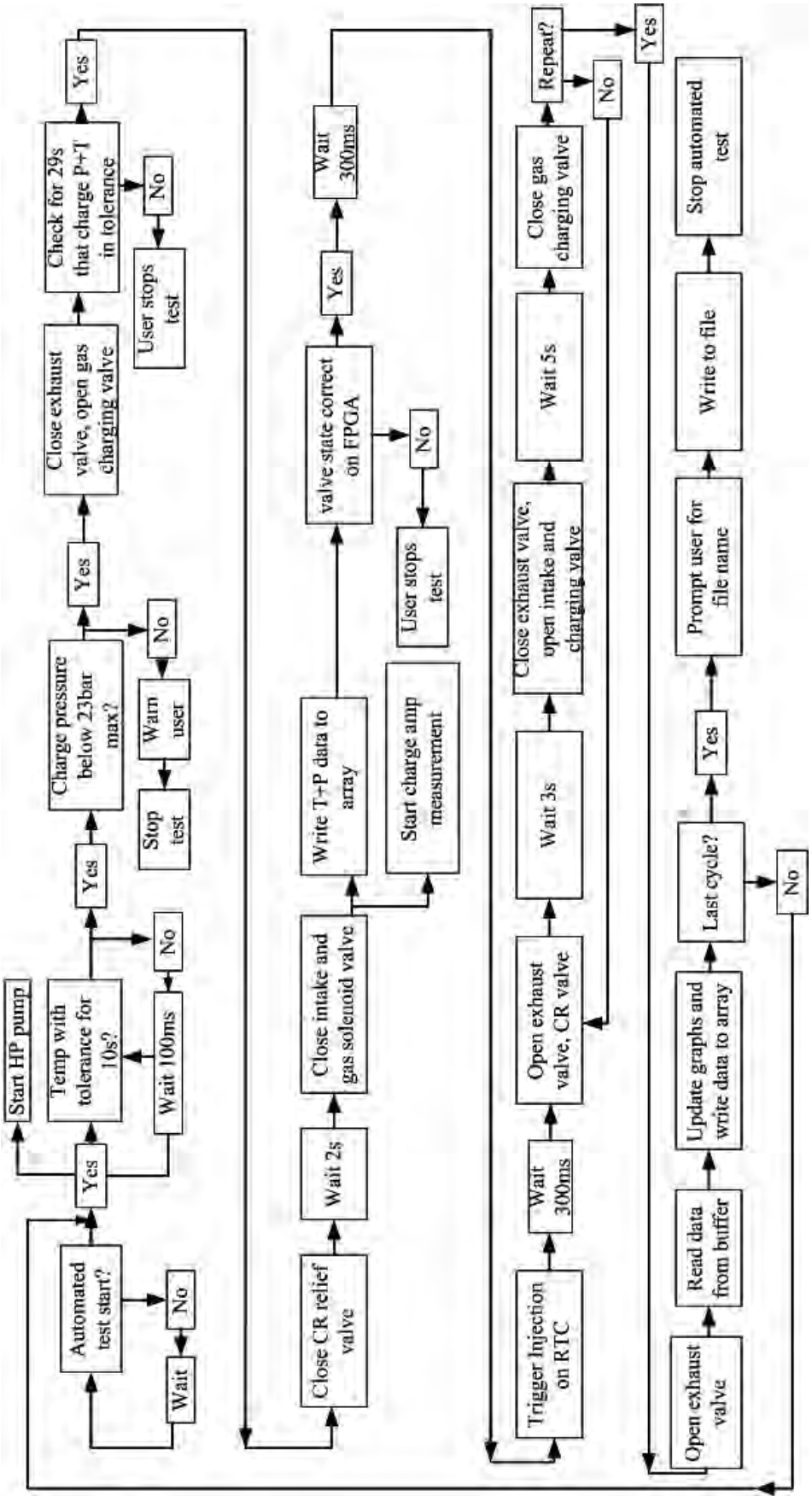

Figure C.2: Host VI automated test schematic

Appendix D

Sample Pressure Uncertainty Calculation

The 9215 NI module was used to measure the output voltages of the respective pressure sensors. The measurement was subject to an uncertainty indicated by the following equation [48]:

$$Module\,uncertainty = 0.02\% \times (gain) + 0.014\% \times (Full\,Range) + Noise\,Uncertainty$$

It was assumed that the module operated at a temperature of 307 K. For temperatures above 303 K the gain error, depicted as the numerical coefficient of the first term in the above equation, increase at a rate of 10 ppm/ K while overall there is an offset drift of 60 μV/ K as well . Using the converted actuator pressure as an example from Table 7.3, its nominal output voltage was 2.025 V. At the afformentioned temperature, the module uncertainty is found as:

$$Module\,uncertainty = \left(\frac{0.02}{100} + 10^{-5} \times (307 - 303)\right) \times 2.025 + \left(\frac{0.014}{100} \times 10.4\right) + 158 \times 10^{-6} + 60 \times 10^{-6}\,(307 - 303)$$

$$Module\,uncertainty = \pm 2.27\,mV$$

At the conversion equation's gradient of 4.2962 Bar/V, this results in a module uncertainty of 0.009 bar. The sensor's uncertainty was estimated to be 0.025 bar and therefore the combined measurement chain uncertainty is found to be 0.027 bar for the actuator pressure.

Appendix E

Technical Drawings

The following pages show the bill of matierals and technical drawings for the components made in this project. Figure E.1 indicates a photo of the rig as it was in situ.

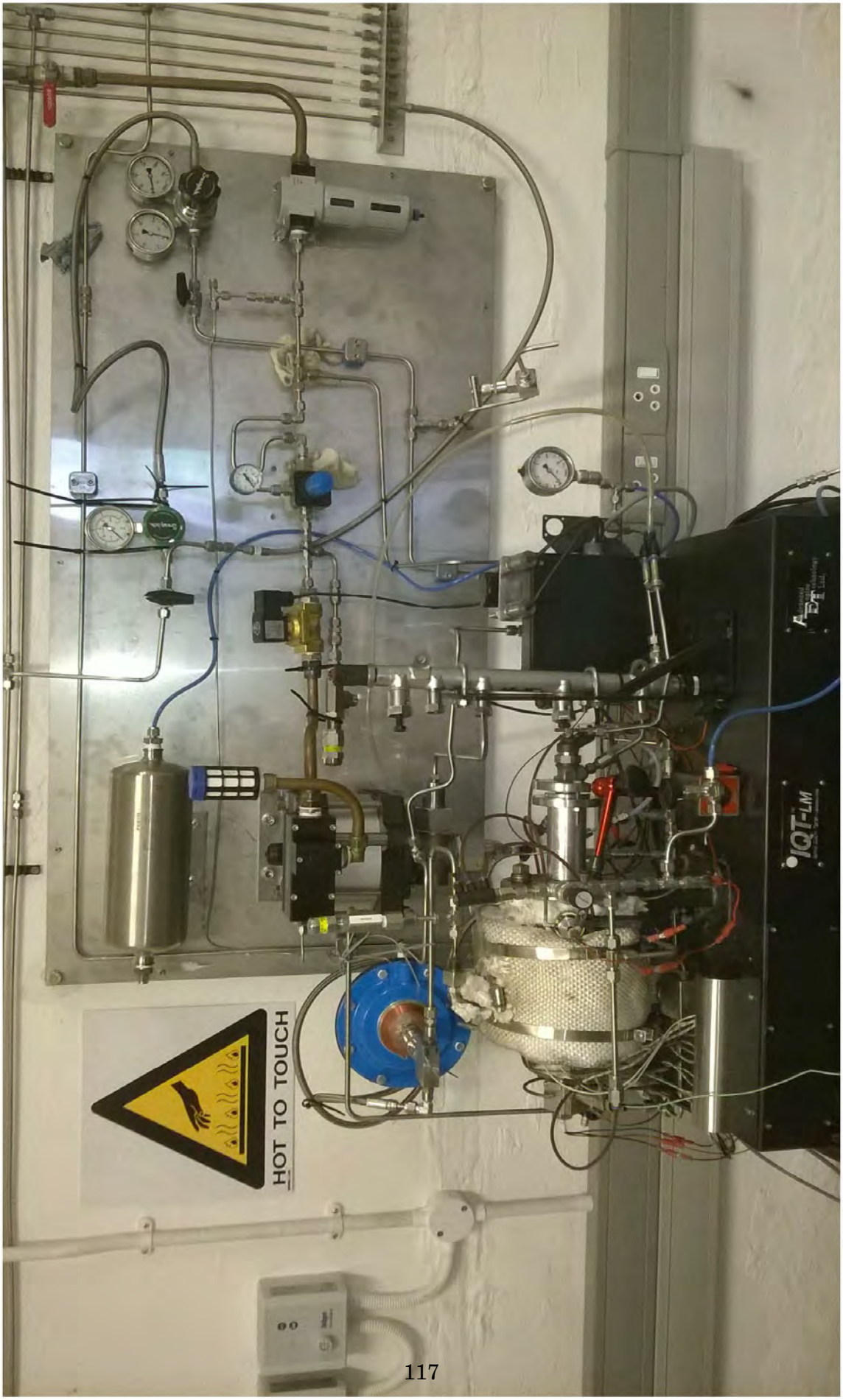

Figure E.1: Modified IQT in situ.

IQT Bill of Matierials

					Drawing #	# of Sheets
IQT assembly					1	3

Item number	Part Name	Quantity	New?	Manufactured/ Bought?	Material	Drawing #	# of Sheets	OEM part #
1	Combustion chamber	1	N		SST			
2	chamber bracket	1	N		painted MS			
3	3/8" UNF x 1/2" Cap screw	2	Y	B	HTS			
	Injector sub-assembly	1						
4	Mounting Plate	1	Y	M	SST	2	4	
5	Mounting plate clamp	1	Y	M	SST	3	1	
6	1/2" UNC nut	3	Y	B	SST			
7	1/2" washers	12	Y	B	SST			
8	Injector Guide	1	Y	M	Alum.	4	1	
9	Injector clamp locator	1	Y	M	SST	5	1	
10	Sol injector clamp	1	Y	M	SST	6	1	
11	Solenoid Injector	1	N		N/A			044 5110 131
12	Injector copper washer	1	N		Copper			
13	M6x1x50	2	Y	B	Grade 8.8			
14	M6 Nut	2	Y	B	Galv. Steel			
15	6mm washer	4	Y	B	Galv. Steel			
16	HP tube	1	Y	B/M	316 SS cold drawn	7	1	65TU4H-316
17	swagelok 1/8"BSP to 1/8" tube	1	Y	B	SST			SS-200-1-2
18	1" ID copper washer	1	N	B	copper			
19	17x2mm o-ring	1	Y	B	Viton			
	Common Rail sub-assembly	1						
20	Common Rail	1	N		SST			646 070 0295
21	Common rail cap	3	Y	M	Bohler M300	8	1	
22	CR_RV_adapter	1	Y	M	SST	9	1	
23	14x1.5mm o-ring	1	Y	B	NBR			
24	M8 U-bolt	2	Y	B	Galv.steel			
25	M8 Nut	4	Y	B	Galv.steel			
26	8mm washer	4	Y	B	Galv.steel			
27	CR Bracket	1	Y	M	Powder coated MS	10	1	
28	3/8" UNF x 1/2" Cap screw	4	Y	B	HTS			
29	Bleed Nut adapter	2	Y	M	SST	11	1	
30	M8x1.25x25 hex head screw	2	Y	B	Grade 10.9			
31	8mm Ball bearing	4	Y	B	HTS			
	Sight glass sub-assembly	**2**						
32	Nipple	1	Y	M	SST	12	1	
33	Window Holder	1	Y	M	SST	13	1	
34	Window Mount	1	Y	M	SST	14	1	
35	Collar	1	Y	M	Brass	15	1	
36	Sight glass	1	N		Quartz			
37	24 mm Ext. circlip	2	Y	B	HTS			
38	9x1.5mm o-ring	1	Y	B	Viton			
39	12x1.5mm o-ring	1	Y	B	Viton			
40	15x1.5mm o-ring	1	Y	B	Viton			
41	22x1.5mm o-ring	2	Y	B	Viton			
42	Festo 3mm swivel elbow	2	Y	B	Galv. Steel			30982
43	Nipple washer	2	Y	M	Copper	16	1	
44	Reciever lead guide	1	Y	M	Teflon	17	1	
45	Optoschmitt guide	1	Y	M	Teflon	25	1	
	Pressure transducer sub-assembly	1						
46	P transducer tee	1	Y	M	SST	18	1	
47	adapter washer	2	Y	M	Copper	19	1	
48	sight glass holder	1	Y	M	Brass	20	1	
49	12x1.5mm o-ring	1	Y	B	Viton			
50	Tee gasket	1	Y	M	Copper	21	1	
51	Kistler 6121 adapter	1	Y	M	SST	22	1	
52	Kistler 6121	1	N		N/A			
53	Kistler washer	1	Y	M	Copper	23	1	
54	Festo 3mm swivel elbow	4	Y	B	Galv. Steel			30982
55	8x1mm o-ring	1	Y	B	Viton			
56	Kistler 6121 guide	1	N		SST			
57	Kistler Nut	1	N		Brass			

58	M3x40 cap screw	4	Y	B	SST			
59	3mm washer	8	Y	B	SST			
60	M3 nut	4	Y	B	SST			
61	Tee cover	2	Y	M	Alum.	24	1	
62	Optoschmitt guide	1	Y	M	Teflon	25	1	
63	17x2mm o-ring	2	Y	B	Viton			
64	sight glass	1	N					
65	9x1.5mm o-ring	1	Y	B	Viton			

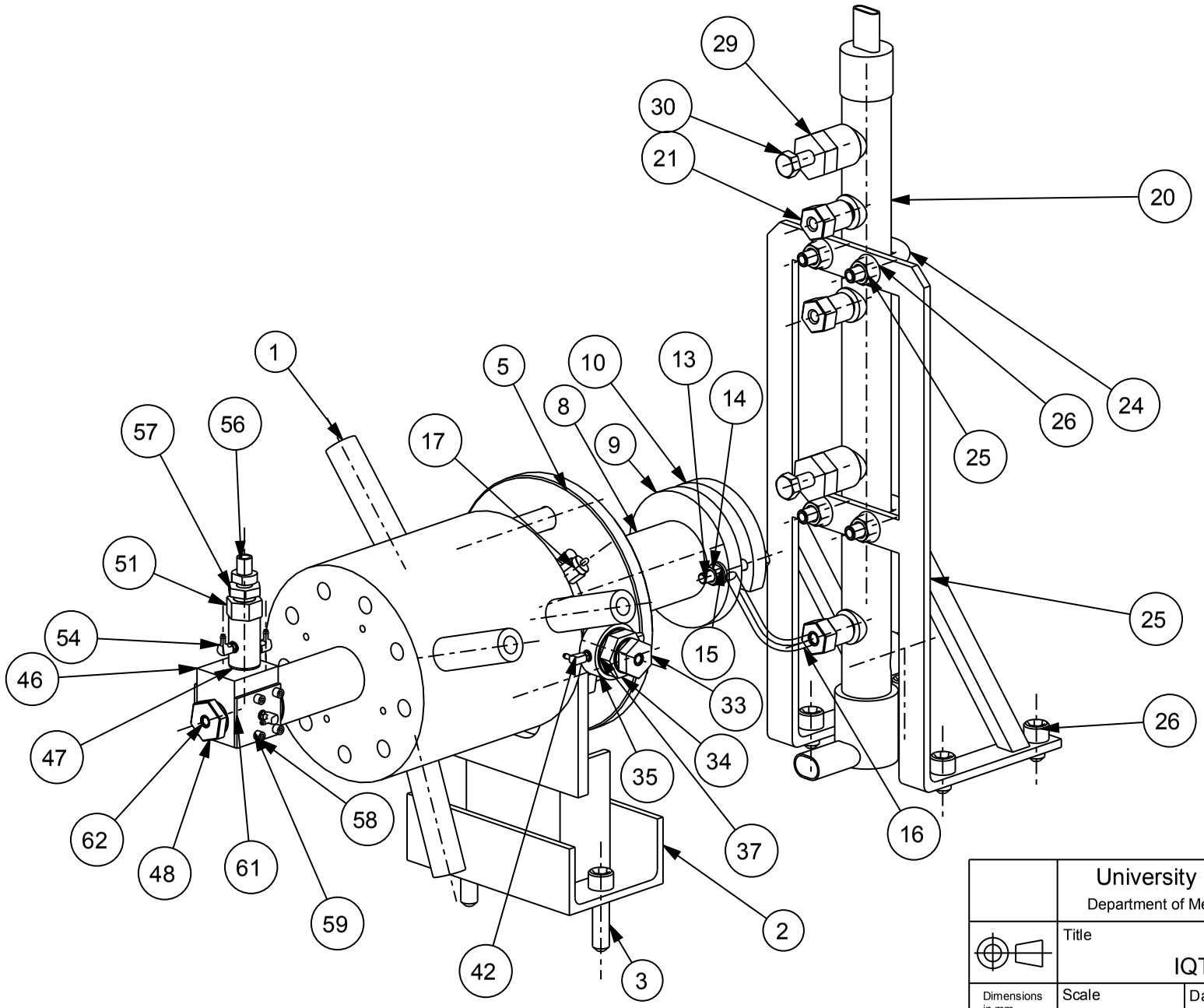

	University of Cape Town Department of Mechanical Engineering			
	Title IQT Assembly			
Dimensions in mm Tolerance U.O.S. 0.1	Scale 1:3	Date 20/06/2014	Sheet 1	of 3
	Drawn By A.Ehrenreich		Drawing Number 1	

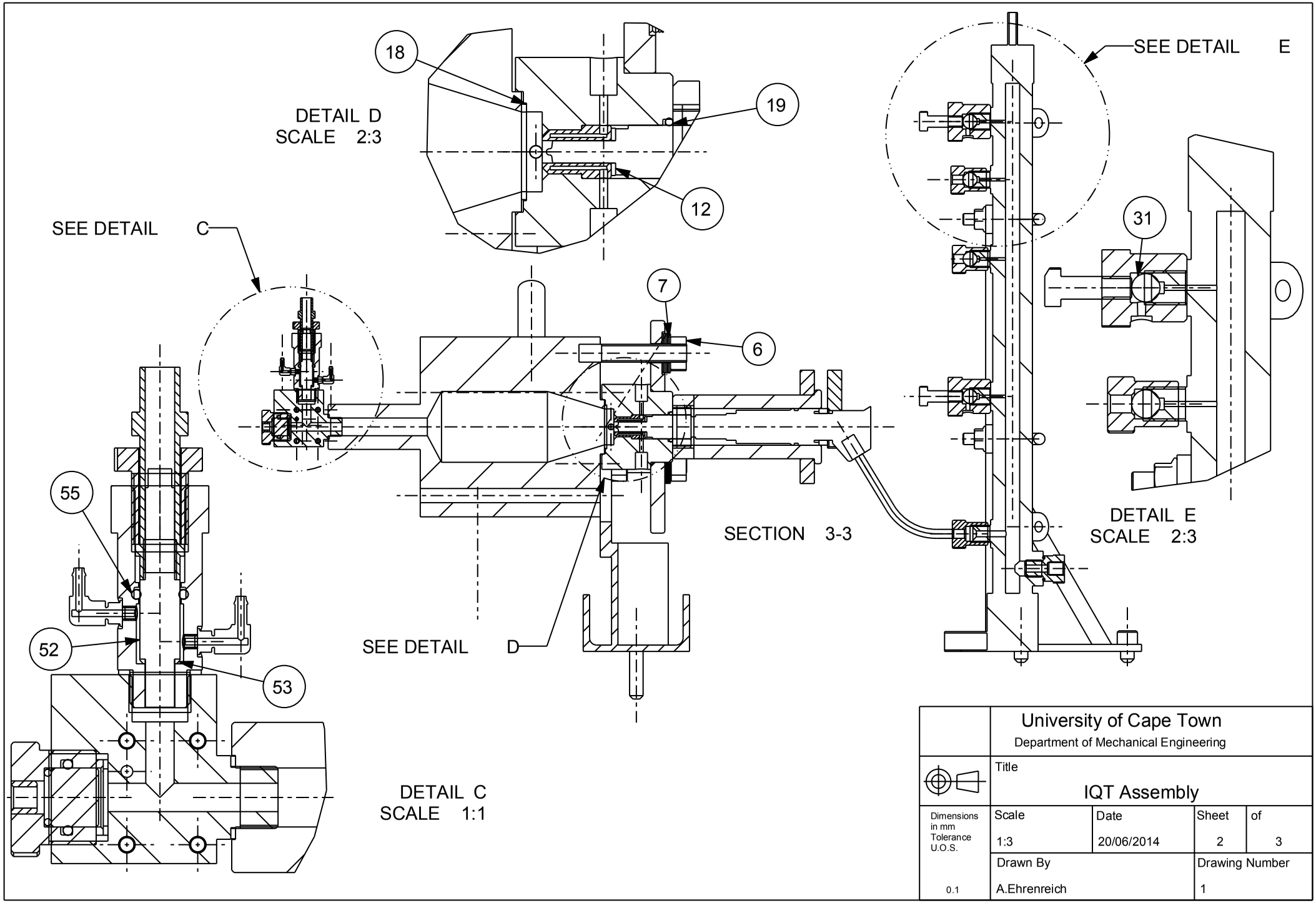

	University of Cape Town Department of Mechanical Engineering			
	Title IQT Assembly			
Dimensions in mm Tolerance U.O.S. 0.1	Scale 1:3	Date 20/06/2014	Sheet 2	of 3
	Drawn By A.Ehrenreich		Drawing Number 1	

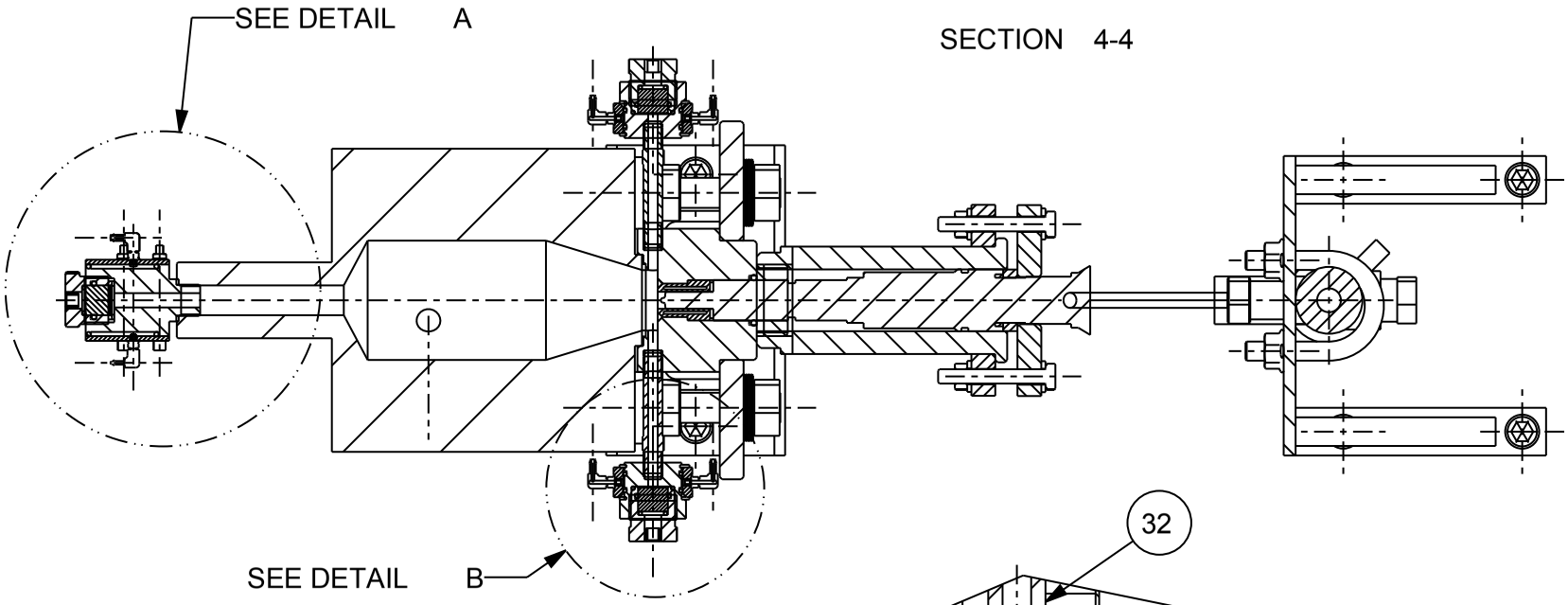

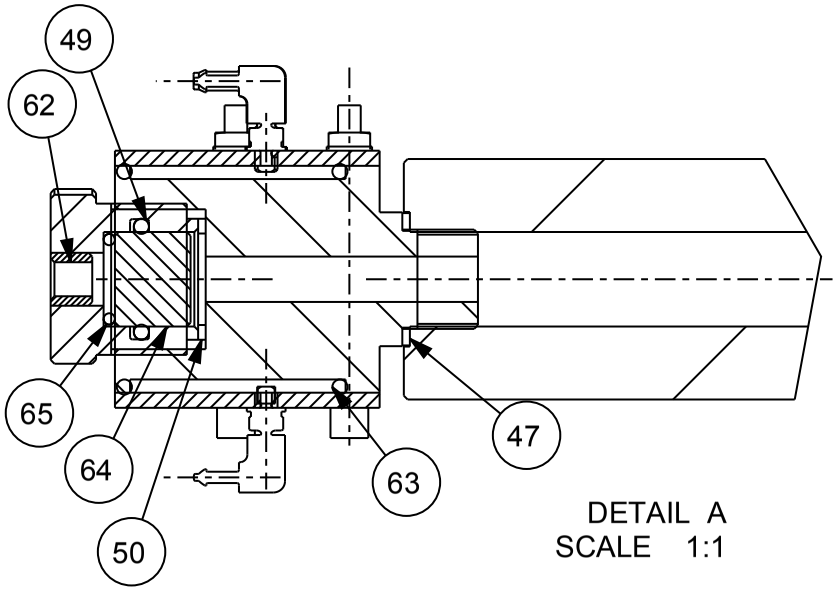

DETAIL A
SCALE 1:1

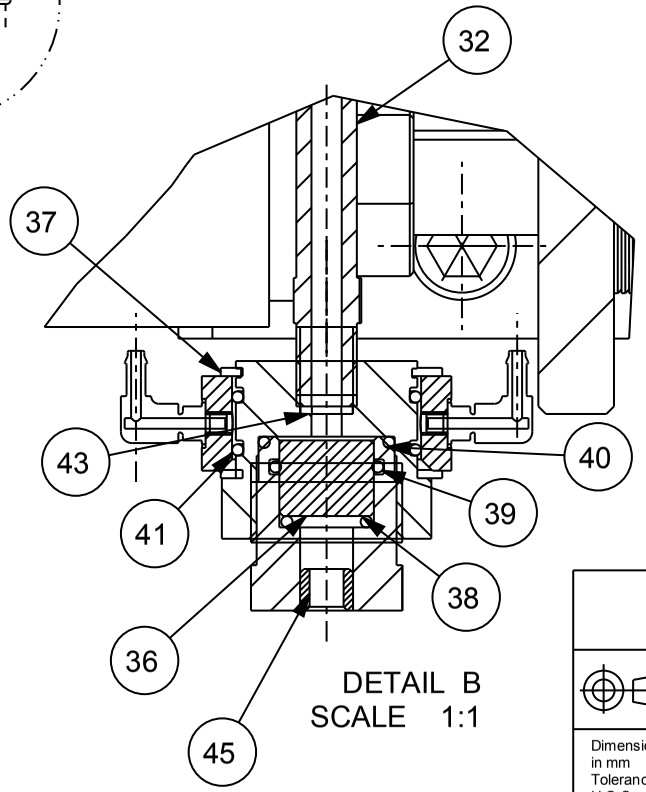

DETAIL B
SCALE 1:1

	University of Cape Town Department of Mechanical Engineering			
	Title IQT Assembly			
Dimensions in mm Tolerance U.O.S. 0.1	Scale 1:3	Date 20/06/2014	Sheet 3	of 3
	Drawn By A. Ehrenreich		Drawing Number 1	

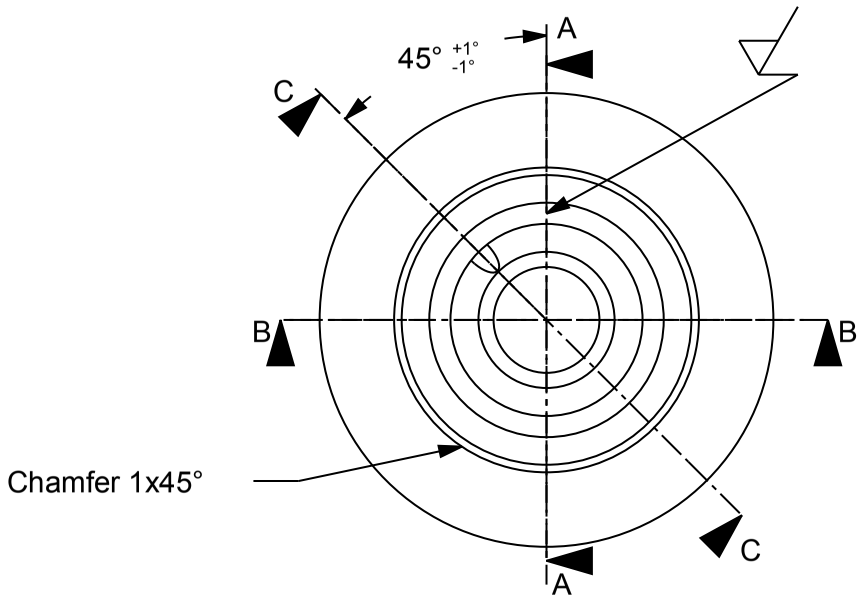

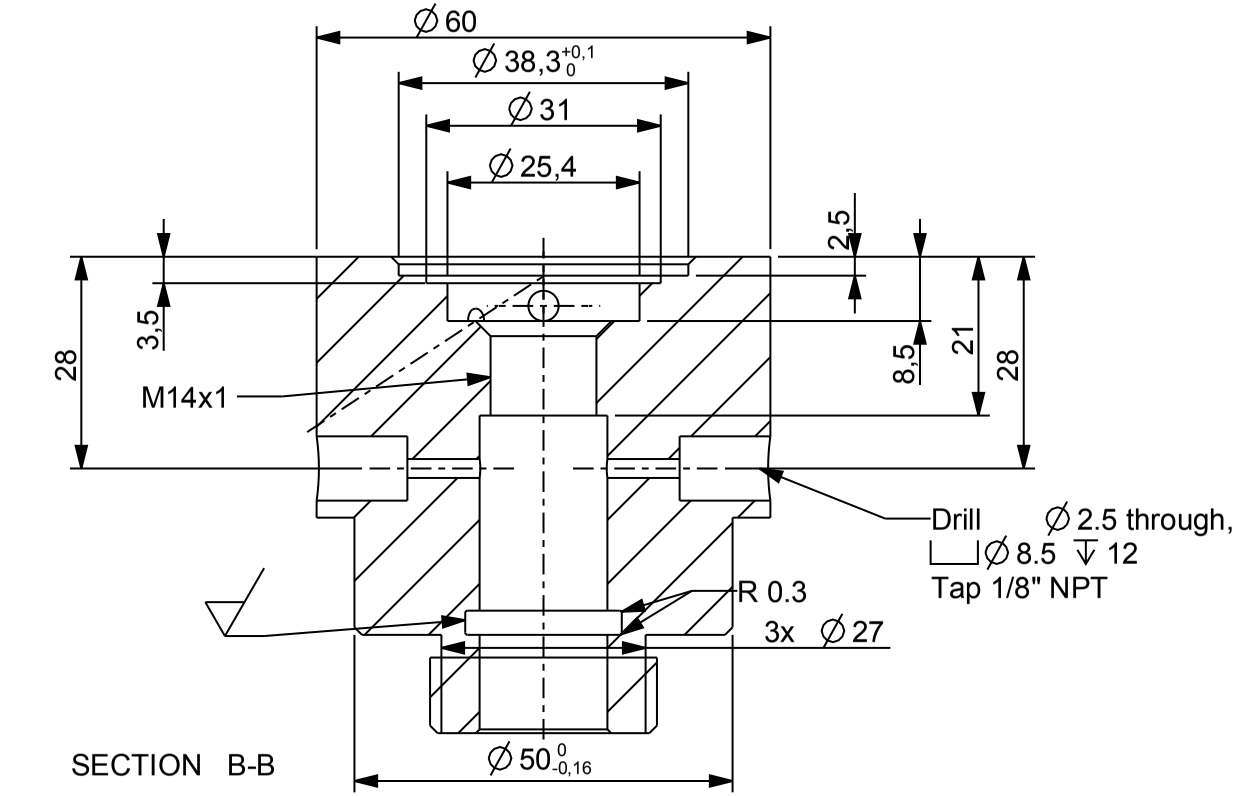

SECTION B-B

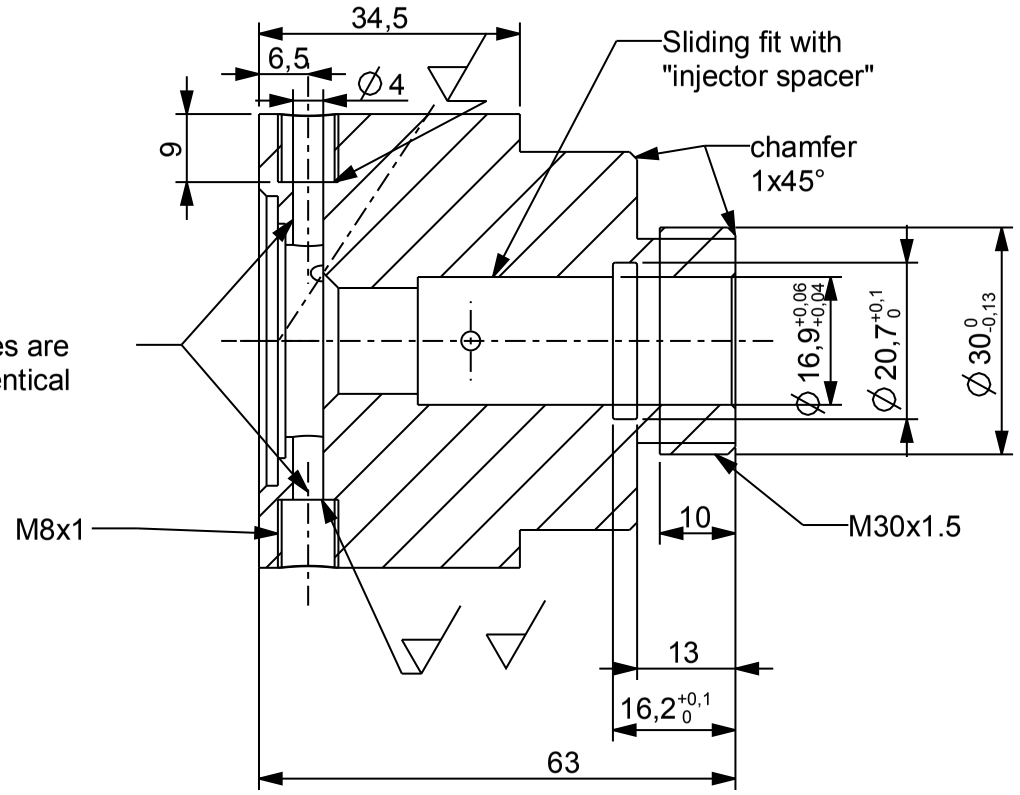

SECTION A-A

4	SST	1	
Item	Material	Qty	Remarks

University of Cape Town
Department of Mechanical Engineering

Title
MOUNTING_PLATE

Dimensions in mm Tolerance U.O.S.	Scale	Date	Sheet	of
	1:1	18/02/2013	1	4
0.1	Drawn By Aidan Ehrenreich (SAFL)		Drawing Number 2	

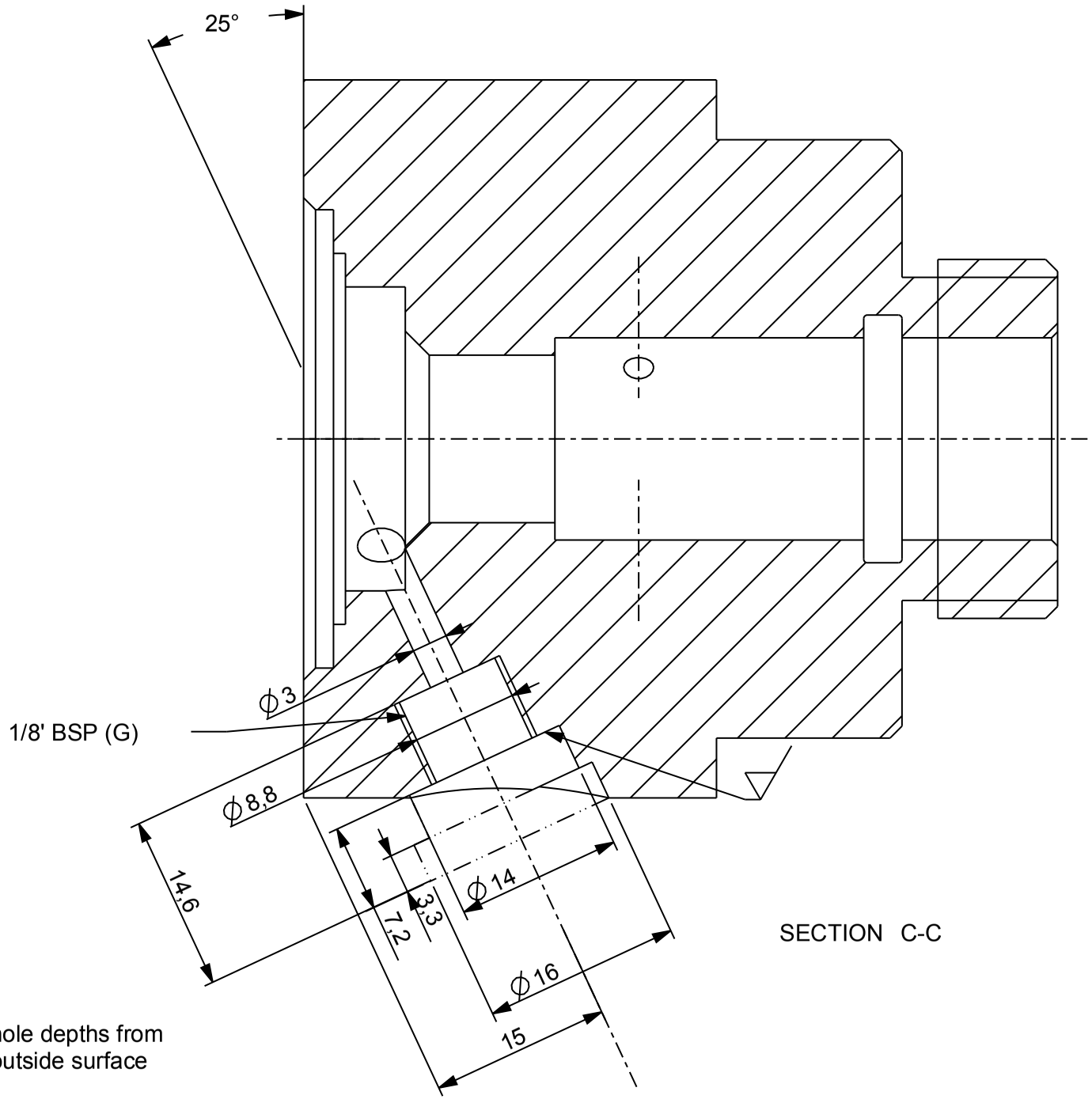

SECTION C-C

hole depths from outside surface

4	SST	1	
Item	Material	Qty	Remarks

University of Cape Town
Department of Mechanical Engineering

Title
MOUNTING_PLATE

Dimensions in mm Tolerance U.O.S.	Scale	Date	Sheet	of
	2:1	26/02/2013	2	4
0.1	Drawn By Aidan Ehrenreich (SAFL)		Drawing Number 2	

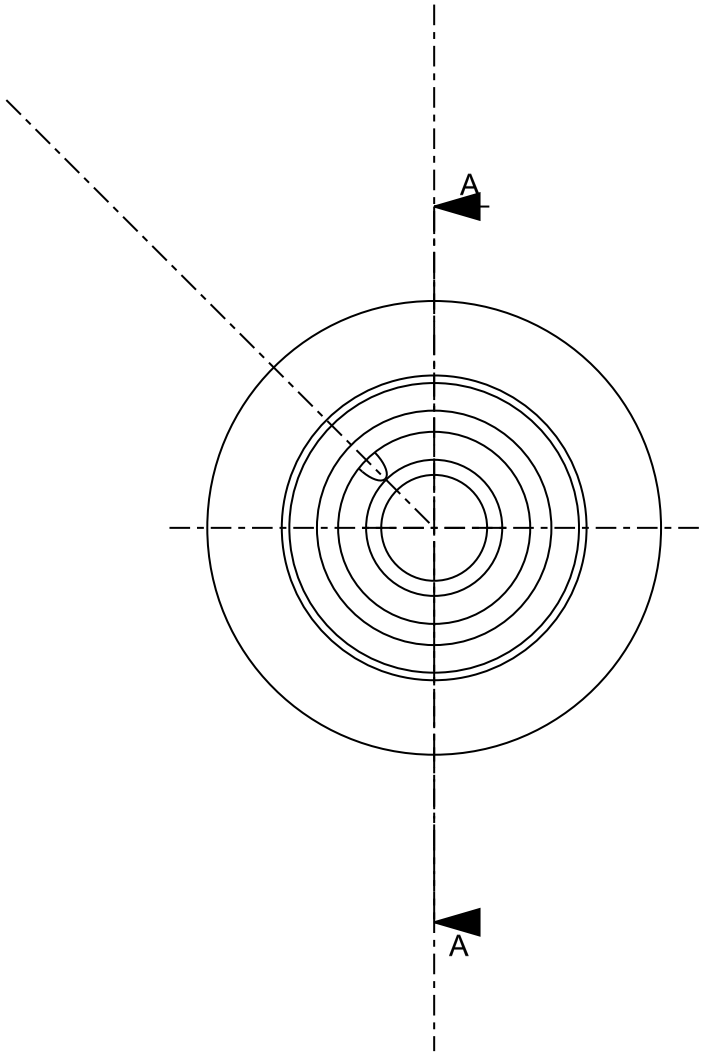

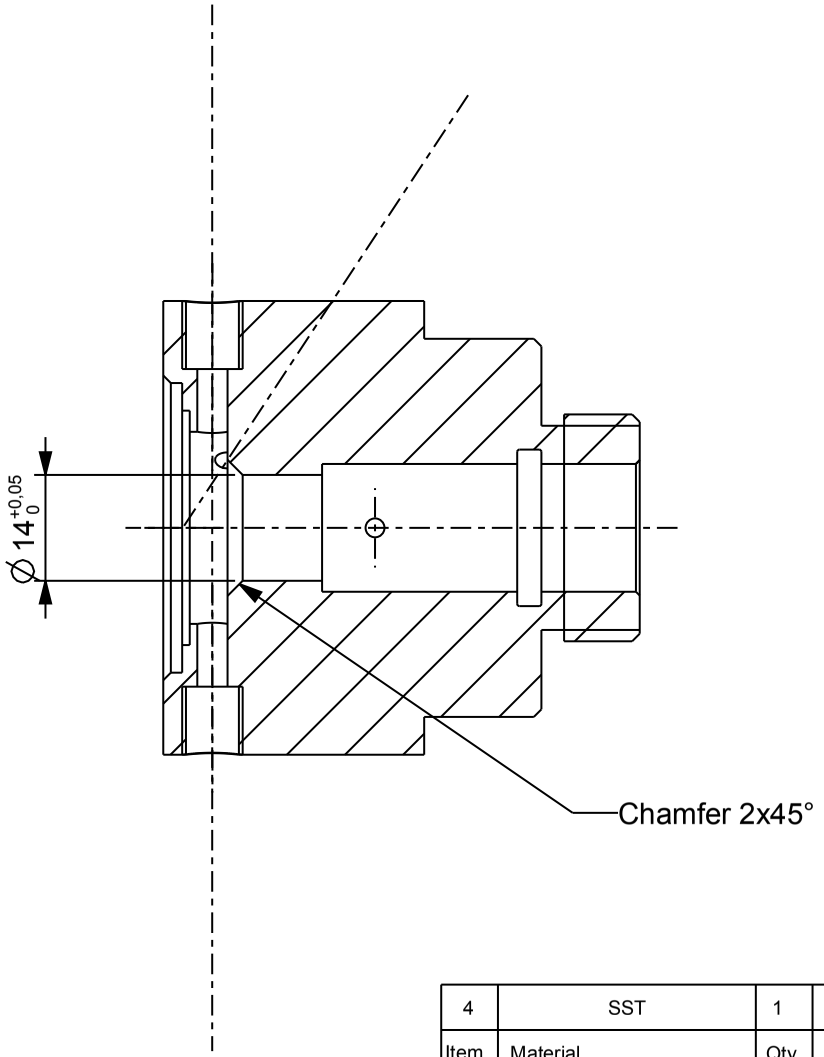

SECTION A-A

Drill out M14 thread and add 2x45° chamfer as indicated

4	SST	1	
Item	Material	Qty	Remarks

University of Cape Town
Department of Mechanical Engineering

Title: MOUNTING_PLATE

Dimensions in mm Tolerance U.O.S.	Scale	Date	Sheet	of
	1:1	20/06/2014	3	4
	Drawn By		Drawing Number	
0.1	A.Ehrenreich		2	

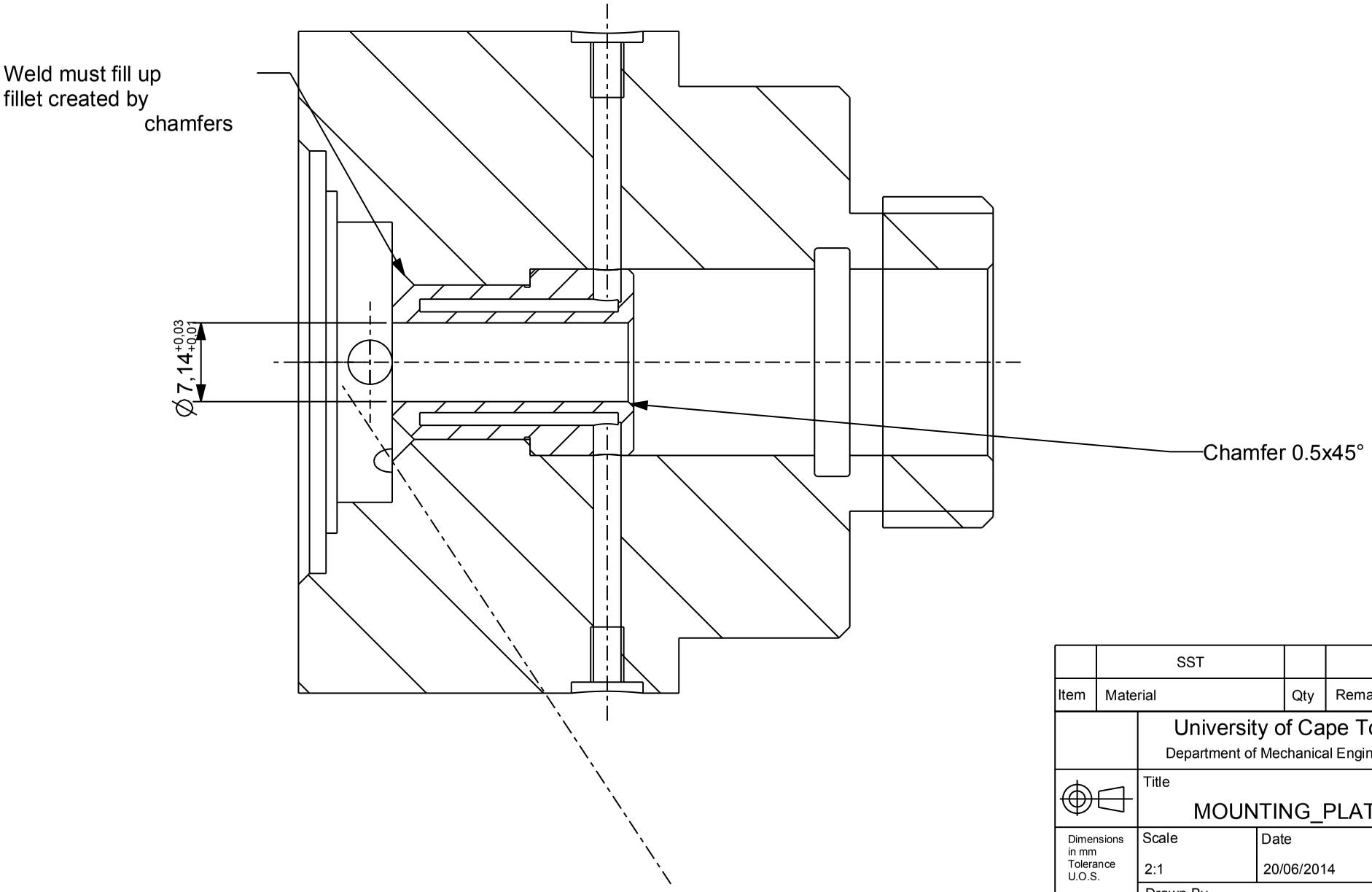

	SST		
Item	Material	Qty	Remarks

University of Cape Town
Department of Mechanical Engineering

Title
MOUNTING_PLATE_FINAL

Dimensions in mm Tolerance U.O.S.	Scale	Date	Sheet	of
	2:1	20/06/2014	4	4
	Drawn By		Drawing Number	
0.1	A.Ehrenreich		2	

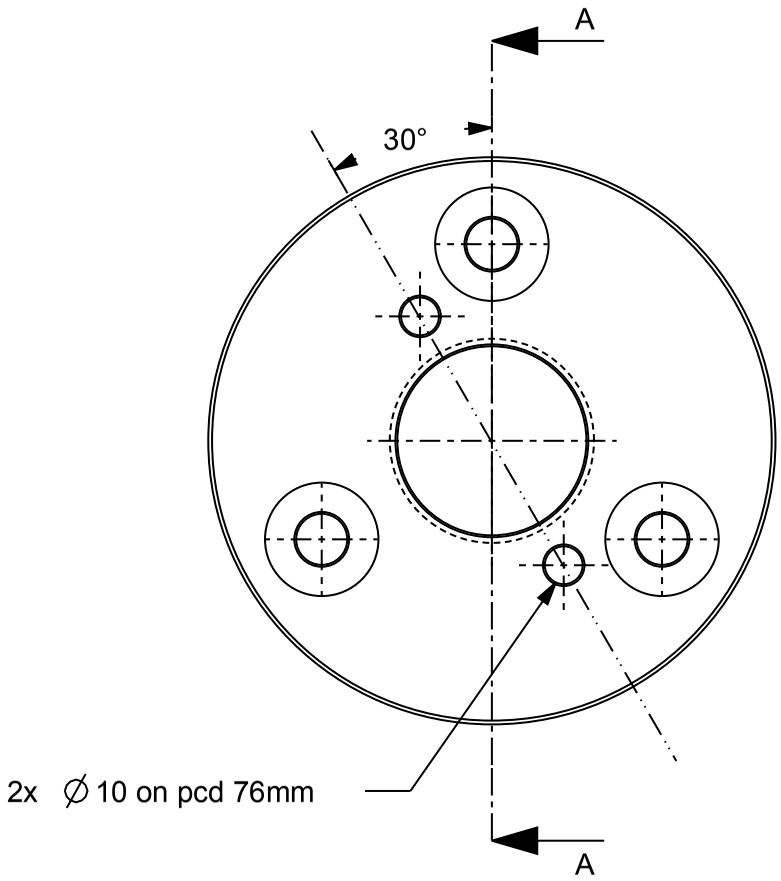

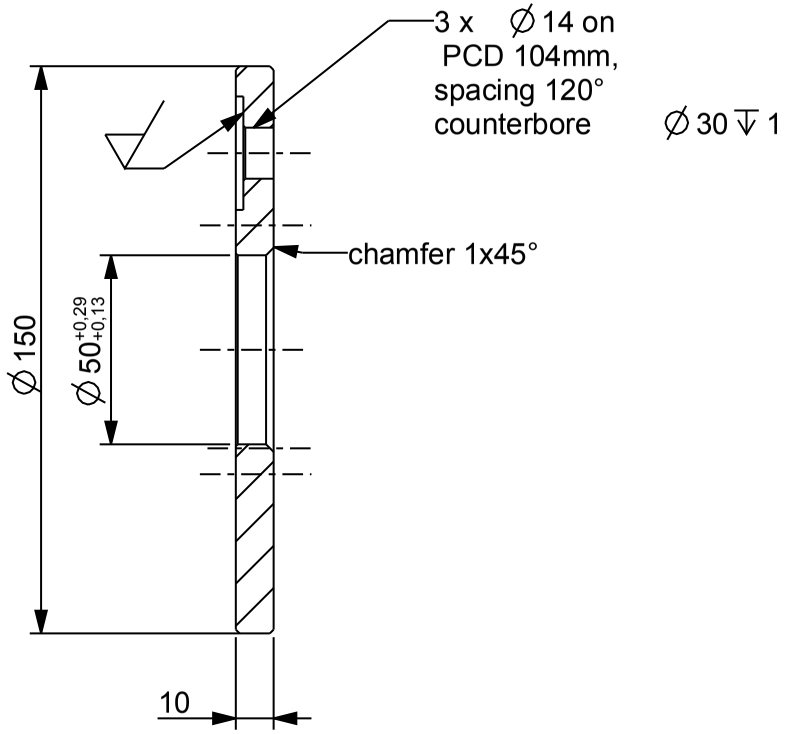

SECTION A-A

Please break all sharp edges

5	SST	1	
Item	Material	Qty	Remarks

University of Cape Town
Department of Mechanical Engineering

Title
MOUNT_PLATE_CLAMP

Dimensions in mm Tolerance U.O.S.	Scale 1:2	Date 11/01/2013	Sheet 1	of 1
0.1	Drawn By Aidan Ehrenreich (SAFL)		Drawing Number 3	

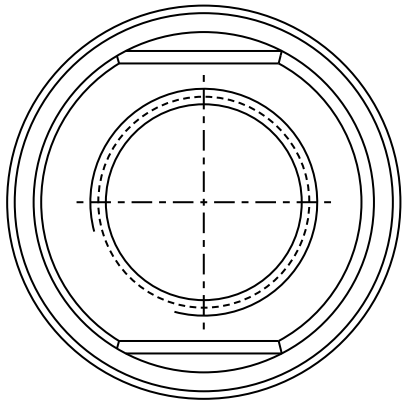

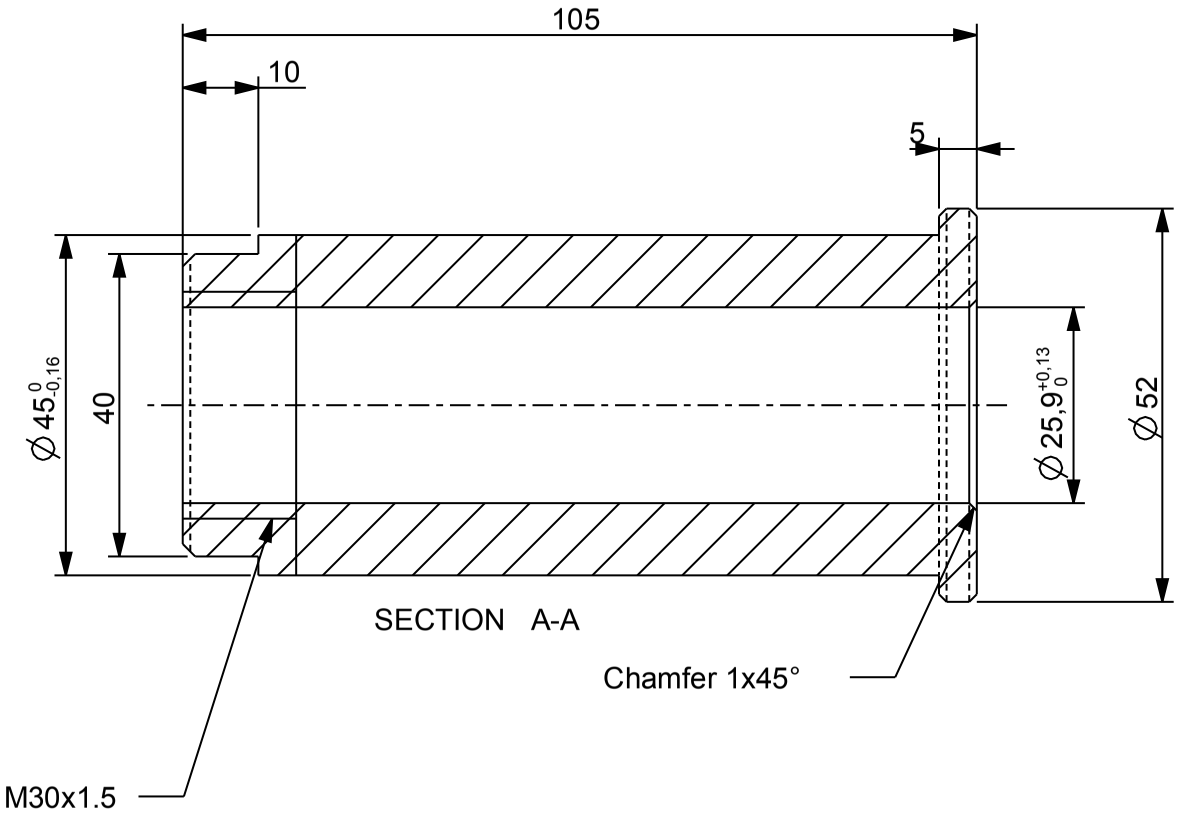

Please break all sharp edges

	ALUMINUM	1	
Item	Material	Qty	Remarks

University of Cape Town
Department of Mechanical Engineering

Title
INJECTOR_GUIDE

Dimensions in mm Tolerance U.O.S.	Scale	Date	Sheet	of
	1:1	18/02/2013	1	1
	Drawn By Aidan Ehrenreich (SAFL)		Drawing Number	
0.1			4	

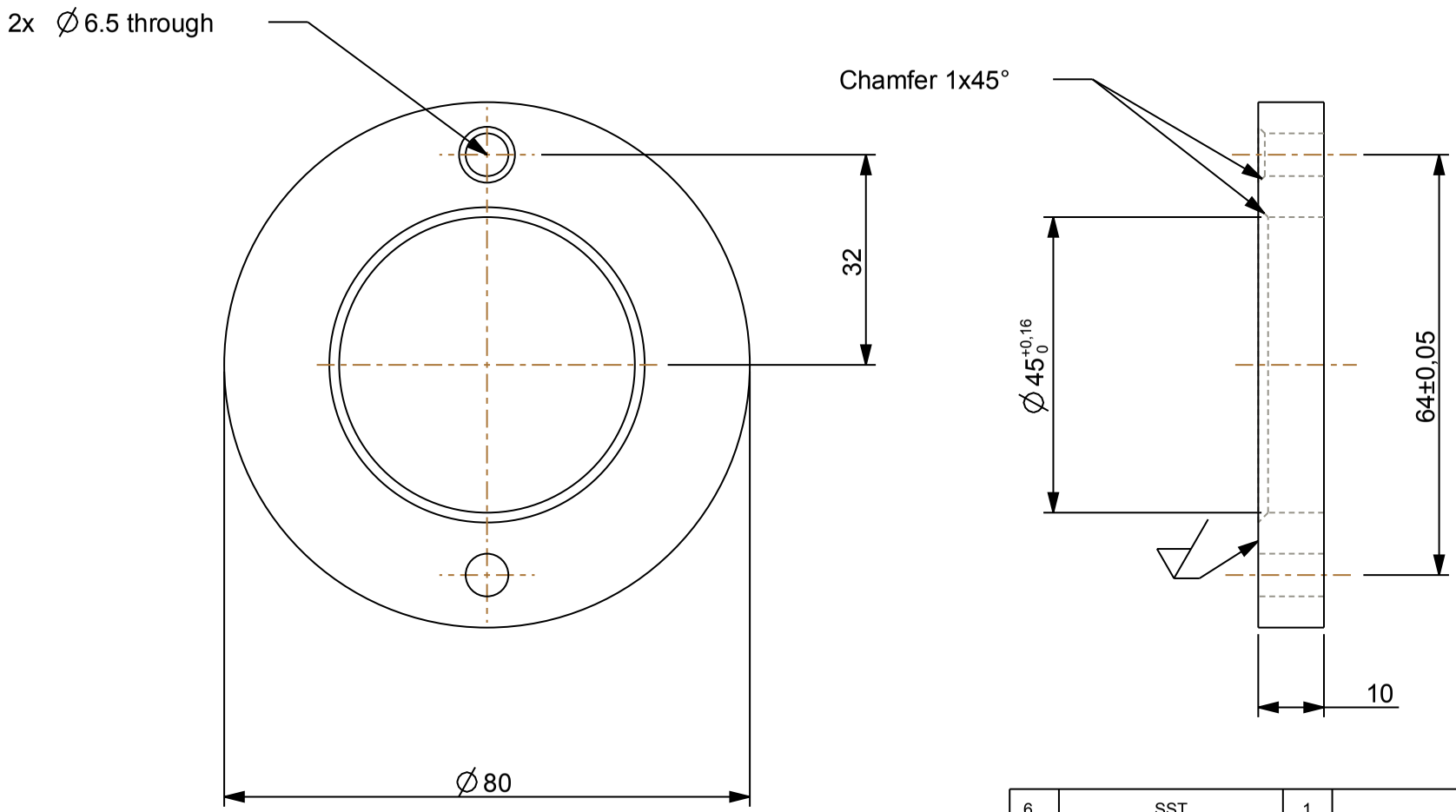

6	SST	1	
Item	Material	Qty	Remarks

University of Cape Town
Department of Mechanical Engineering

Title
INJECTOR_CLAMP_LOCATOR

Dimensions in mm Tolerance U.O.S.	Scale	Date	Sheet	of
	1:1	08/01/2013	1	1
	Drawn By Aidan Ehrenreich (SAFL)		Drawing Number	
0.1			6	

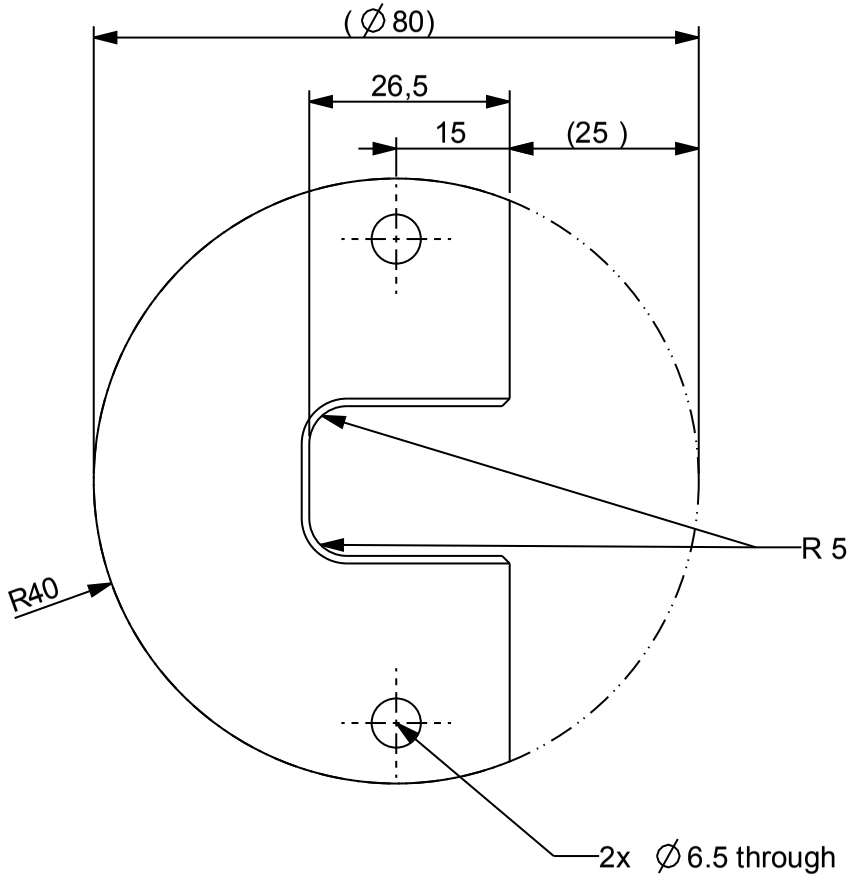

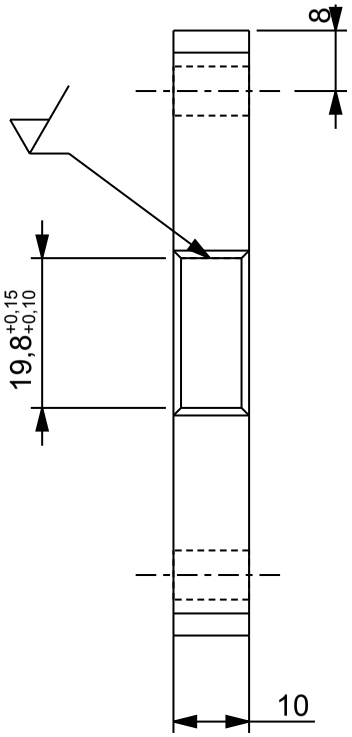

Please break all sharp edges

10	SST	1	
Item	Material	Qty	Remarks

University of Cape Town
Department of Mechanical Engineering

Title: SOL_INJECTOR_CLAMP

Dimensions in mm Tolerance U.O.S.	Scale	Date	Sheet	of
0.1	1:1	08/01/2012	1	1

Drawn By: Aidan Ehrenreich (SAFL)

Drawing Number: 6

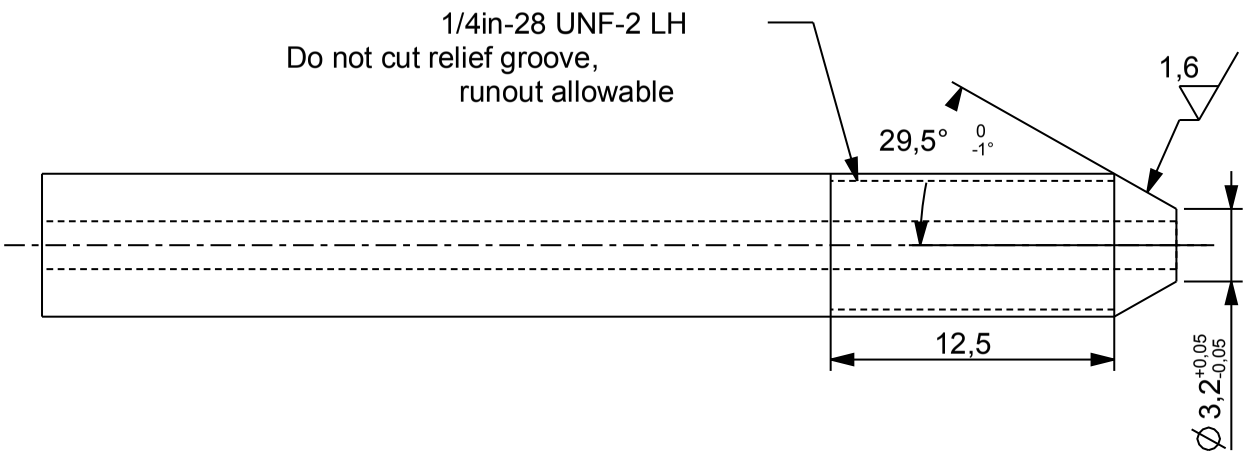

All tube ends the same

16	316 S.S. Cold drawn	1	
Item	Material	Qty	Remarks

University of Cape Town
Department of Mechanical Engineering

Title: HP_TUBE

Dimensions in mm Tolerance U.O.S.	Scale	Date	Sheet	of
0.1	3:1	04/06/2013	1	1

Drawn By: Aidan Ehrenreich (SAFL)

Drawing Number: 7

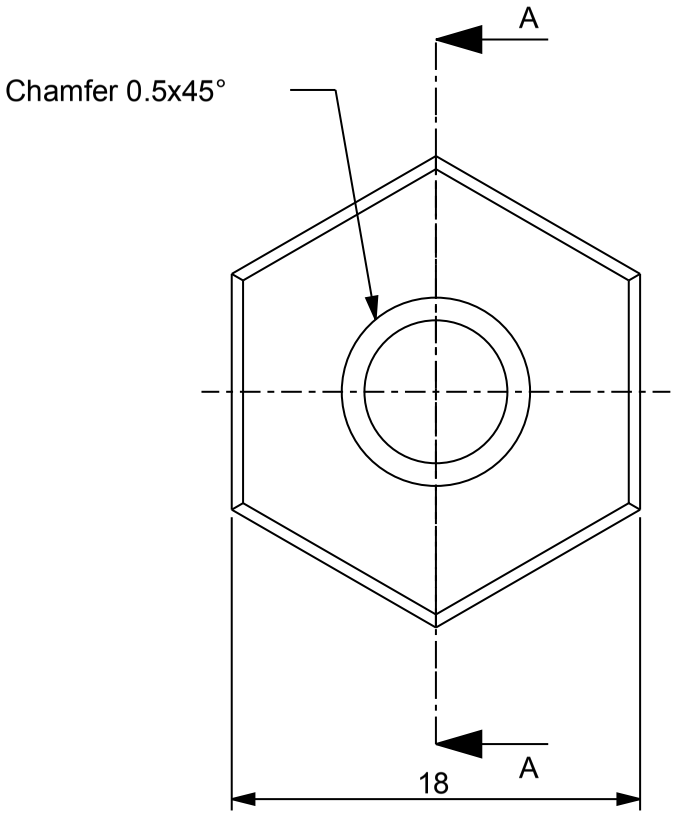

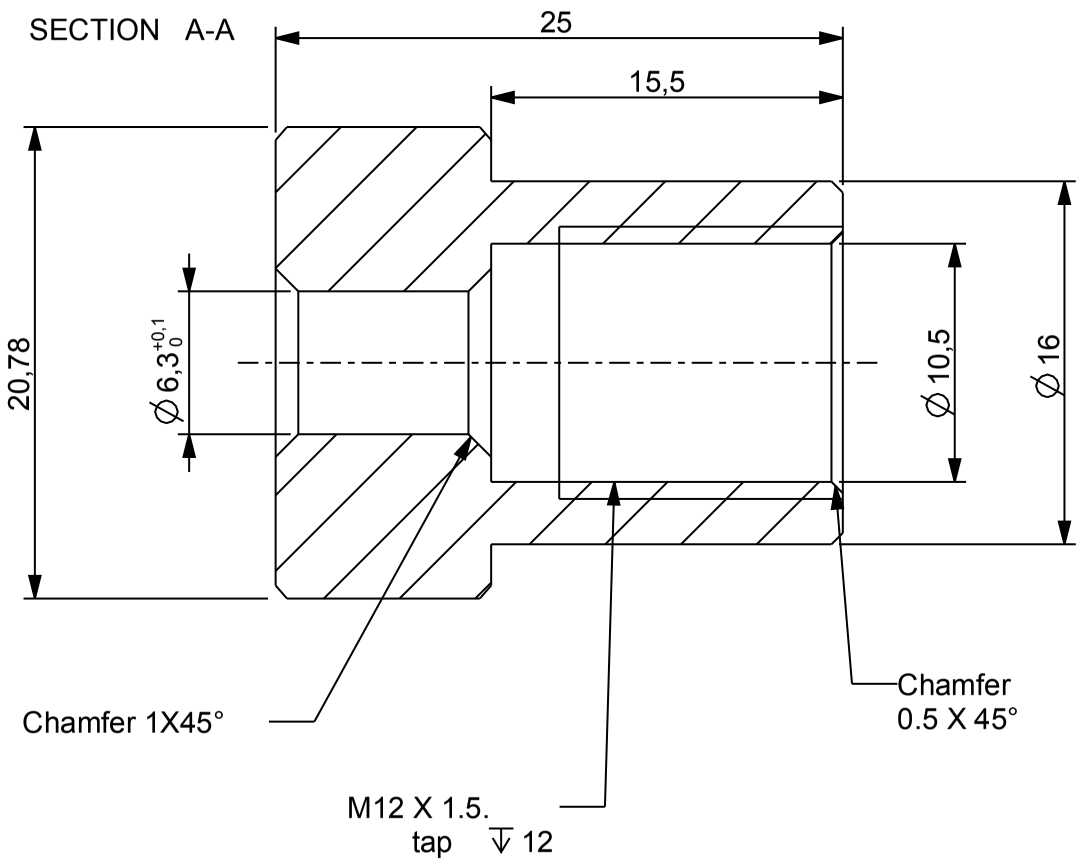

Please break all sharp edges

19	Bohler M300	3	
Item	Material	Qty	Remarks

University of Cape Town
Department of Mechanical Engineering

Title: COMMON_RAIL_CAP

Dimensions in mm Tolerance U.O.S.	Scale	Date	Sheet	of
	3:1	02/12/2012	1	1
	Drawn By		Drawing Number	
0.1	Aidan Ehrenreich (SAFL)		8	

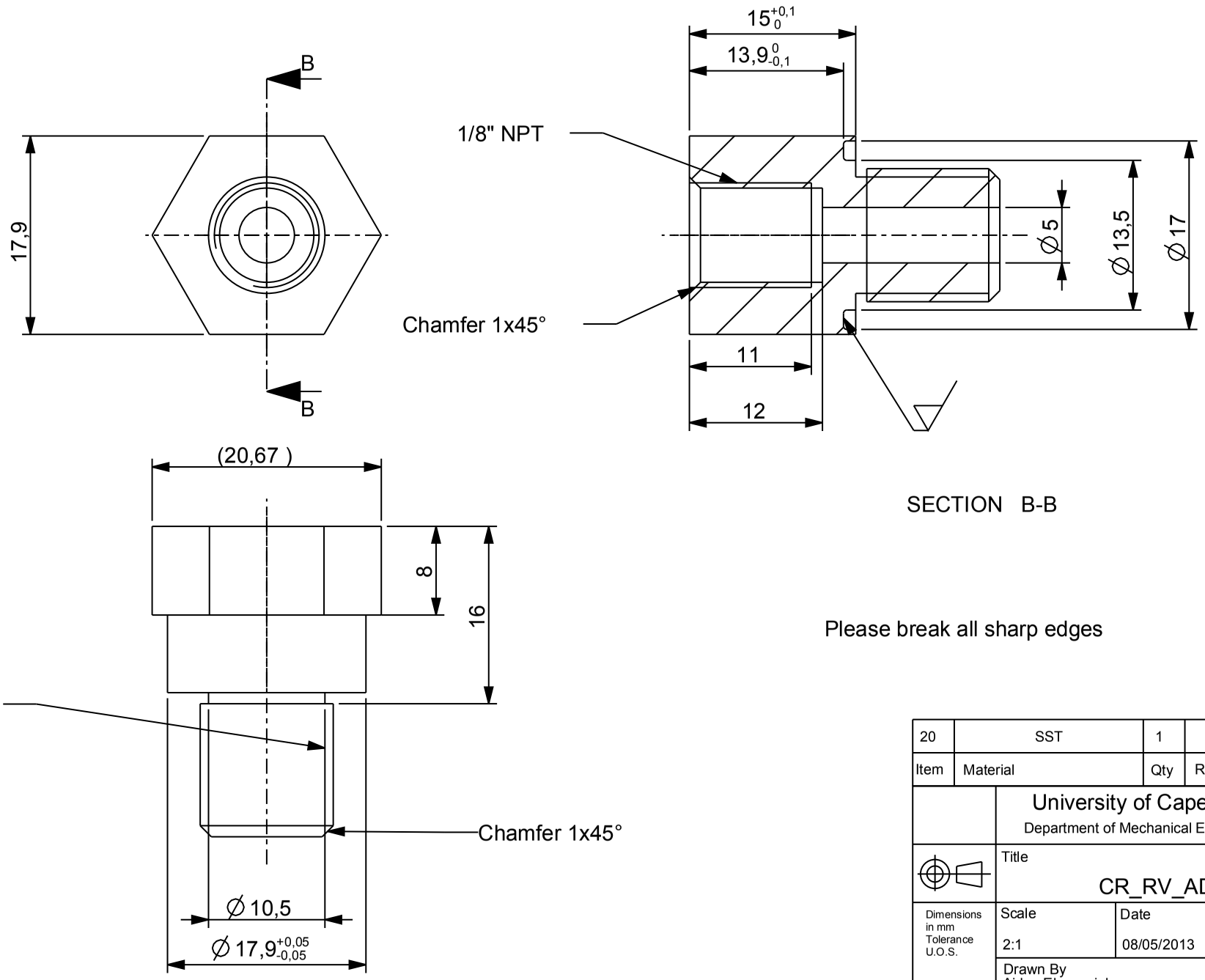

20	SST	1	
Item	Material	Qty	Remarks

University of Cape Town
Department of Mechanical Engineering

Title: CR_RV_ADAPTER

Dimensions in mm Tolerance U.O.S.	Scale	Date	Sheet	of
0.1	2:1	08/05/2013	1	1

Drawn By: Aidan Ehrenreich (SAFL)

Drawing Number: 9

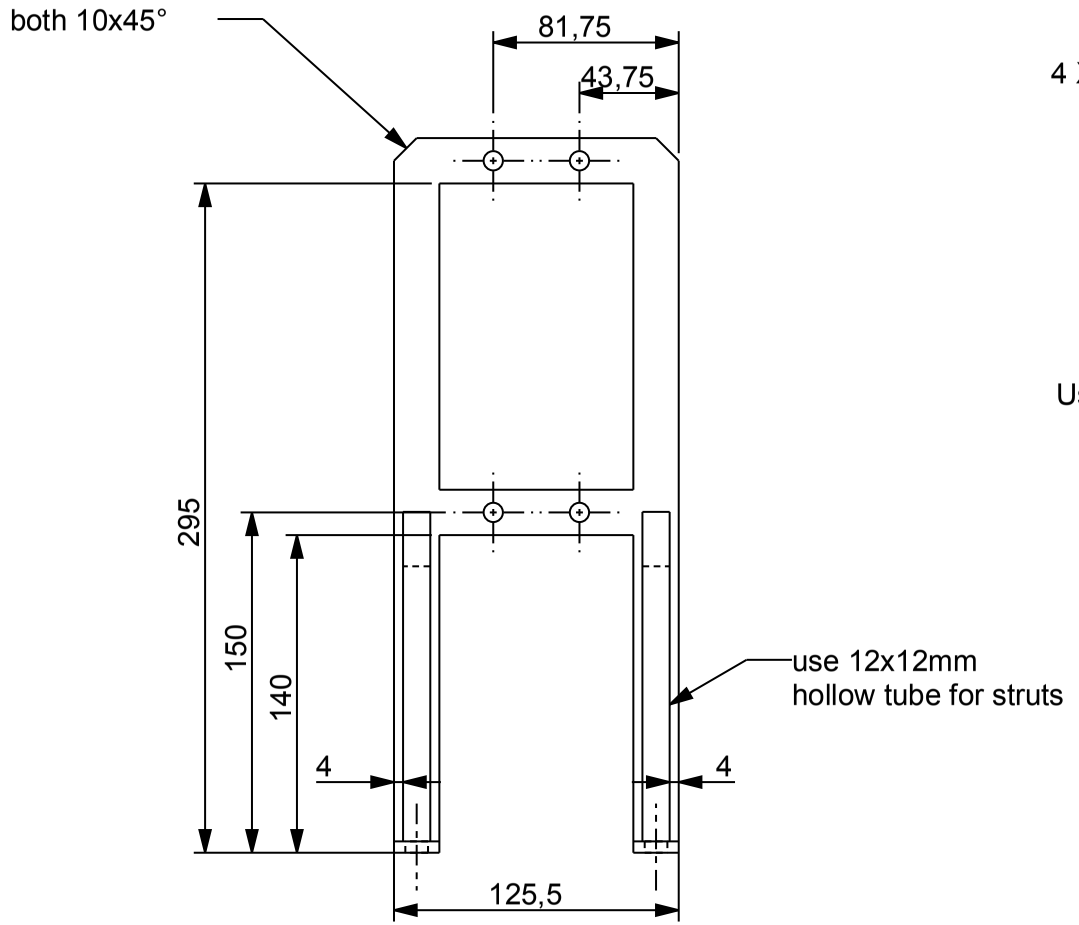

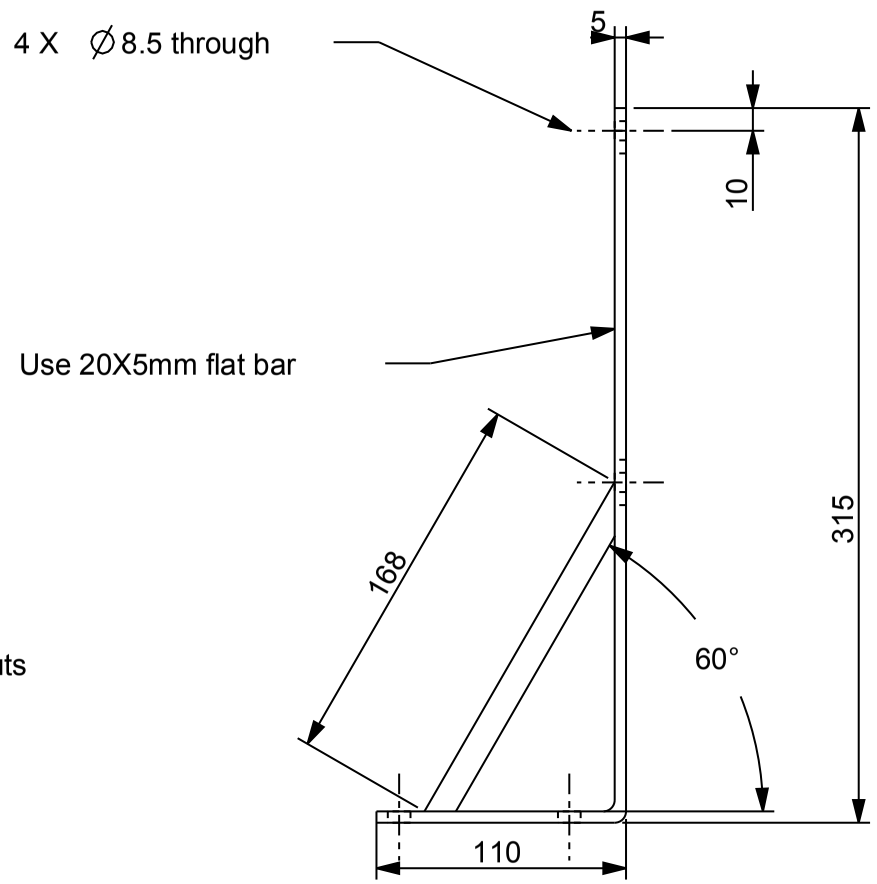

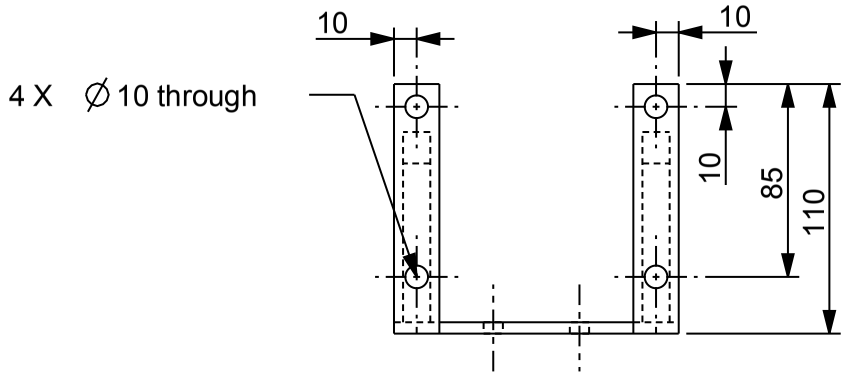

25	STEEL_LC	1	
Item	Material	Qty	Remarks

University of Cape Town
Department of Mechanical Engineering

Title: CR_BRACKET

Dimensions in mm Tolerance U.O.S.	Scale	Date	Sheet	of
0.1	3:10	08/05/2013	1	1

Drawn By: Aidan Ehrenreich (SAFL)

Drawing Number: 10

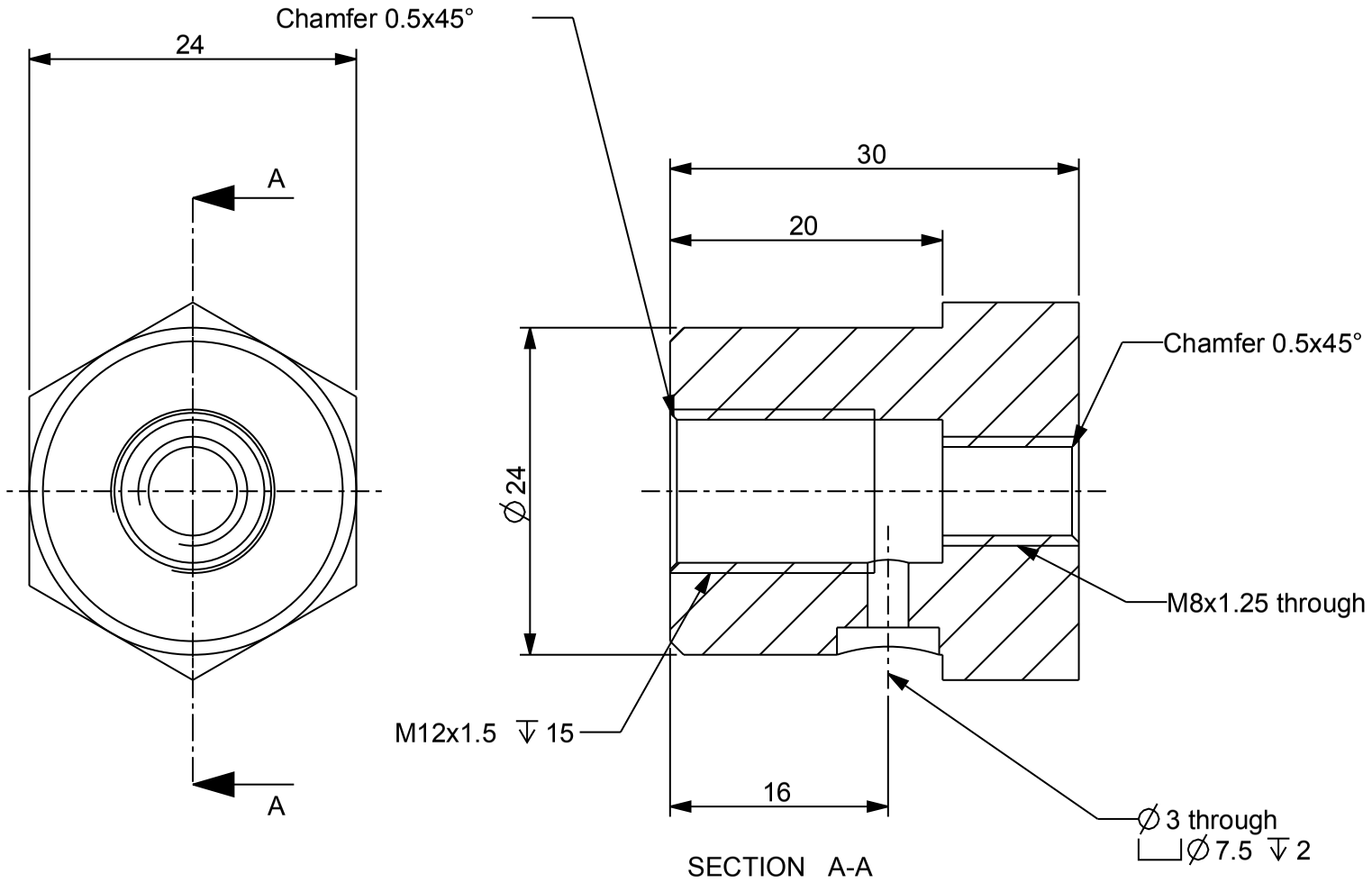

SECTION A-A

27	SST	2	
Item	Material	Qty	Remarks

University of Cape Town
Department of Mechanical Engineering

Title: BLEED_NUT_ADAPTER

Dimensions in mm Tolerance U.O.S.	Scale	Date	Sheet	of
0.1	2:1	06/02/2015	1	1

Drawn By	Drawing Number
A. Ehrenreich	11

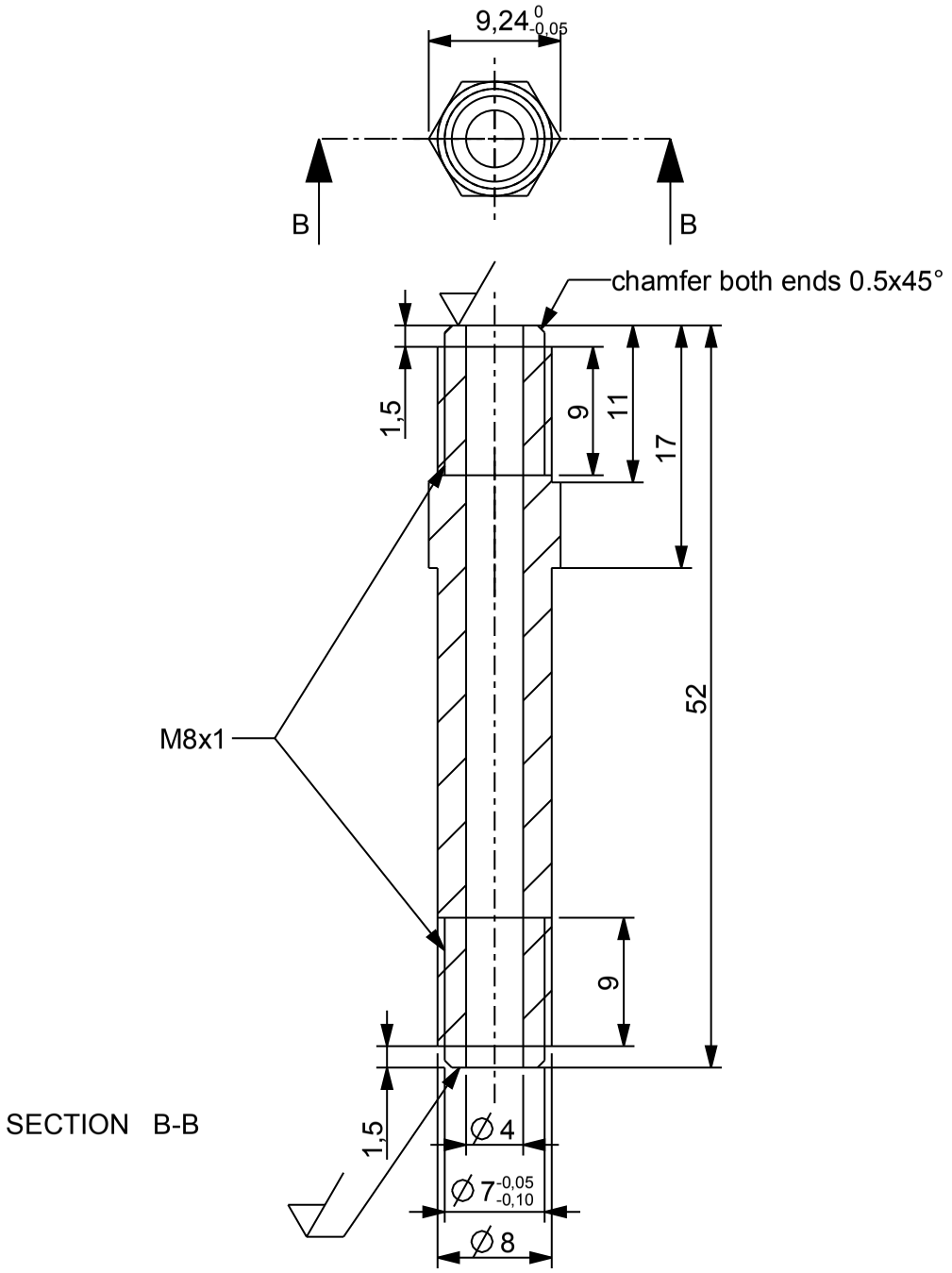

SECTION B-B

30	SST	2	
Item	Material	Qty	Remarks

University of Cape Town
Department of Mechanical Engineering

Title
NIPPLE

Dimensions in mm Tolerance U.O.S.	Scale 2:1	Date 18/02/2013	Sheet 1	of 1
0.1	Drawn By Aidan Ehrenreich (SAFL)		Drawing Number 12	

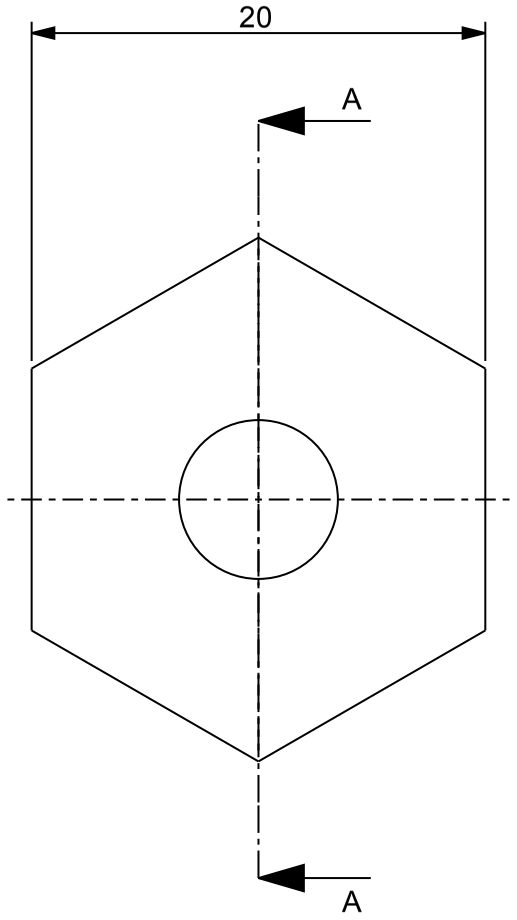

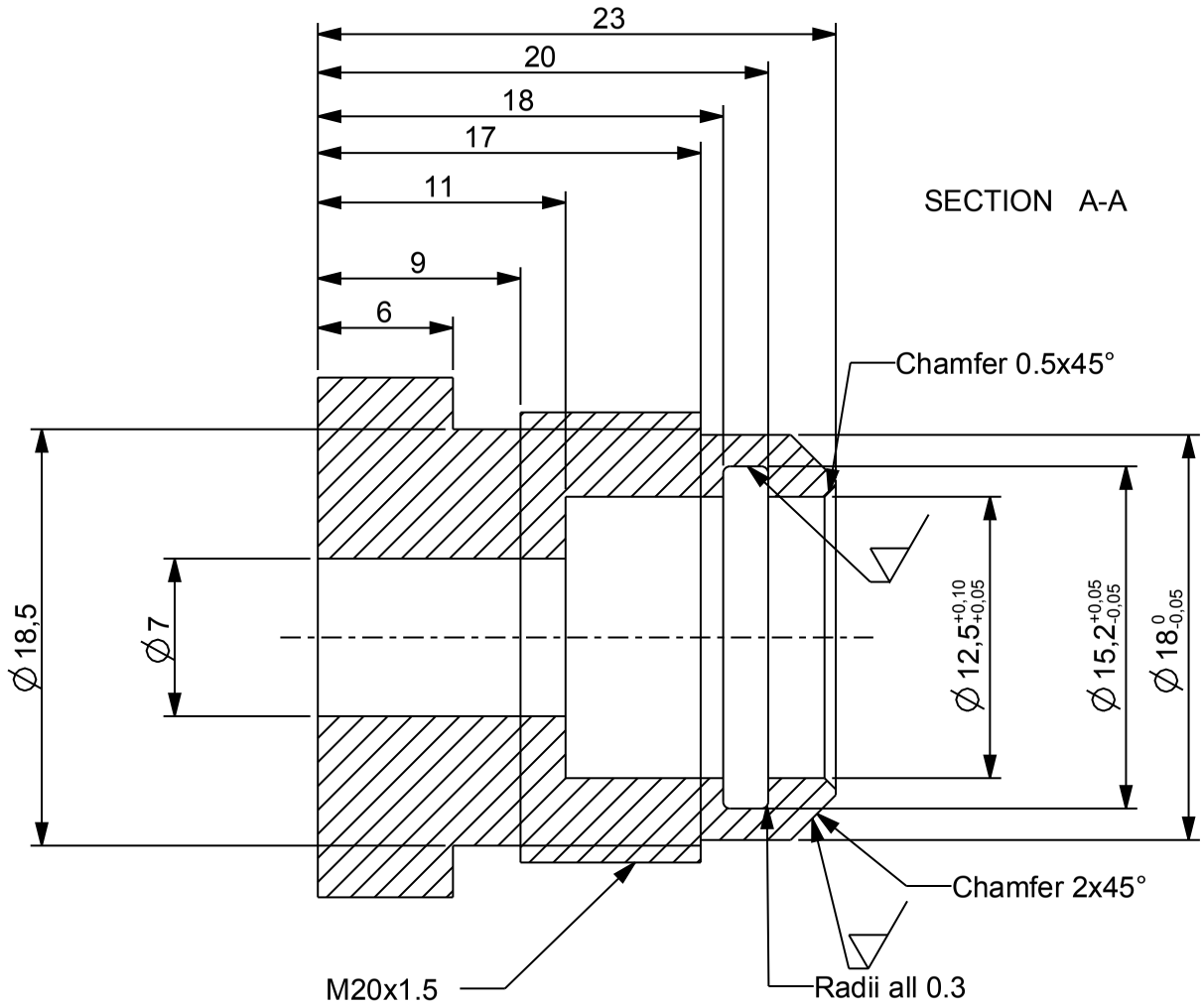

SECTION A-A

31	SST_304	2	
Item	Material	Qty	Remarks

University of Cape Town
Department of Mechanical Engineering

Title
WINDOW_HOLDER

Dimensions in mm Tolerance U.O.S.	Scale	Date	Sheet	of
	3:1	20/06/2014	1	1
	Drawn By		Drawing Number	
0.1	A.Ehrenreich		13	

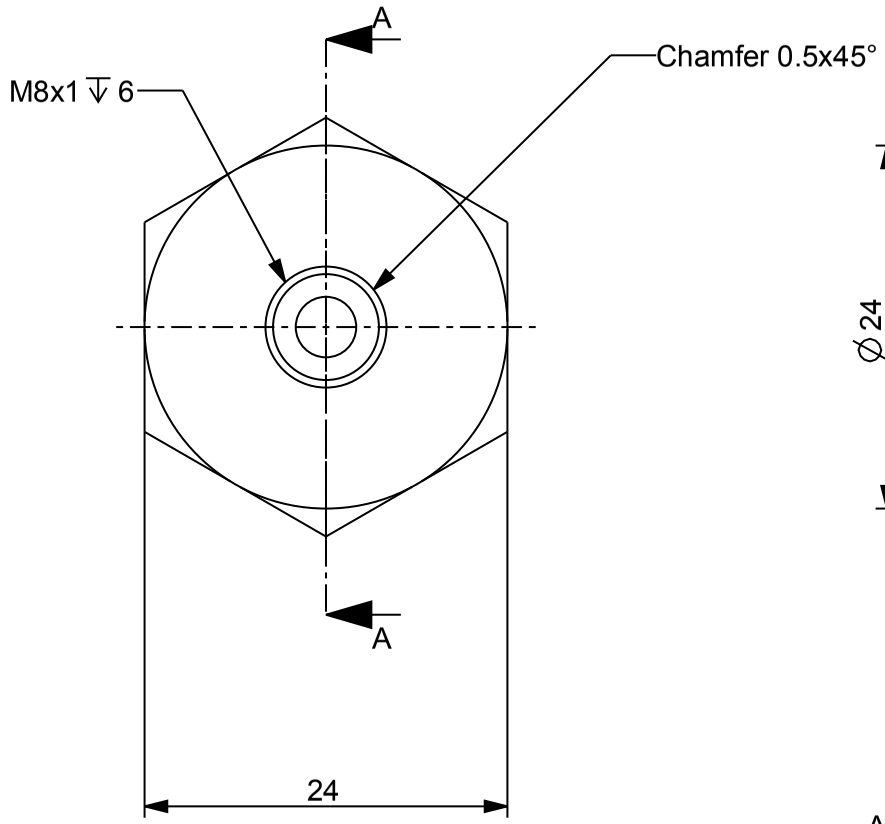

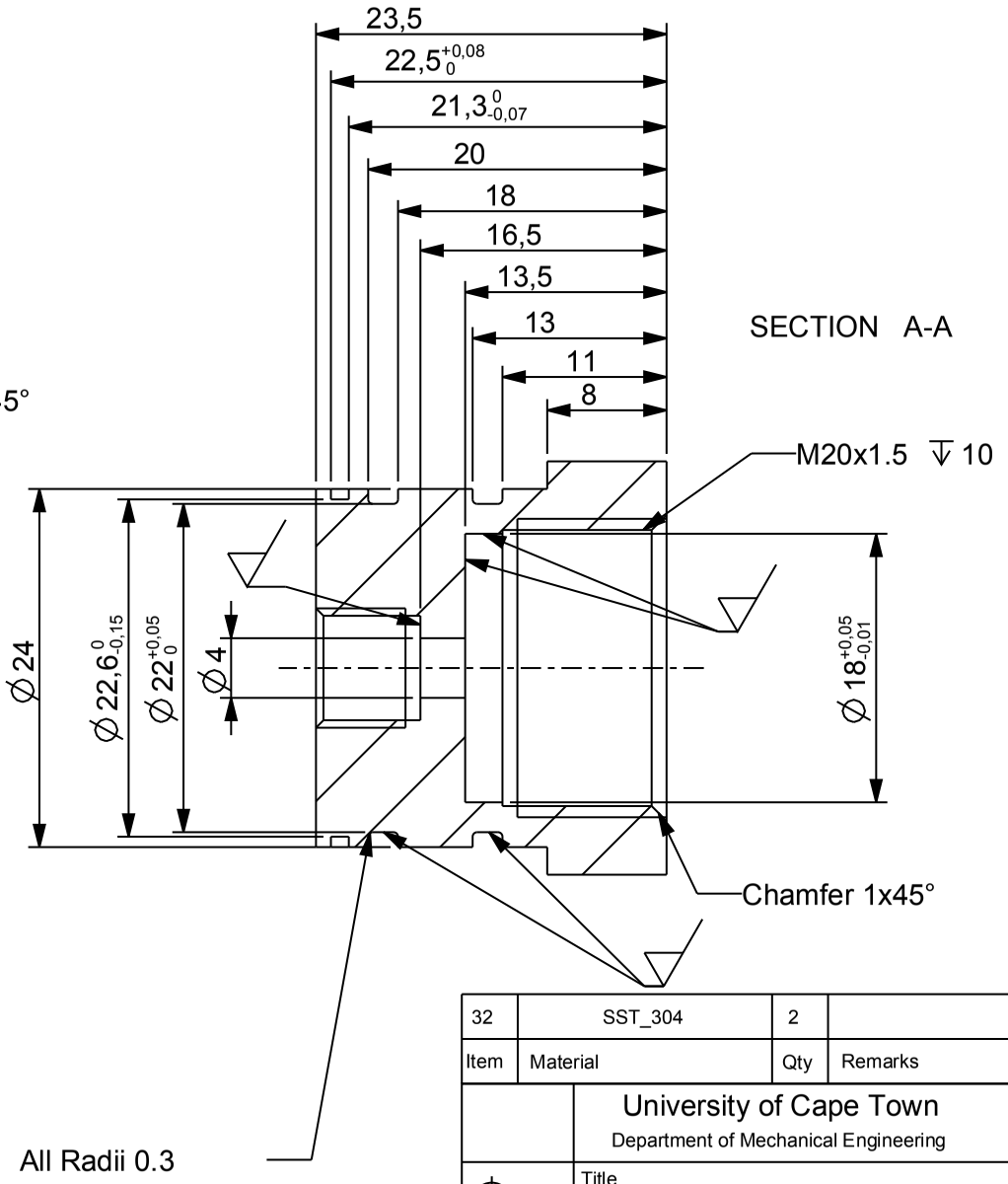

32	SST_304	2	
Item	Material	Qty	Remarks

University of Cape Town
Department of Mechanical Engineering

Title: WINDOW_MOUNT

Dimensions in mm Tolerance U.O.S.	Scale	Date	Sheet	of
	2:1	20/06/2014	1	1
	Drawn By		Drawing Number	
0.1	A.Ehrenreich		14	

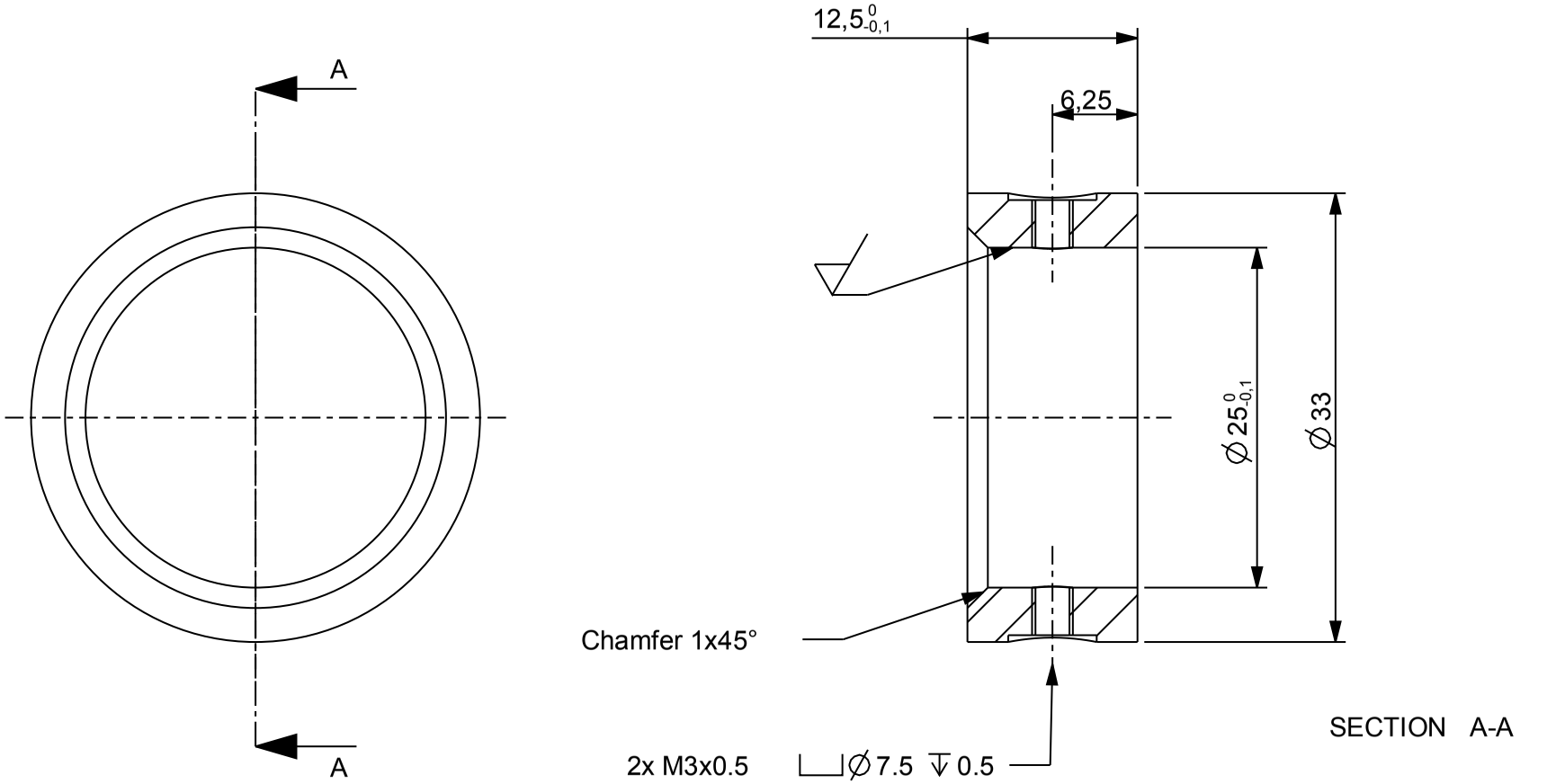

33	BRASS	2	
Item	Material	Qty	Remarks

University of Cape Town
Department of Mechanical Engineering

Title: COLLAR

Dimensions in mm Tolerance U.O.S.	Scale 2:1	Date 20/06/2014	Sheet 1	of 1
	Drawn By A.Ehrenreich		Drawing Number 15	
0.1				

must drop into M8x1 holes
on "mounting plate"

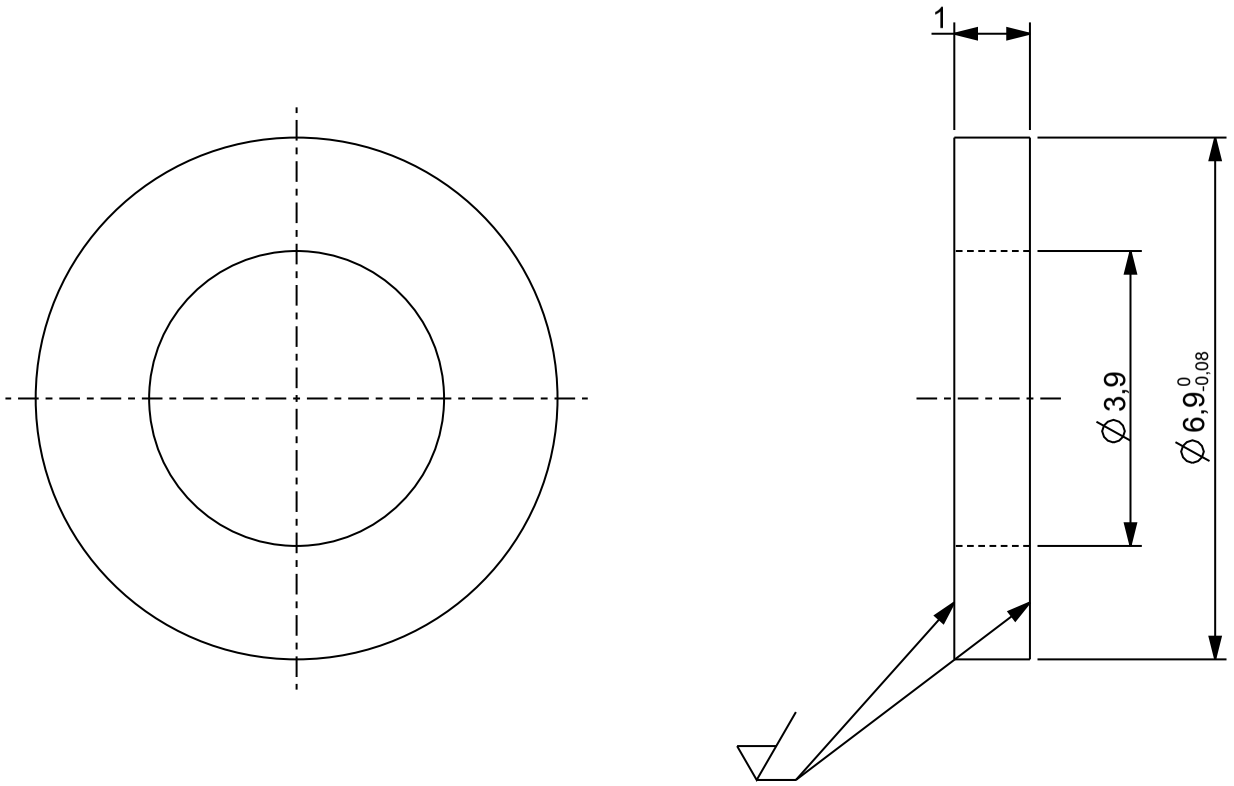

41	annealed copper	2	
Item	Material	Qty	Remarks

University of Cape Town
Department of Mechanical Engineering

Title
NIPPLE_WASHER

Dimensions in mm Tolerance U.O.S.	Scale	Date	Sheet	of
0.1	10:1	18/02/2013	1	1

Drawn By
Aidan Ehrenreich
(SAFL)

Drawing Number
16

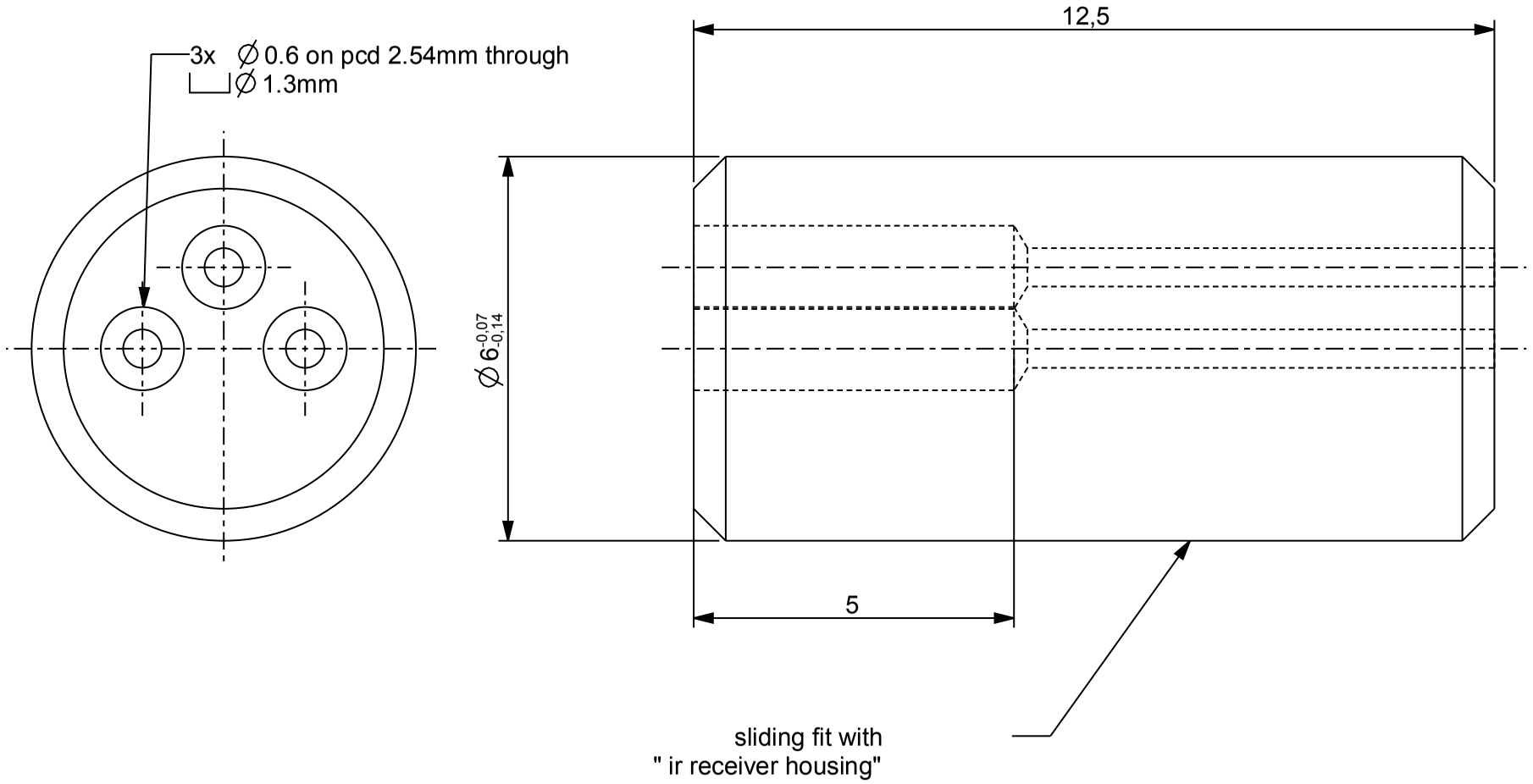

42	Teflon	1	
Item	Material	Qty	Remarks

University of Cape Town
Department of Mechanical Engineering

Title
RECEIVER_LEAD_GUIDE

Dimensions in mm Tolerance U.O.S.	Scale	Date	Sheet	of
	10:1	19/02/2013	1	1
	Drawn By: Aidan Ehrenreich (SAFL)		Drawing Number: 17	

0.1

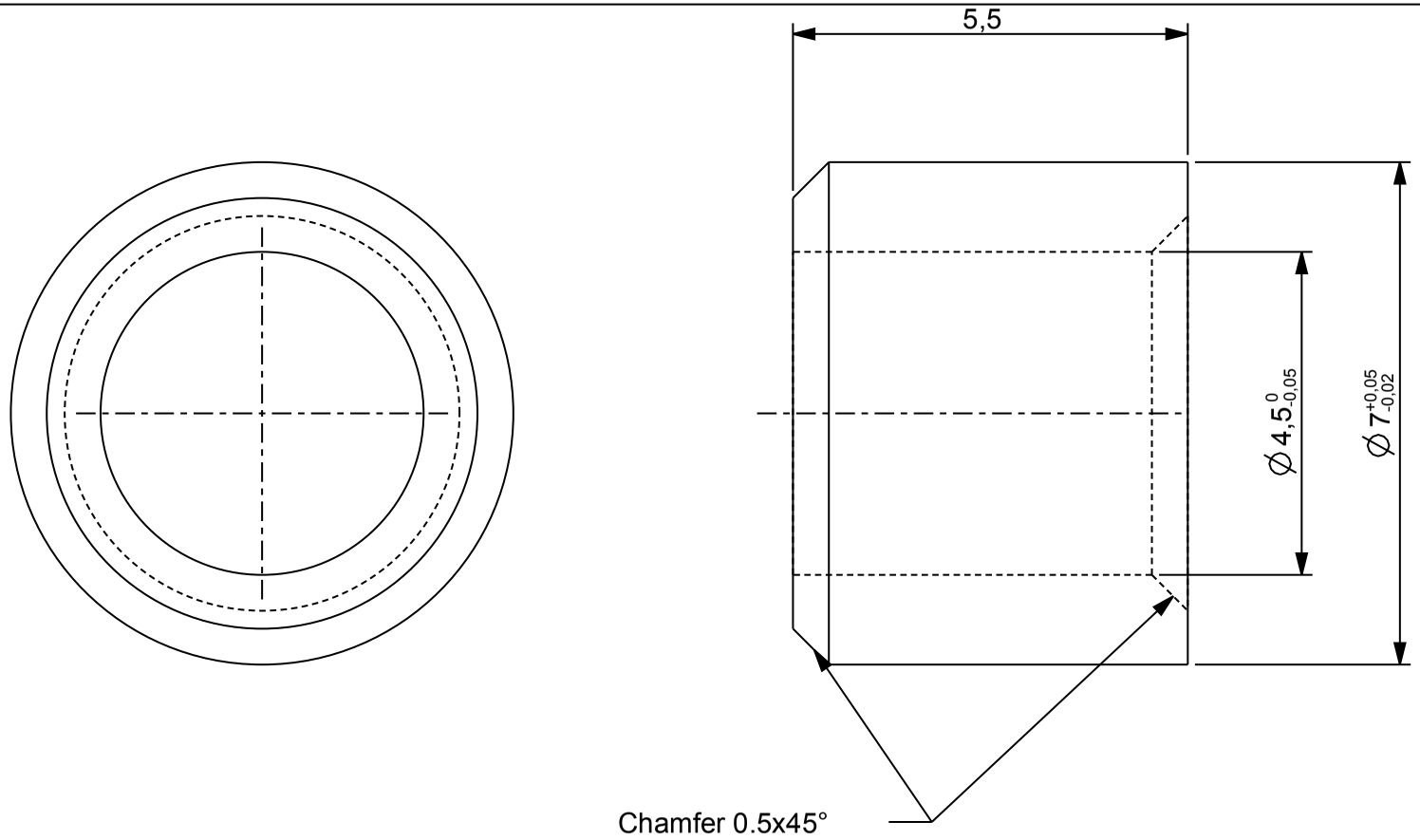

43,60	Teflon	1	
Item	Material	Qty	Remarks

University of Cape Town
Department of Mechanical Engineering

Title
OPTOSCHMITT_GUIDE

Dimensions in mm Tolerance U.O.S.	Scale	Date	Sheet	of
	10:1	10/06/2014	1	1
	Drawn By		Drawing Number	
0.1	A.Ehrenreich		25	

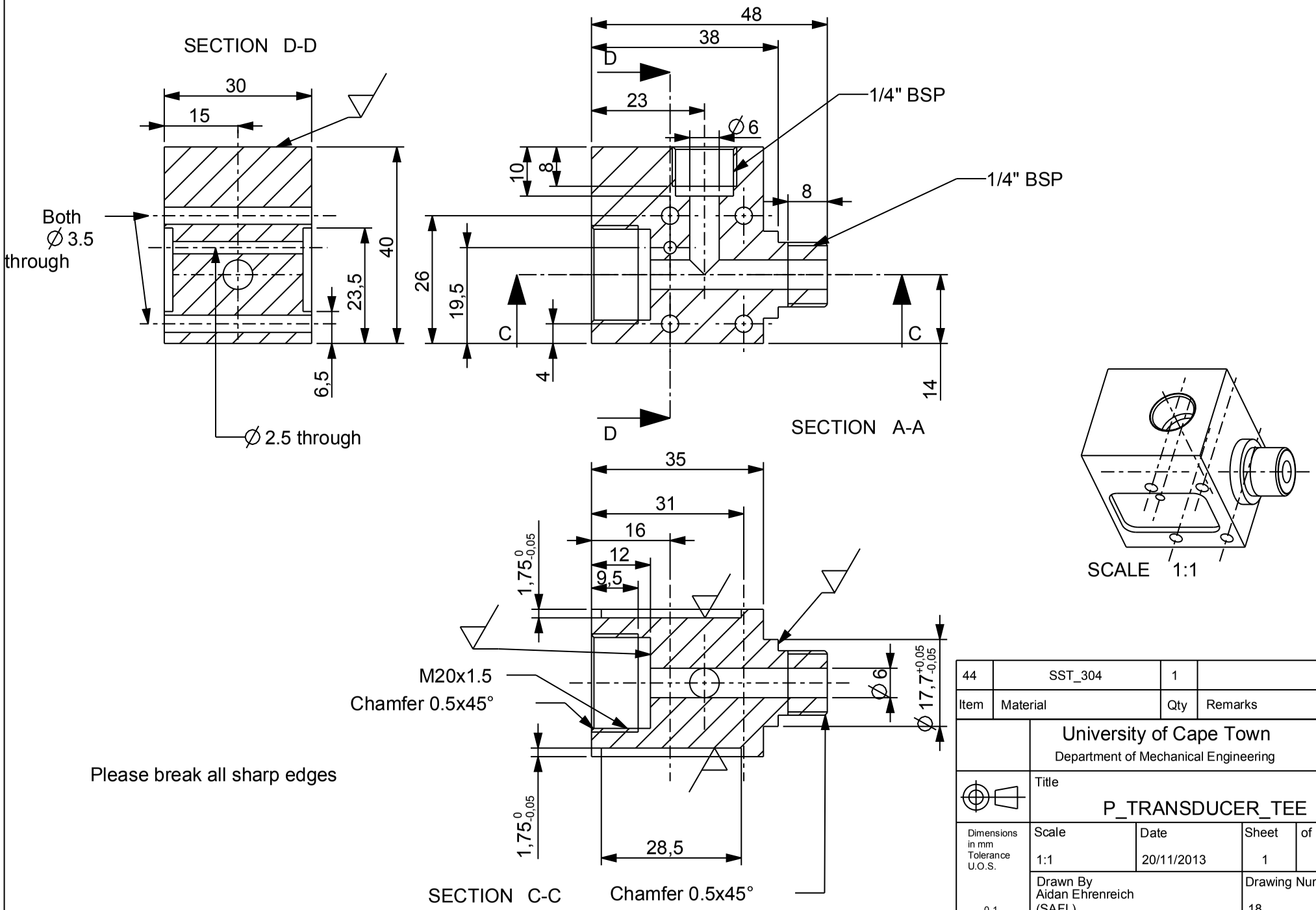

44	SST_304	1	
Item	Material	Qty	Remarks

University of Cape Town
Department of Mechanical Engineering

Title
P_TRANSDUCER_TEE

Dimensions in mm Tolerance U.O.S.	Scale	Date	Sheet	of
	1:1	20/11/2013	1	1
0.1	Drawn By Aidan Ehrenreich (SAFL)		Drawing Number 18	

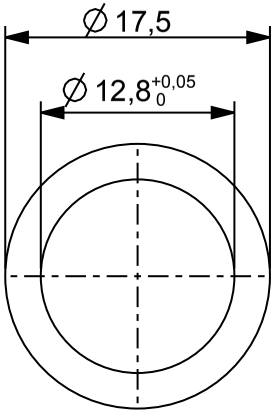

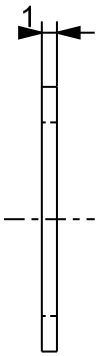

45	Annealed Copper	1	
Item	Material	Qty	Remarks

University of Cape Town
Department of Mechanical Engineering

Title
ADAPTER_WASHER

Dimensions in mm Tolerance U.O.S.	Scale	Date	Sheet	of
	2:1	26/04/2013	1	1
0.1	Drawn By Aidan Ehrenreich (SAFL)		Drawing Number 19	

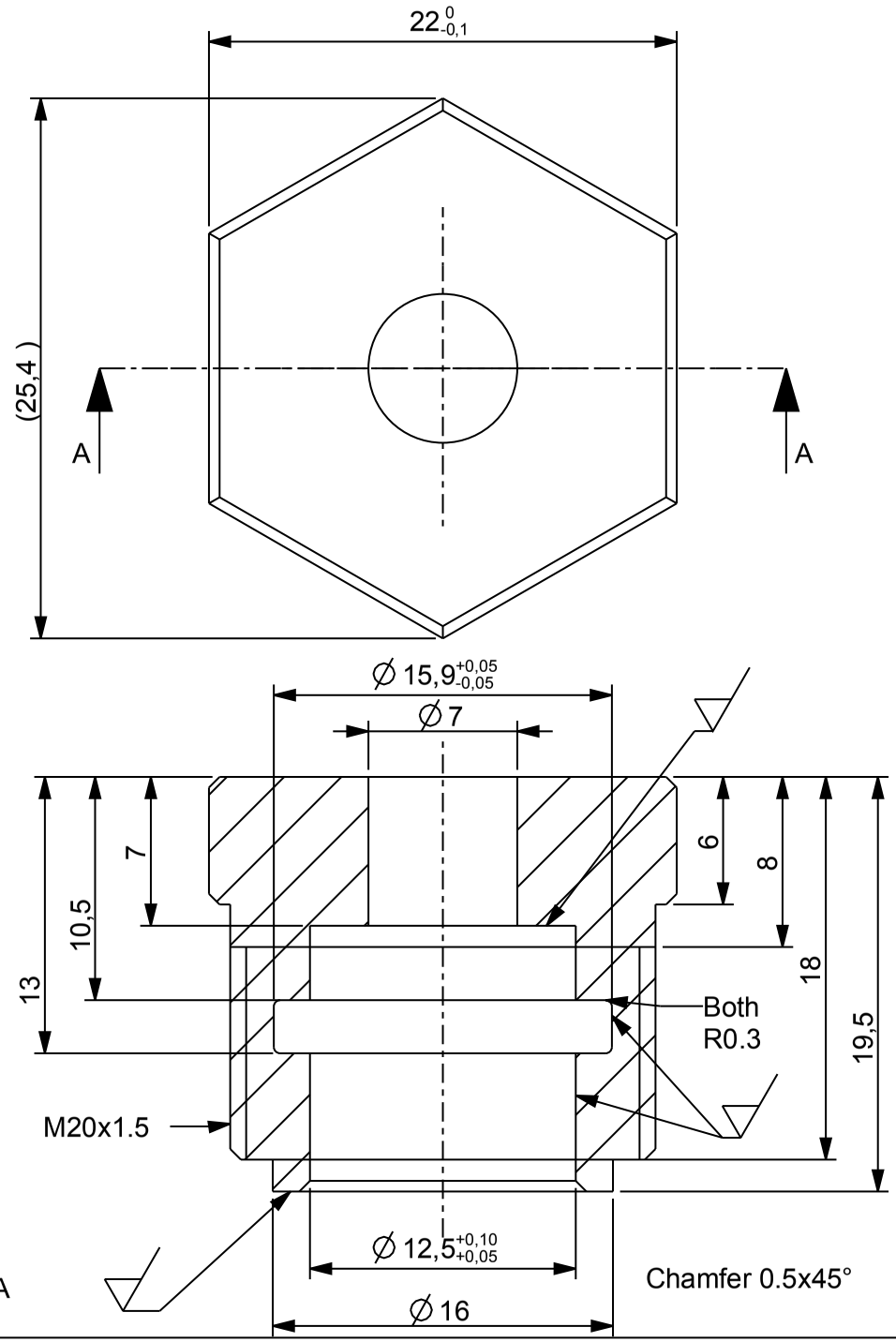

Please break all sharp edges

46	BRASS	1	
Item	Material	Qty	Remarks

University of Cape Town
Department of Mechanical Engineering

Title
SIGHT_GLASS_HOLDER

Dimensions in mm Tolerance U.O.S.	Scale	Date	Sheet	of
	3:1	20/11/2013	1	1
	Drawn By Aidan Ehrenreich (SAFL)		Drawing Number	
0.1			20	

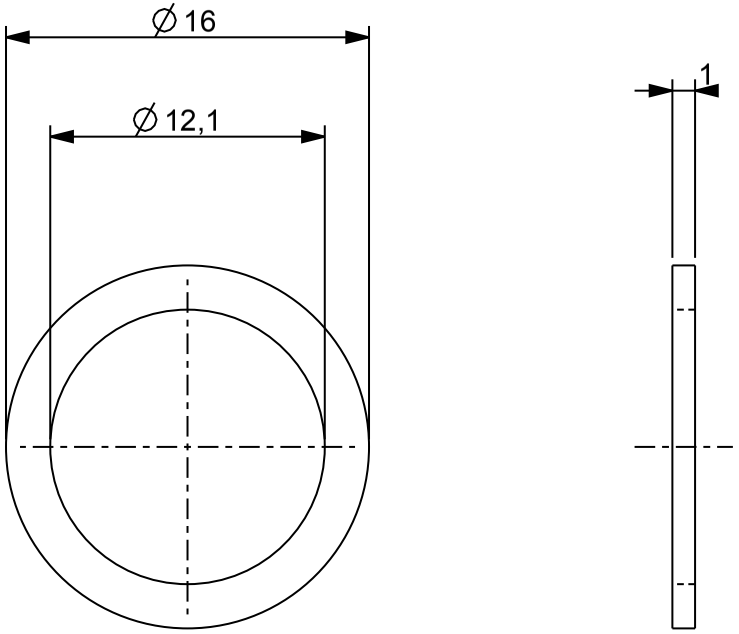

48	Copper	1	
Item	Material	Qty	Remarks

University of Cape Town
Department of Mechanical Engineering

Title
TEE_GASKET

Dimensions in mm Tolerance U.O.S.	Scale	Date	Sheet	of
	3:1	20/11/2013	1	1
0.1	Drawn By Aidan Ehrenreich (SAFL)		Drawing Number 21	

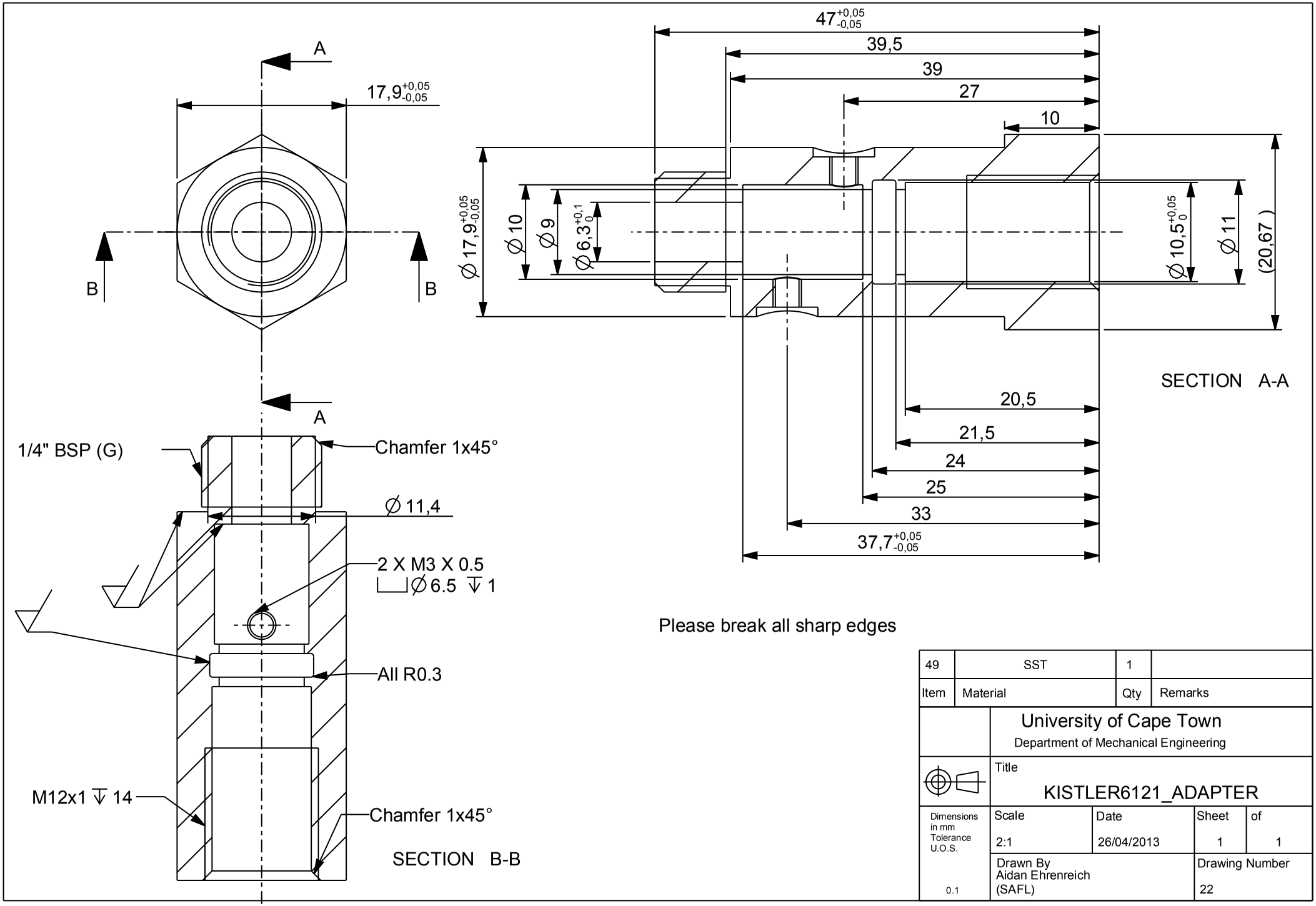

49	SST	1	
Item	Material	Qty	Remarks

University of Cape Town
Department of Mechanical Engineering

Title: KISTLER6121_ADAPTER

Dimensions in mm Tolerance U.O.S.	Scale	Date	Sheet	of
0.1	2:1	26/04/2013	1	1

Drawn By: Aidan Ehrenreich (SAFL)

Drawing Number: 22

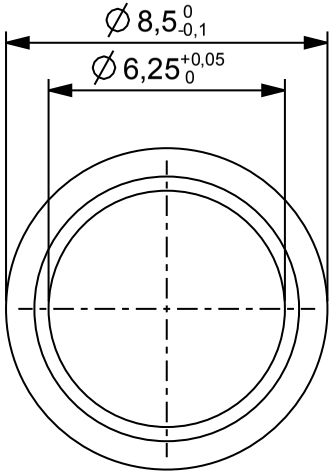

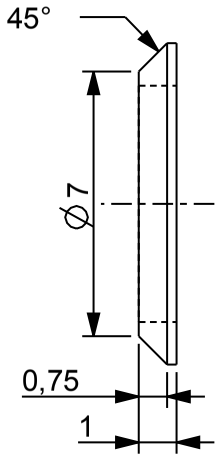

51	Annealed Copper	1	
Item	Material	Qty	Remarks

University of Cape Town
Department of Mechanical Engineering

Title
KISTLER_6121_WASHER

Dimensions in mm Tolerance U.O.S.	Scale	Date	Sheet	of
	5:1	09/07/2013	1	1
	Drawn By Aidan Ehrenreich (SAFL)		Drawing Number 23	
0.1				

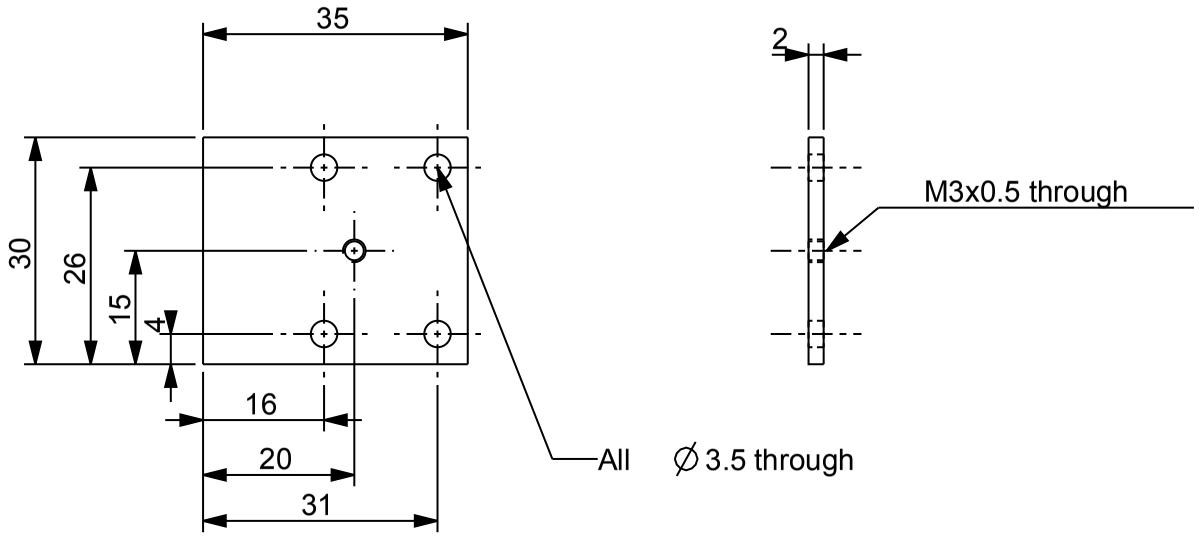

59	BRASS	2	
Item	Material	Qty	Remarks

University of Cape Town
Department of Mechanical Engineering

Title
TEE_COVER

Dimensions in mm Tolerance U.O.S.	Scale	Date	Sheet	of
	1:1	20/10/2013	1	1
	Drawn By Aidan Ehrenreich (SAFL)		Drawing Number 24	
0.1				